

European Coating Symposium 2023
Paris — 13-15 September

Book of Abstracts

version: September 12, 2023



Contents

Introduction	9
List of participants	11
<hr/> Tuesday Sept 12 <hr/>	17
Pre-Symposium Course Program : Wetting, Drying, Coating and Adhesion: Theory and Applications	17
Goehring Lucas, <i>Drying colloidal films, from a liquid dispersion to a rigid coating</i>	17
Benkreira Hadj, <i>Coating Flows: Principles & Operation</i>	18
Talini Laurence, <i>Wetting of solids by liquids: how is the dynamics modified by a complex substrate or a complex liquid?</i>	19
Ciccotti Matteo, <i>Adhesion and adhesives fundamentals</i>	20
<hr/> Wednesday Sept 13 <hr/>	21
Opening Keynote Lectures	21
Rémy Deleurence, <i>Wet Coating Processes at Saint-Gobain: Products and Industrial Realities</i>	21
Doris Vollmer, <i>How to clean a contaminated surface with a water drop ?</i>	22
Parallel Session 1: Material Coating	23
Jain Adarsh, <i>Developing Anode Architectures to Enhance Hydrogen Production in Alkaline Water Electrolysis</i>	23
Jacobs Marijke, <i>Development of tuned SOEC electrode by spray coating</i>	24
Heckmann Thilo, <i>Sorption and Diffusion Processes in Cathode Active Materials for Lithium-ion Batteries during the production of electrodes</i>	25
Parallel Session 2: Drying and Wetting	26
Rigutto Damien, <i>Experimental analysis of dynamic menisci in dip coating</i>	26
Bintein Pierre-Brice, <i>Contact line dynamics with inertia</i>	27
Boulogne François, <i>The coffee stain on a fiber</i>	28

Parallel Session 3: Drying and Wetting	29
Quarz Philipp, <i>About the production of catalyst layers for PEM-fuel cells and PEM-electrolysis</i>	29
Masato Yamamura, <i>Particle migration in evaporating alcohol-water bimodal slurry films</i>	30
Jung Hyun Wook, <i>Particle dynamics in coating and drying processes of particulate suspensions</i>	34
Wilson Stephen, <i>The effect of the spatial variation of the evaporative flux on the deposition from a sessile droplet</i>	35
Limat Laurent, <i>Drops sliding down an inclined soft coating</i>	36
Parallel Session 4: Interface Dynamics	37
Pino Fabio, <i>Absolute/convective instability threshold for a liquid film over a moving substrate via linear stability analysis</i>	37
Scholle Markus, <i>Bilayer Couette and Film Flow over a Profiled Substrate</i> . . .	38
Djambov Simeon, <i>Weakly non-parallel stability of a condensing film flow</i>	42
Martin Jérôme, <i>Condensation-induced self-patterning of a thin clayey layer. Impact on painted caves.</i>	46
Barreiro-Villaverde David, <i>High and low fidelity models to understand the physics of air-knife coating</i>	47
Poster Session	48
Jee Sanghun, <i>Analysis of edge formation in intermittent slot coating process</i> . .	48
Quarz Philipp, <i>About the production of catalyst layers for PEM-fuel cells and PEM-electrolysis</i>	49
Mounkaila Noma Djibrilla, <i>Drying of slurry for manufacturing of battery electrodes: microfluidic studies of binder migration</i>	50
Janning Linus, <i>Investigation of microstructure formation and pore emptying in relation to drying conditions and particle properties</i>	51
Barbig Philipp, <i>Mass transport through battery electrode coatings during post-drying and humidity management</i>	52
Loedige Lukas, <i>Multi-component drying of electrolyte solvents from porous electrodes and separators for recycling processes of lithium-ion batteries</i> .	53
Hoffmann Alexander, <i>CFD simulation of slot-die coating for single- and multi-layered lithium-ion battery electrodes in OpenFOAM</i>	54
Kim Donguk, <i>Data-driven modeling-based design of dual-shim configuration for uniform coating of non-Newtonian liquids in the PEMFC slot coating process</i>	55
Borho Julian, <i>Multi-stage drying of battery electrodes and comparison of drying process and energy efficiency with NIR and laser energy input</i>	56
Yun Jinseong, <i>Simulation study on cooperative motion of particles in a quasi-two-dimensional colloidal glass-forming liquid</i>	57

Ly Kevin, <i>Towards an optimized electrode production - Recent approaches in flexibility and efficiency</i>	58
Gosset Anne, <i>Experimental characterization of the rivulets in a liquid film down an inclined plane</i>	59
Darhuber Anton, <i>Transient deformation and swelling of paper by aqueous co-solvent solutions</i>	60
Song Jisoo, <i>Quantifying the coating layer shape in finite depth dip coating</i> . . .	61
Yoon Jihwan, <i>Simplified model for stable operating condition of thick-film battery electrode slot coating</i>	63
<hr/>	
Thursday Sept 14	64
Keynote Lectures	64
Odile Sonnevile-Aubrun, <i>A journey into cosmetic coatings through mascara deposition</i>	64
Alexander Routh, <i>Cracking, stratification and instabilities in drying of colloidal dispersions</i>	65
Parallel Session 5: Interface Dynamics	66
Hadj Benkreira, <i>Air Entrapment during Coating of Viscous Fluids</i>	66
Rabehi Fateh, <i>Hydrodynamics of Short Curtain Coating</i>	67
Omer Atasi, <i>Multiscale numerical modeling of antibubbles combining CFD and lubrication approach</i>	69
Gosset Anne, <i>Three-dimensional damping of defects on coating films</i>	70
Parallel Session 6: Material Coating	71
Hoffmann Alexander, <i>Simultaneous multilayer coating for battery electrodes and numerical simulations with model material systems</i>	71
Min Kyengmin, <i>Coating thickness analysis The numerical analysis of battery slurry passing slot die cavity using a thixotropy model</i>	72
Ly Kevin, <i>A new concept for an energy- and cost-efficient battery electrode production - Drying investigation of a highly-concentrated granule-based system</i>	73
Doell Harald, <i>Cleaning station for slot dies</i>	74
Parallel Session 7: Drying and Wetting	75
Moorhead Annie, <i>Stress and Fracture During the Drying of Aqueous Particulate Coatings</i>	75
Salmon Jean-Baptiste, <i>Mass transport and drying-induced stresses in charged colloidal dispersions</i>	76
Lequeux François, <i>Formation of glassy skins in drying polymer solutions</i>	77
Bouvier Antoine, <i>Coalescence of multiple sessile drops on a substrate</i>	78

Parallel Session 8: Printing Technology	79
Darhuber Anton, <i>Chromatographic Effects in Inkjet Printing</i>	79
Darhuber Anton, <i>Inkjet printing of surfactant solutions onto thin moving porous media</i>	80
Mauron Muriel, <i>Smart materials by inkjet</i>	81
Brogly Amélie, <i>The role of the dispersing agent on latency issues for water-based inkjet inks: drying aspect</i>	82
Parallel Session 9: Interface dynamics	84
Ruyer-Quil Christian, <i>Falling films on a slippery wall: a revisited formulation</i> .	84
Dietze Georg, <i>Falling liquid film subject to a counter-current turbulent gas flow: beyond the absolute instability limit</i>	85
Milne Laura, <i>Modelling thin-film flow over a spinning disk</i>	86
Parallel Session 10: Interface dynamics	87
Gasser Mary-Ann, <i>Fluid invasion front within a confined copper pillar array for microelectronic</i>	87
Di Mauro Gabrielle, <i>Thickness gradients induced by defects in liquid deposition</i>	88
Talini Laurence, <i>Drying liquid coatings with an evaporation mask</i>	89
Keynote Lecture	90
François Gallaire, <i>Stable and unstable coating flows on curved substrates</i> . . .	90
Friday Sept 15	91
Keynote Lecture	91
Jacco Snoeijer, <i>Wetting flows with viscoelasticity</i>	91
Parallel Session 11: Drying and Wetting	92
Pelosse Alice, <i>Free surface flows and contact line motions with suspensions</i> . .	92
Varlet Anthony, <i>Delayed coating of a liquid film on a soft substrate in a partially wetted condition</i>	93
Le Lay Grégoire, <i>Acoustically-Induced Sinuous-Varicose Coupling in Falling Fluid Rivulets</i>	94
Pingulkar Hrishikesh, <i>Microfluidic study of evaporation through steady colloidal crust</i>	95
Kumar Satish, <i>Capillary flow of evaporating liquid solutions in open rectangular microchannels</i>	96
Waquier Louis, <i>Optomechanical measurement of single nanodroplet evaporation with millisecond time-resolution</i>	97

Parallel Session 12: Material Coating	98
Kobayashi Hirokazu, <i>Effect of gas wiping temperature on coating weight reduction in hot-dip galvanizing on steel strip</i>	98
Klemens Julian, <i>Film Formation of Lithium-Ion- and Sodium-Ion-Battery Electrodes During Drying: Challenges and Opportunities due to Particle Properties and Process Conditions</i>	103
Zimmerer Nadine, <i>Structural optimisation of catalyst layers for PEM electrolysis</i>	104
Harris Tequila, <i>Fabrication of Reduced Graphene Oxide Nanofiltration Membranes by an Integrated Roll-to-Roll (R2R) Process</i>	105
Burger David, <i>About the pore emptying during drying of water-based battery electrodes</i>	106
Mohacsi Jonas, <i>New methods for optimized inline monitoring of the drying process of battery electrodes</i>	107
 Parallel Session 13: Interface dynamics	 108
Chateaubinois Antoine, <i>Friction of poroelastic contacts with hydrogel coatings</i>	108
Verneuil Emilie, <i>Hydrogel films as anti-fog coatings : swelling and debonding</i> .	109
 Parallel Session 14: Printing Technology	 110
Darhuber Anton, <i>Transport and evaporation of aqueous co-solvent mixtures in thin porous media</i>	110
Kessler Philip, <i>Digital printing of coatings by direct-to-shape inkjet printing with industrial robot</i>	111
 Keynote Lecture	 112
Thomas Séon, <i>Freezing contact line</i>	112

Introduction

The European Coating Symposium is now reaching its 15th edition. It follows, two years after, a remarkable event at the exit of the last pandemic, that was a fair success in Bruxelles (ECS2021). For us, it is also the second time that ECS occurs in Paris, the previous occasion being ECS2007. The local conditions have a bit changed, it is not the University Paris Diderot that now welcomes this original community, which mixes scientists and engineers, from both academics and industry. In place, it is the new University Paris Cité that results from a fusion between Paris Diderot and Paris Descartes Universities, together with Institut de Physique du Globe (IPGP), and for this occasion, in close association with University Paris Saclay. Two labs have federated here their efforts, “Matière et Systèmes Complexes” (MSC) from Paris Cité, and also “Fluides, Automatique et Systèmes Thermiques” (FAST) from Université Paris-Saclay. Both are UMR (Unité Mixtes de Recherche) associated to CNRS, Centre National de la Recherche Scientifique.

Just as for Bruxelles, in 2021, this new event is a fair success. In addition to 7 invited conferences, from people coming from different European Countries, and 4 pre-Symposium Training Course, it is not less than 54 oral talks and 15 posters, that are presented, while the Symposium also hosts 3 different Society booths from Industry (TSE Troller, nTACT and Polytype Converting). ECS demonstrates again its strong vitality and the fact that there is a true community that needs to be federated each two years by our Symposium. As for the previous events, the classical division between wetting, drying and coating, does not hide the fact that very different new subjects are emerging, a tendency that we have tried to encourage. Many talks are presenting original progresses on energy, batteries, solar cells, fracture in art painting, soft matter compounds and materials, inkjet printing, glass industry and cosmetic films... Exploring new fields is essential to maintain the dynamism of the event. Above all, the Symposium will be the occasion for many people and old friends to meet again a new time. We have tried to make the event very festive with a cruise banquet on the Seine river, and a degustation of French wines and cheeses during the poster session.

We now thank our sponsors: Centre National de la Recherche Scientifique (CNRS), Université Paris Cité, especially its Sciences Faculty, Labex SEAM on smart materials, and the three societies TSE Troller, nTact and Polytype Con-

verting from Olbrich group. Above all, organizing this meeting was a collective adventure, in which each member of the organizing committee has invested many efforts (Ludivine Allée, Philippe Brunet, Adrian Daerr, Julien Dervaux, Frédérique Giorgiutti, Luc Lebon, Laurent Limat, Ludovic Pauchard, Benoit Scheid) and offered his or her own qualities in a complementary way. A lot of thanks are due to each of them. The success of this meeting is the result of sharing all our efforts. We also thank ECS Committee for having elected our team for this year event, and we wish a pleasant stay to all participants on the Seine borders.

L. Limat and **L. Pauchard**, co-chairmen, ECS2023.

Paris, September 3, 2023.

Atasi, Omer omer.atasi@ulb.be

TIPs, Université libre de Bruxelles (ULB), Belgique

Barbig, Philipp barbig.philipp@googlemail.com

Thin Film Technology, Karlsruhe Institute of Technology, Germany

Bintein, Pierre-Brice pierre-brice.bintein@u-paris.fr

Matière et Systèmes Complexes, CNRS & Université Paris Cité, France

Borho, Julian julian.borho@kit.edu

Thin Film Technology, Karlsruhe Institute of Technology, Germany

Boulogne, François fboulogne@sciunto.org

Université Paris Saclay, CNRS, France

Bouteille, Barbara babou.bouteille@gmail.com

Saint-Gobain Thin Films departement, Saint-Gobain Research Paris, France

Bouvier, Antoine antoine.bouvier@espci.fr

PMMH, CNRS - ESPCI Paris - Université PSL - Sorbonne Université - Université Paris Cité, France

Brogly, Amélie amelie.brogly@grenoble-inp.fr

LGP2, Université Grenoble Alpes, France

Brunet, Marine marine.brunet@saint-gobain.com

Saint-Gobain Research Paris, France

Brunet, Philippe philippe.brunet@univ-paris-diderot.fr

Matière et Systèmes Complexes, CNRS, France

Burger, David david.burger@kit.edu

Thin Film Technology, Karlsruhe Institute of Technology, Germany

Chateauminis, Antoine antoine.chateauminis@espci.fr

SIMM UMR 7615, Ecole Supérieure de Physique et Chimie Industrielles (ESPCI) - CNRS, France

Ciccotti, Matteo matteo.ciccotti@espci.fr

SIMM, ESPCI Paris PSL, France

Daerr, Adrian adrian.daerr@univ-paris-diderot.fr

Matière et Systèmes Complexes, Université Paris Cité, France

Darhuber, Anton a.a.darhuber@tue.nl

Department of Applied Physics, Eindhoven University of Technology, Netherlands

David, Barreiro david.barreiro1@udc.es

von Karman Institute, Belgique

Dervaux, Julien julien.dervaux@univ-paris-diderot.fr
Matière et Systèmes Complexes, CNRS, France

Di Mauro, Gabrielle gabrielle.dimauro@saint-gobain.com
CNRS & Saint Gobain, France

Dietze, Georg F. georg.dietze@universite-paris-saclay.fr
FAST, CNRS, France

Djambov, Simeon simeon.djambov@epfl.ch
Laboratory of Fluid Mechanics and Instabilities, Ecole Polytechnique Fédérale de Lausanne, Suisse

Doell, Harald harald.doell@tse-coating.ch
TSE Troller AG, Suisse

Etienne-Simonetti, Alice alice.etienne-simonetti@universite-paris-saclay.fr
Laboratoire de Physique des Solides (LPS), Université Paris-Saclay, France

Gallaire, Francois francois.gallaire@epfl.ch
Ecole Polytechnique Fédérale de Lausanne, Suisse

Gasser, Mary-Ann mary-ann.gasser@cea.fr
LETI, CEA, France

Goehring, Lucas lucas.goehring@ntu.ac.uk
School of Science and Technology, Nottingham Trent University, United Kingdom

Gosset, Anne anne.gosset@udc.es
University of A Coruña, Spain

Gugler, Gilbert gilbert.gugler@heFrance.ch
iPrint Institut, HES-SO University of Applied Science of Western Switzerland, Suisse

Hadj, Benkreira H.Benkreira@bradford.ac.uk
Dept of Chemical Engineering, University of Bradford, United Kingdom

Harris, Tequila tharris3@gatech.edu
Highly Advanced Roll-to-Roll iManufacturing System Lab, Georgia Institute of Technology, USA

Heckmann, Thilo thilo.heckmann@kit.edu
Thin Film Technology, Karlsruhe Institute of Technology, Germany

Hoeng, Fanny fanny.hoeng@symbio.one
Symbio, France

- Hoffmann, Alexander** alexander.hoffmann@kit.edu
Thin Film Technology, Karlsruhe Institute of Technology, Germany
- Ishimura, Misa** ishimura-misa-kx@ynu.ac.jp
Nishino laboratory, Yokohama National University, Dept. of Mechanical Engineering, Japan
- Jain, Adarsh** adarsh.jain@uni-due.de
*Instit. for Energy and Materials processes - Particle Science and Technology (EMPI-PST),
University of Duisburg-Essen, Germany*
- Janning, Linus** linus.janning@googlemail.com
Thin Film Technology, Karlsruhe Institute of Technology, Germany
- Jee, Sanghun** jeesh0123@grtrkr.korea.ac.kr
Korea University, Korea
- Jung, Hyun wook** hwjung@grtrkr.korea.ac.kr
Korea University, Korea
- Kessler, Philip** philip.kessler@hefr.ch
iPrint Institut, HES-SO University of Applied Science of Western Switzerland, Suisse
- Kim, Donguk** kdu0309@grtrkr.korea.ac.kr
Korea University, Korea
- Klemens, Julian** julian.klemens@kit.edu
Thin Film Technology, Karlsruhe Institute of Technology, Germany
- Kobayashi, Hirokazu** hirok-kobayashi@jfe-steel.co.jp
Steel Research Laboratory, JFE Steel Corporation, Japan
- Koczorowski, Mélanie** melanie.koczorowski@tarkett.com
Tarkett, Luxemburg
- Kumar, Satish** kumar030@umn.edu
Department of Chemical Engineering and Materials Science, University of Minnesota, USA
- Kusina, Christophe** christophe.kusina@loreal.com
Invention Domain Sciences and Process of Formulation, L'Oréal, France
- Laura, Milne** l.milne@strath.ac.uk
University of Strathclyde, United Kingdom
- Lebon, Luc** luc.lebon@univ-paris-diderot.fr
Matière et Systèmes Complexes, CNRS et Université Paris Cité, France
- Le Lay, Grégoire** gregoire.le-lay@u-paris.fr
Matière et Systèmes Complexes, Université Paris Cité, France

Le Verge, Danielle danielle.leverge@loreal.com

Advanced Research-Formulation Science & Process, L'Oréal, France

Lequeux, François francois.lequeux@espci.fr

SIMM, ESPCI, France

Limat, Laurent laurent.limat@univ-paris-diderot.fr

Matière et Systèmes Complexes, CNRS & Université Paris Cité, France

Loedige, Lukas lukas.loedige@kit.edu

Thin Film Technology, Karlsruhe Institute of Technology, Germany

Ly, Kevin kevin.ly@kit.edu

Thin Film Technology (TFT) & Material Research Center for Energy Systems (MZE), Karlsruhe Institute of Technology (KIT), Germany

Martin, Jérôme martin@fast.u-psud.fr

FAST, CNRS & Université Paris Saclay, France

Masato, Yamamura yamamura@che.kyutech.ac.jp

Kyushu Institute of Technology, Japan

Mauron, Muriel muriel.mauron@hefr.ch

iPrint institut, HEIA-FR HES-SO University of Applied Science of Western Switzerland, Suisse

Min, Kyengmin minsstar@snu.ac.kr

Microfluidics and Coating Process Laboratory, Seoul National University, Korea

Mohacsi, Jonas jonas.mohacsi@kit.edu

Thin Film Technology, Karlsruhe Institute of Technology, Germany

Moorhead, Annie moorh030@umn.edu

University of Minnesota, USA

Müller, Max max.mueller.mm1@roche.com

Roche Diagnostics GmbH, Germany

Pauchard, Ludovic ludovic.pauchard@universite-paris-saclay.fr

FAST, CNRS & Université Paris Saclay, France

Pelosse, Alice alice.pelosse@ens-lyon.fr

Matière et Systèmes Complexes, Université Paris Cité, France

Pingulkar, Hrishikesh hrishikesh.pingulkar-ext@solvay.com

Laboratoire du Futur (LOF), CNRS-Solvay-Université de Bordeaux, France

Pino, Fabio fabio.pino@vki.ac.be

The von Karman Institute for Fluid Dynamics & Université libre de Bruxelles, Belgique

Quarz, Philipp philipp.quarz@kit.edu

Thin Film Technology, Karlsruhe Institute of Technology, Germany

Rabehi, Fateh fateh.rabehi@etu.u-paris.fr

Matière et Systèmes Complexes, CNRS & Université Paris Cité, France

Rigutto, Damien damien.rigutto@vki.ac.be

EA Department, von Karman Institute for Fluid Dynamics, Sint-Genesius-Rode, Belgique

Routh, Alexander afr10@cam.ac.uk

University of Cambridge, United Kingdom

Ruyer-Quil, Christian ruyerquc@univ-smb.fr

Laboratoire procédés Energie Bâtiment, Université Savoie Mont Blanc (Chambéry), France

Salem-Tabet, Allan allan.salem-tabet@crpp.cnrs.fr

Centre de Recherche Paul Pascal (UMR 5031 Pessac) & Laboratoire de Génie Chimique (UMR 5503 Toulouse), CNRS, France

Salmon, Jean-Baptiste jean-baptiste.salmon-exterieur@solvay.com

LOF UMR5258, France

Schabel, Wilhelm Wilhelm.Schabel@kit.edu

Thin Film Technology, Germany

Scharfer, Philip philip.scharfer@kit.edu

Thin Film Technology, Karlsruhe Institute of Technology, Germany

Scheid, Benoit Benoit.Scheid@ulb.be

Transfers Interfaces and Processes, Université Libre de Bruxelles, Belgique

Schnoklake, Sven sschnoklake@olbrich.com

Polytype Converting AG, Suisse

Scholle, Markus markus.scholle@hs-heilbronn.de

Heilbronn University, Germany

Schweizer, Peter M. ps@schweizer-coating.ch

Suisse

Seon, Thomas thomas.seon@gmail.com

Institut d'Alembert, CNRS, France

Snoeijer, Jacco j.h.snoeijer@utwente.nl

Fac. of Science and Technology, University of Twente, Netherlands

Somoano Marfull, Javier javier.somoano@arcelormittal.com
ArcelorMittal Global R&D, ArcelorMittal, Spain

Song, Jisoo jeesoo9595@snu.ac.kr
Microfluidics and Coating Process Laboratory, Seoul National University, Korea

Sonneville-Aubrun, Odile odile.aubrun@loreal.com
Physical-Chemistry Group / Process & Formulation Science Invention Domain, L'OREAL, France

Talini, Laurence laurence.talini@cnrs.fr
Surface du Verre et Interfaces, CNRS, France

Toivakka, Martti Martti.Toivakka@abo.fi
Laboratory of Natural Materials Technology, Åbo Akademi University, FI

Varlet, Anthony anthony.vrlt91230@gmail.com
Matière et Systèmes Complexes, Université Paris Cité, France

Verneuil, Emilie emilie.verneuil@espci.fr
SIMM, ESPCI Paris, France

Victor, Gracia victor.alfonso.gracia.medrano.bravo@audi.de
Audi, Germany

Wang, Shuo s.wang2@tue.nl
F&F group, Tu/e, Netherlands

Waquier, Louis louis.waquier@u-paris.fr
Matériaux et Phénomènes Quantiques, Université Paris Cité, CNRS, France

Wilson, Stephen K. s.k.wilson@strath.ac.uk
University of Strathclyde, United Kingdom

Yoon, Jihwan jw1080@snu.ac.kr
School of Chemical and Biological Engineering, Seoul National University, Korea

Yun, Jinseong jsyun@grtrkr.korea.ac.kr
Department of Chemical and Biological Engineering, Korea University, Korea

Zimmerer, Nadine nadine.zimmerer@kit.edu
Thin Film Technology, Karlsruhe Institute of Technology, Germany

Drying colloidal films, from a liquid dispersion to a rigid coating

Lucas Goehring
Nottingham Trent University, UK

Colloidal dispersions are the basis of diverse types of coatings including paints, varnishes, foodstuffs, cosmetics and medical materials. These are prepared as complex mixtures of different phases of matter, such as nanoscopic particles, polymers and emulsions, dispersed in a liquid, applied to a surface and then dried. Such processes involves complex changes in appearance and properties, as the material changes from a liquid into a solid. Often, drying materials also pass rapidly through intermediate states, like gels or glasses. These states affect the structure of the final product but are challenging to control or measure. This is important not only in academic settings but also crucial to a wide variety of industries, as coating and drying processes are widely used in many production routes. Over the past twenty years there has been considerable research progress made in the understanding of these drying processes, for example including the search to replace more harmful solvents with water, or to prepare dispersions with bespoke, designer properties.

In this workshop I will walk through the key stages of how a dispersion dries. I will begin by covering the underlying theory of colloidal dispersions and colloidal interactions that control the properties of the liquid product. Then I will identify the key stages of drying, and the process of importance to understand how a drying film solidifies. I will then turn to look at the properties of the solid product itself, and how drying can lead to mechanical instabilities like fracture, shear banding and peeling, and how such undesirable effects can be minimised. Finally, I will summarise some more recent specialist topics, including drying blood droplets, and dispersions that stratify by particle size as they dry.



European Coating Symposium 2023

12-15 Sep 2023 Paris (France)

PRE-CONFERENCE TRAINING

Professor Hadj Benkreira (CEng, FIChemE, FHEA)

Dept of Chemical Engineering, University of Bradford, United Kingdom

Coating Flows: Principles & Operation

Abstract

Coating operations are many and varied and in many ways challenging to understand. This is because the coating fluids used are inherently non-Newtonian and the flows are free surfaces flows that exhibit instabilities. Inherently non-Newtonian they are because a coating formulation is a mix of particles that will eventually form the coating after the solution is coated, a liquid carrier (the solvent- that could be water) and binders. As for instabilities, it is easy to imagine that if the operation is carried out at high speeds, surface defects will appear and or air will be entrained in the coated film. Both instabilities ruin the uniformity required for the final product to perform as designed.

The purpose of this course is to help anyone who is entering the field of coating (whether it is for research studies or for engineering practice) to develop a good insight to help build a good understanding of their operations. In the course the following aspects will be covered:

- Introduction and definition of a coating flow in terms of its essential features.
- Classification of coating flows: free coating (dip coating), metered coating (blade and roll coating), exact coating (slide, slot and curtain coating) and gravure coating.
- Fluid mechanics of the above coating flows to enable the calculation of the final coated film thickness as a function of operating conditions and the determination of the critical conditions that trigger instabilities (surface defect and air entrainment)
- Consideration of Non-Newtonian effects on the above.

Wetting of solids by liquids: how is the dynamics modified by a complex substrate or a complex liquid?

Laurence Talini
SVI, Saint Gobain, France

When a droplet of pure liquid spreads on a rigid, non-soluble, substrate, the dynamics of its contact line is determined by a balance between the energy associated with the driving capillary force and the energy dissipated by the viscous shear in the liquid. This balance is expressed by the Cox-Voinov law, which relates the spreading speed to the contact angle. In recent years, complex situations have been examined in which dissipation may be strongly modified, leading to sometimes spectacular effects on wetting dynamics. We will review the case of soft substrates, including those dissolved by the spreading fluid. We will also consider multi-component fluids, such as solutions or suspensions. In all cases, we will discuss the nature of the dissipative mechanisms at stake, and their consequences on spreading kinetics.

Adhesion and adhesives fundamentals

Matteo Ciccotti
ESPCI Paris PSL, France

This lecture presents an introduction to the science of adhesion and the mechanics of adhesive coatings. After a brief historical introduction, the multidisciplinary and multiscale nature of adhesion science is presented starting from the molecular scale and then growing towards the macroscopic scale of mechanics. The consequences of the peculiar soft viscoelastic rheology of adhesives will be discussed on the three fundamental phases of the life of an adhesive joint, which are respectively the contact formation, the holding phase and the final debonding. Fracture mechanics concepts will finally be presented to deal with several kinds of debonding tests such as peel, tack, and shear.

'Wet Coating Processes at Saint-Gobain: Products and Industrial Realities'

Rémi Deleurence & Jérémie Teisseire
Saint-Gobain Research Paris, Aubervilliers, France

Saint-Gobain designs, manufactures and distributes materials for the markets of construction, transport and industry. The surface of these materials is often treated with thin liquid coatings (paint, silver, etc.) in order to obtain specific aesthetic and functional properties. There exists a lot of possible techniques to coat substrates with a treatment layer (or coating) with well-controlled properties. However, products for construction market typically represent very large volumes and surfaces which make the use of common processes very challenging in terms of homogeneity along all dimensions, thickness ranges, and productivity.

For instance, widespread processes such as curtain or roller coating can be quite complex when dealing with glass plates of several meters width, uneven thickness, conveyed at high speed, and on a discontinuous “batch” mode. Another example is the treatment of building-scale fibrous products, where coating must reach the proper repartition in the tridimensional network to ensure final product properties while keeping reasonable costs.

In this presentation, we will present a few of these challenges and discuss how research performed in Saint-Gobain R&D centers can help to provide guidelines on formulations or process levers, or to select the proper technique and equipment.

How to clean a contaminated surface with a water drop

Abhinav Naga, Florian Geyer, Hans-Jürgen Butt, Rüdiger Berger, Doris Vollmer

Max Planck Institute for Polymer Research, Ackermannweg 10, 55128 Mainz, Germany

vollmerd@mpip-mainz.mpg.de

The contamination of surfaces by dirt particles is problematic in many applications. For example, the accumulation of dirt on solar panels leads to a reduction in efficiency. To improve our understanding of how to clean contaminated superhydrophobic or hydrophobic surfaces, we developed a method of slowly moving a drop over a contaminated surface while imaging the region close to three-phase contact line by laser scanning confocal microscopy simultaneously. This enabled us to monitor in slow motion how a drop takes up dirt while rolling over the surface.¹ The friction force can be quantified from the deflection of the blade that holds the drop in position while the contaminated substrate is pulled at well-defined velocity. On a superhydrophobic surface, particulate contaminants are picked up at the receding side of the drop (Fig. 1a,b).¹ On a hydrophobic surface, the particle remains attached to the drop at low speeds (Figure 1c) whereas the particle enters and exits the drop at high speeds (Fig. 1c,d).² We showed that particle removal is possible when the maximum capillary force that the drop can exert on the particle is greater than the resistive force experienced by the particle. Both the capillary and resistive forces depend on the geometry of the particle, its surface properties, and how it moves over the surface.

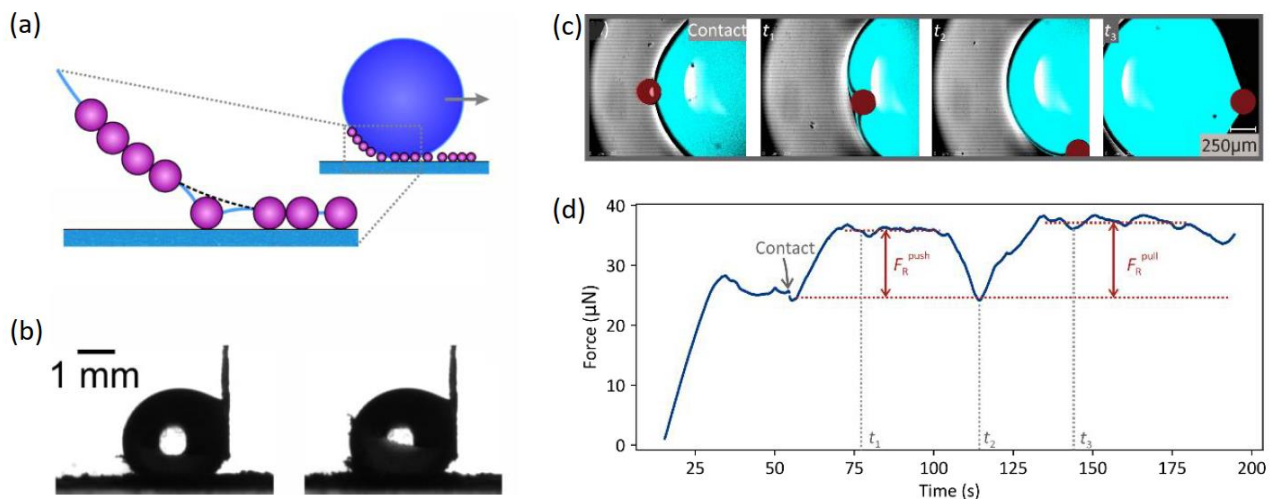


Fig. 1: a) Sketch of a drop rolling over a contaminated superhydrophobic surface. b) Snapshots of the drop partially covered with particles. From the deflection of the blade the friction force can be quantified. c) Confocal image of the collision between a particle (dark red) and a water drop (cyan) at 50 $\mu\text{m/s}$ on a hydrophobic surface. (d) Force experienced by the drop during the collision.

References

1. F. Geyer, M. D'Acunzi, A. Sharifi-Aghili, A. Saal, N. Gao, A. Kaltbeitzel, T.F. Sloot, R. Berger, H.J. Butt, D. Vollmer, When and how self-cleaning of superhydrophobic surfaces works, *Science Advances*, **6**: eaaw9727 (11p) (2020)
2. A. Naga, A. Kaltbeitzel, W. S. Y. Wong, L. Hauer, H.-J. Butt, and D. Vollmer, How a Water Drop Removes a Particle from a Hydrophobic Surface, *Soft Matter*, **17**, 1746 (2021). Selected as "Soft matter hot article 2021".

Developing Anode Architectures to Enhance Hydrogen Production in Alkaline Water Electrolysis

Adarsh Jain^{1,2}, Vineetha Vinayakumar¹, Christian Marcks³, Andre Olean Oliveira⁴, Corina Andronesu^{4,5}, Anna K. Mechler³, Doris Segets^{1,2,5*}

¹ Institute for Energy and Materials Processes–Particle Science and Technology (EMPI–PST), University of Duisburg–Essen, Duisburg, Germany

² Max Planck Institute for Chemical Energy Conversion (IMPRS-RECHARGE), Muelheim an der Ruhr, Germany

³ Electrochemical Reaction Engineering, RWTH Aachen University, Aachen, Germany

⁴ Chemical Technology III, University of Duisburg–Essen, Duisburg, Germany

⁵ Center for Nanointegration Duisburg-Essen (CENIDE), University of Duisburg-Essen (UDE), Duisburg, Germany

Corresponding author: doris.segets@uni-due.de

Alkaline water electrolysis has shown potential as a promising technique for producing green hydrogen and improving the power sector. However, despite its well-established status, there remains for significantly enhancing the affordability, functionality, and durability of the components used in the electrolyser [1,2]. To achieve these objectives, it is crucial to unravel morphology-activity relationships of spray-coated anode catalyst layers to establish feedback loops and enable optimization of ink formulation and the coating process.

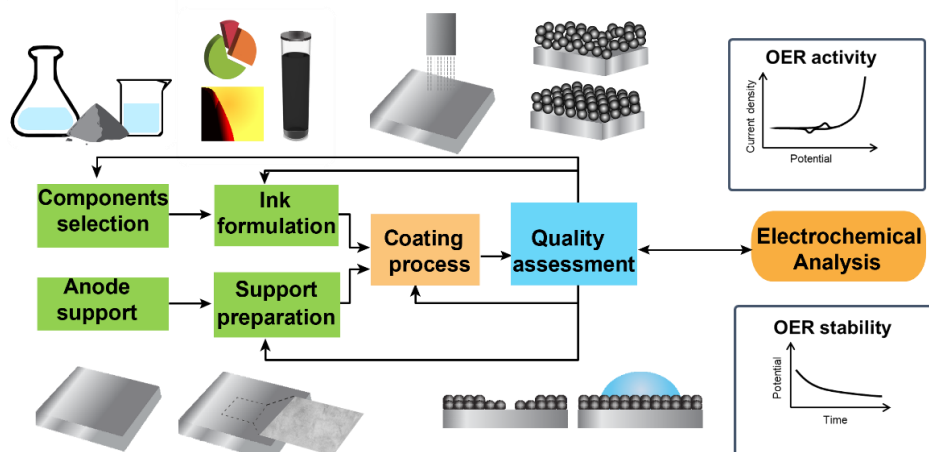


Fig. 1. Developed strategy for electrode fabrication and feedback loops for controlling the process parameters with correlation into electrochemical analysis.

This work aims to address the relevant sub-sections of electrode fabrication, i.e., powder characterization, ink formulation, coating and drying as shown in Figure 1. In the initial stage of the work, we found that quantitative analysis of the nanoscale structure of the electrodes produced by ultrasonic spray coating is an excellent indicator, in terms of a descriptor, for judging the quality of particle-based catalyst coatings. Atomic force microscopy (AFM) is a powerful tool for analyzing the nanoscale microstructure of electrodes. However, its application in large-scale fabrication is limited by its inability to measure large electrodes and qualitative morphological analysis hinders the correlation of local surface features with the electrochemical activity. To overcome these limitations, we developed a multi-stage data quantification technique to comprehensively assess the representative structural features of the catalyst layer. These machine-readable features are then correlated with the electrochemical activity of the catalyst layer and fed back into the process development chain for further improvement or can be used for the development of proxies ready for inline measurement. The framework provides a statistically supported representation of the entire surface from a controllable number of spot measurements of AFM images on catalyst layers with centimetre sized area. We demonstrate the effectiveness of our method by characterizing anodes fabricated using different spray coating processing conditions. Furthermore, the utilized approach can be easily transferred to similar systems for faster and more effective evaluation of electrodes. It has the potential to enable complex navigation through a large parameter space of numerous factors throughout electrode formation, such as ink formulations and coating processes.

References

1. Michalski, J., et al. International Journal of Hydrogen Energy **42**, 13427 – 13443 (2017)
2. Siegmund, D., et al. JACS Au **5**, 527-535 (2021)
3. Bapat, S. and D. Segets, ACS Applied Nano Materials, **3(8)**, 7384-7391(2020)
4. Anwar, O., et al., Nanoscale **14(37)**, 13593-13607 (2022)

Development of tuned SOEC electrode by spray coating

Marijke Jacobs¹, Fatima-Ezzahra El Bassiri², Aurélie Rolle², Rose-Noëlle Vannier² and Vesna Middelkoop¹

¹ Flemish Institute for Technological Research – VITO, Boeretang 200, B-2400 Mol, Belgium

² Univ. Lille, CNRS, Centrale Lille, Univ. Artois, UMR 8181 - UCCS - Unité de Catalyse et Chimie du Solide, F-59000 Lille, France

Corresponding author: Marijke.jacobs@vito.be

Solid Oxide Electrolysis Cell (SOEC) is a key technology for the ongoing energy transition towards a low carbon future. It is the most viable route for the efficient utilization of renewable electricity to produce green hydrogen and fuels [1]. Although SOEC do not make use of expensive Pt, it still consists of rare earth elements (REE). To overcome the environmental and criticality challenges of REE, alternative materials are needed or REE should be recycled. Therefore, the European NOUVEAU project aims to make Solid Oxide Electrolysis Cell (SOEC) technology more sustainable and reusable by developing novel electrode coatings and interconnect. Besides the material choice, the microstructure of the electrode coatings is important as well to obtain an optimal use of critical materials and to achieve an efficient working SOEC for green hydrogen production. The electrode microstructure will be tuned in (La-free) composition along the thickness of the electrode to have an improved thermal expansion match between the different layers. Such a structure can be achieved by spray coating as it allows to vary the composition along the thickness of the electrode and to create uniform electrode coatings [2].

In this work, a symmetric cell is fabricated by applying the electrode layers on yttria-stabilized zirconia (YSZ) planar substrates, which serve as the electrolyte layer. As electrode material, a La-free oxide is selected by Centrale Lille to have a reduced amount of REE and produced by Marion Technologies. This material is mixed with Gd doped Ce oxide to obtain a tuned composition. This mixture was continuously varied so that the layer consists of 100 % of Gd doped Ce oxide near the interlayer and 25/75 % Gd doped Ce oxide/La-free oxide at the surface (see Fig. 1). The coating parameters such as atomization pressure, coating speed and suspension flow were optimized to obtain uniform coatings and to control the microstructure and thickness. The suspension formulation was adjusted to improve the adhesion and the quality of the coating. Profilometry and microscopy were used to determine the coating thickness and porosity of the structure. Furthermore, electrochemical impedance spectroscopy were carried out.

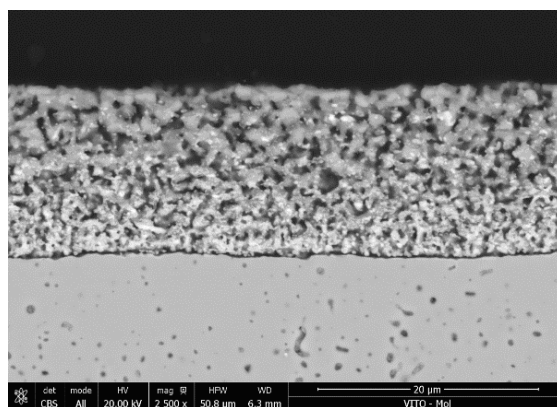


Fig. 1. An illustration of tuned porosity of electrodes obtained by spray coating.

References

1. A. Nechache and S. Hody, *Renewable and Sustainable Energy Reviews* **149**, 111322 (2021).
2. M. Jacobs, L. O. Jøssang, V. Rangasamy and V. Middelkoop, *Journal of Coatings Technology and Research* **20**, 41–50 (2023).

Acknowledgement

This project has received funding from the European Union's Horizon Europe research and innovation programme under grant agreement N°101058784. The present publication reflects only the author's views. The Commission is not responsible for any use that may be made of the information contained therein.

Sorption and Diffusion Processes in Cathode Active Materials for Lithium-ion Batteries during the production of electrodes

Thilo Heckmann, Philip Scharfer, Wilhelm Schabel

Thin Film Technology (TFT), Material Research Center for Energy Systems (MZE), Karlsruhe Institute of Technology (KIT), Karlsruhe

Corresponding author: thilo.heckmann@kit.edu

Moisture content in Li-ion batteries affects device performance. Therefore, the energy-intensive moisture management and post-drying is necessary to adjust the optimal moisture levels in the electrodes during their production. These processes pose an optimization challenge as they require a large share of the total energy demand of the electrode production and are crucial for performance of the final product. This challenge consists of reducing the energy demand of the moisture management and post-drying while maintaining a high level of device performance.[1]

Tackling this challenge demands a precise understanding of the sorption and heat and mass transfer processes during the production of the battery electrodes. These physical processes vary depending on the materials of the electrodes, e.g., cathode and anode material. Especially cathode active materials such as lithium nickel manganese cobalt oxides (NMC) can be susceptible to degradation in form of chemical sorption due to moisture and other species in the production atmosphere. This chemical sorption can be irreversible in the temperature range that is usable during post-drying (the process step that removes residual moisture). Therefore, the degradation of the cathode active material needs to be avoided to maintain a high level of device performance.[2]

The focus of this study lies on the interaction of the cathode active material NMC 622, in form of thin films and raw material, with species of the production atmosphere such as moisture and CO₂. This interaction is investigated by a magnetic suspension balance with a conditioned and continuously perfused measurement cell.[3] Gases such as nitrogen, air, and CO₂ can be saturated and mixed with dry gases to adjust the desired relative humidity of the perfusing gas flow through the measurement cell. The measured mass uptake over time changes as a function of the composition of the gas flow as well as temperature and allows conclusions about sorption and mass transport mechanisms. The species that form during this sorption are characterized and evaluated regarding its reversibility to counteract this degradation. The results show that hydroxides, hydrates, and carbonates form on the surface of the cathode active material.

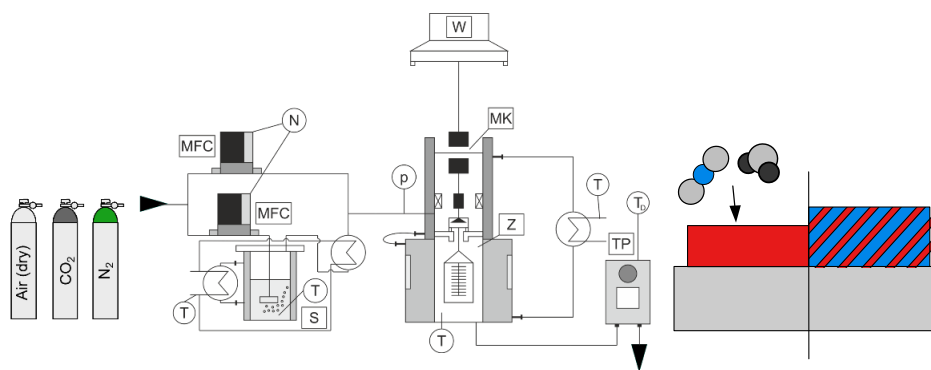


Fig. 1. Experimental setup for sorption experiments in perfusion mode (left) and schematic of the chemical sorption of CO₂ and water in the cathode active material (right).

This work contributes to the research performed at CELEST (Center for Electrochemical Energy Storage Ulm Karlsruhe) and the Material Research Center for Energy Systems (MZE). The authors would like to acknowledge financial support of the Federal ministry of Education and Research (BMBF) via the ProZell cluster project “Epic” (Grant No. 03XP0295A).

References

1. A. Kwade, et al., K. Droeder, Current status and challenges for automotive [...], *Nature Energy* **3**, 290-300 (2018).
2. R. Jung, et al., H. Gasteiger, Effect of Ambient Storage on the [...], *J. Electrochem. Soc.*, **165**, A132-A141 (2018).
3. J. Eser, et al., P. Scharfer and W. Schabel, Moisture Adsorption Behaviour [...], *Energy Technology* **8**, 1801162 (2020).

Experimental analysis of dynamic menisci in dip coating

Damien Rigutto¹, Jean-Marie Buchlin¹, Miguel Alfonso Mendez¹

¹ EA Department, von Karman Institute for Fluid Dynamics, Sint-Genesius-Rode, Belgium
Corresponding author: damien.rigutto@vki.ac.be

Dynamic wetting is fundamental in many coating processes. In static conditions, a meniscus is produced when a liquid is in contact with a solid wall. The intersection between the gas-liquid interface and the solid surface occurs at a specific angle known as a static contact angle. When the solid and the interface are in relative motion, the angle is known as dynamic. Most of the theoretical and experimental efforts in its characterization have been focused on highly viscous fluids, for which inertia has a negligible effect. A fundamental contribution is the empirical correlation proposed by Hoffman (1975) [1], which links the dynamic contact angle to the Capillary number. This correlation was derived at the limit of $Ca \ll 1$, but many industrial configurations are characterized by large Ca . The dynamics of the contact angle influence the shape of the meniscus and its ability to remain attached to the solid even in the presence of surface defects. Moreover, the meniscus dynamic is also influenced by the velocity field underneath it. The flow field in the proximity of the contact line is characterized by large gradients required to allow for the velocity to be zero at the wall despite a relative motion between the contact line and the surface (see the triple point paradox (Huh and Scriven, 1970)) [2].

This work investigates the meniscus dynamics on a moving surface and the flow fields underneath it. The configuration of interest is sketched in Figure 1a: the dynamic meniscus is formed as a gas-liquid interface in contact with a tilted flat plate entering a bath with an angle θ_e and velocity U_p . This configuration is relevant to hot dip galvanization and was reproduced in a facility developed at the von Karman Institute (VKI). The facility consists of a large rotating cylinder partially immersed in a water bath. The cylinder is made of stainless steel and has a diameter of 60 cm and 20 cm in width. It can reach tangential velocities up to 2 m/s. The large velocities and the possibility of altering the water properties by changing the bath temperature allow for covering a wide range of Weber and Capillary numbers.

The facility is instrumented with (1) a device for Laser-Induced Fluorescence (LIF) visualization and detection of the meniscus interface and (2) image velocimetry. A snapshot of the interface detection process is shown in Figure 1b, where Rhodamine is used to amplify the contrast between air and water. Concerning the image velocimetry, PTV is applied to the acquired images, resulting in the velocity field shown in Figure 1c. The flow field reveals various relevant flow features, including the growth of the boundary layer on the cylinder wall and the large curvature of the streamlines near the immersion point.

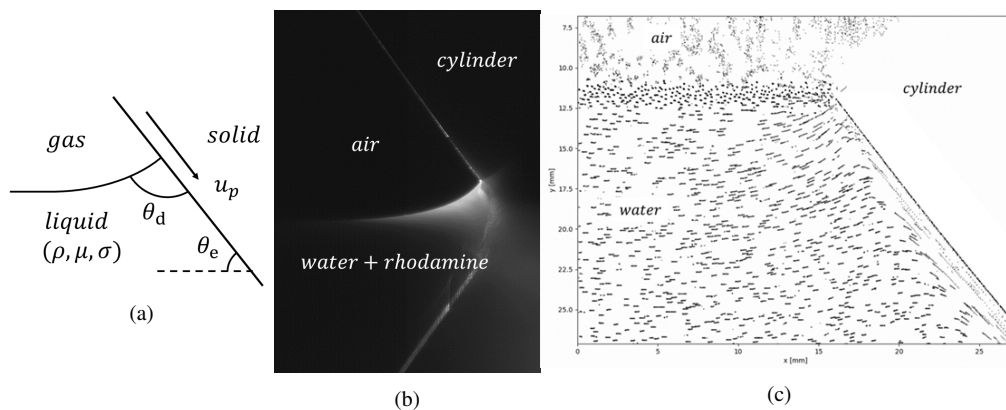


Figure 1: (a) Dynamic entering contact angle, schematic of the investigated configuration and main parameters. (b) Snapshot of the interface detection with LIF. (c) Example of flow field determined with PTV

References

- [1] HOFFMAN L. RICHARD, [Optional: A Study of the Advancing Interface I. Interface Shape in Liquid-Gas Systems.] *Journal of Colloid and Interface Science*, **50**, 228 (1975).
- [2] HUH CHUN AND SCRIVEN L. E., [Optional: Hydrodynamic Model of Steady Movement of a Solid / Liquid / Fluid Contact Line.] *Journal of Colloid and Interface Science*, **35**, 85 (1970).

Contact line dynamics under oscillating forcing

Pierre-Brice Bintein¹, Arnaud Grados¹, François Gallaire², Laurent Limat¹, Philippe Brunet¹

¹Laboratoire Matière et Systèmes Complexes, Université Paris Cité, CNRS, Paris, France

²LFMI-STI-IGM, EPFL, Lausanne, Switzerland

Corresponding author: pierre-brice.bintein@u-paris.fr

A liquid forced to spread or recede on a solid surface can be frequently observed in every-day life (like raindrops blown away on the windshield of a car) as well as in industrial processes (as for coatings of solids by liquid deposition). Liquid motion is then governed by the wetting dynamics of the contact line (where the three phases intersect) which is determined by the hydrodynamics near the liquid-wall interface (viscous shear stress) and by the physicochemical interactions with the substrate. These molecular interactions translate macroscopically into the contact angle between liquid and solid, and the relation between the dynamic contact angle and the contact line velocity is a way to understand and characterize the wetting dynamics that has been intensively studied in the recent years, at the crossroads of fluid mechanics, chemistry and engineering [1]. Specific studies have been devoted to the influence of inertia on such interface dynamics [2,3] which can occur in unsteady conditions.

Here we study the response of a drop contact-line under an oscillating, low-frequency horizontal forcing. The drop sits on a surface with non-wetting conditions and a low hysteresis while its upper part is pinned on an adhesive cover, see figure 1(a), so that the response of the contact-line involves a significant inertial component. Indeed, under such a periodic forcing, the mobility law relating velocity and contact-angle is not ruled anymore by a classical visco-capillary equilibrium (Cox-Voinov law) [2-4]. In order to propose constitutive laws taking inertia into account, we measure the dynamic contact angle as a function of the triple line velocity (figure 1(b)) and relate the emerging hysteretic cycles to the oscillations (amplitude and frequency), liquid and substrate properties.

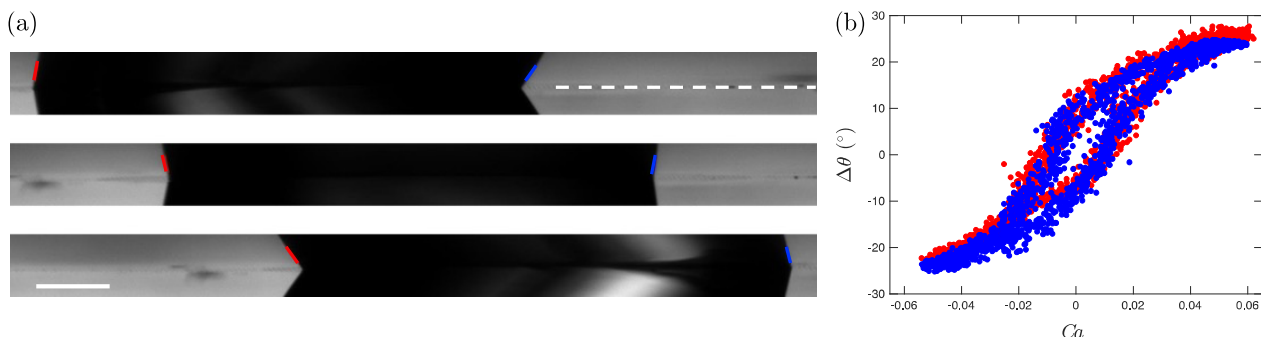


Fig. 1. (a) Pictures of moving contacts line of a water droplet on an oscillating surface with low hysteresis. Liquid appears in dark while solid surface is indicated by white dashed line; contact angles (marked in colors) are measured in the reflected part of the drop. Time interval between pictures is 0.1 s, scale bar is 1 mm. (b) Corresponding plot of the contact angle minus its equilibrium value (around 100°) as a function of the capillary number $Ca = \eta V/\gamma$, where η and γ are the viscosity and surface tension of water, while V is the algebraic velocity of the contact line in the frame of reference of the oscillating plate. Colors hold for both sides of the drops as in (a); eight successive cycles are overlapped for each side.

References

1. J.H. Snoeijer and B. Andreotti, Moving Contact Lines: Scales, Regimes, and Dynamical Transitions, *Annu. Rev. Fluid. Mech.* **45**, 269-292 (2013).
2. R.G. Cox, Inertial and viscous effects on dynamic contact angles, *J. Fluid. Mech.* **357**, 249-278 (1998).
3. D. Fiorini, M. A. Mendez, A. Simonini, J. Steelant, and D. Seveno, Effect of inertia on the dynamic contact angle in oscillating menisci, *Phys. Fluids* **34**, 102116 (2022).
4. C.-L. Ting and M. Perlin, Boundary conditions in the vicinity of the contact line at a vertically oscillating upright plate: an experimental investigation, *J. Fluid. Mech.* **295**, 263-300 (1995).

The coffee stain on a fiber

Marie Corpart¹, Frédéric Restagno¹ François Boulogne¹,

¹ Université Paris-Saclay, CNRS, Laboratoire de Physique des Solides, 91405, Orsay, France.

Corresponding author: francois.boulogne@cnrs.fr

Presented by F. Boulogne.

The drying of a drop of a colloidal suspension is known to generate a transport of the particles towards the contact line, which is called the "coffee stain" effect [1]. This transport is caused by the volume change, which triggers an internal flow to stay within the minimum of the surface tension energy, *i.e.* a spherical cap for a sessile spherical cap for a sessile drop [2, 3].

In this presentation, we will analyze the origin of the difference between the coating from a sessile drop and an axisymmetric in an axisymmetric drop deposited on a fiber as illustrated in figure 1 [4]. First, we model the shape of a drop on a fiber and its evaporation flow with some approximations with some approximations to derive analytical calculations. Then, in the case of pinned contact lines, we solve the hydrodynamic equations in the liquid phase under the lubrication approximation to determine the flow velocity to the contact lines. We comment on these results by comparing them to those of a sessile drop under similar evaporation conditions, and we show that the show that the curvature of the substrate plays a role on the thinning of the the contact line, the local evaporation flux and the liquid flow field. The competition between advection and Brownian motion indicates that the transport of the particles to the contact line contact line occurs in a localized volume near the contact lines for a drop on a contact lines for a drop on a fiber. Thus, the geometry of the fiber induces a lower accumulation of particles at the contact line compared to a sessile drop, which changes the common sense that the community has developed over the last 20 years, and that can be used in industrial applications where fibers are involved such as construction materials, filters, textiles.

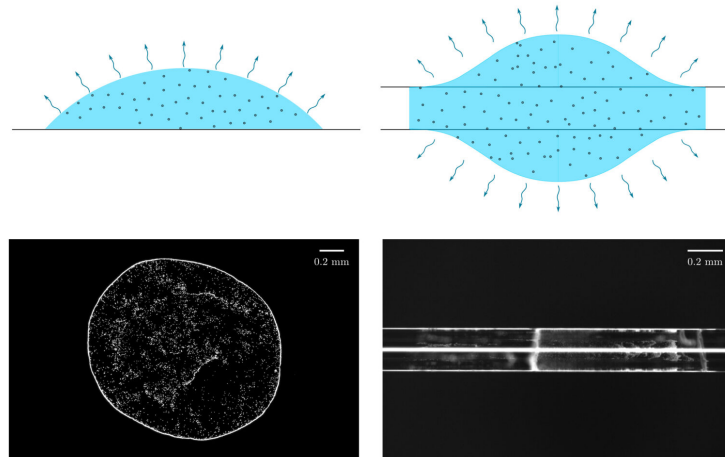


Figure 1: Comparison of deposits on a flat surface (left) and on a fiber (right). The geometries are schematized at the top and the deposits are photographed by fluorescence microscopy in top view. Note the circular deposition of the drop edge on the flat surface while the deposition on a fiber shows a weak deposit at the initial positions of both drop edges. The particles are one micrometer in diameter.

References

- [1] Deegan, R., Bakajin, O., Dupont, T., Huber, G., Nagel, S. & Witten, T. Capillary flow as the cause of ring stains from dried liquid drops. *Nature*. **389**, 827-829 (1997)
- [2] Popov, Y. Evaporative deposition patterns: Spatial dimensions of the deposit. *Phys. Rev. E*. **71**, 036313 (2005)
- [3] Berteloot, G., Hoang, A., Daerr, A., Kavehpour, H., Lequeux, F. & Limat, L. Evaporation of a sessile droplet: Inside the coffee stain. *Journal Of Colloid And Interface Science*. **370** pp. 155-161 (2012)
- [4] Corpart, M., Restagno, F. & Boulogne, F. Coffee stain effect on a fibre from axisymmetric droplets. *Journal Of Fluid Mechanics*. **957** pp. A24 (2023)

About the production of catalyst layers for PEM-fuel cells and PEM-electrolysis

Philipp Quarz^{1,2}, Nadine Zimmerer^{1,2}, Philip Scharfer^{1,2}, Wilhelm Schabel^{1,2}

¹ Thin Film Technology (TFT), Karlsruhe Institute of Technology (KIT), Karlsruhe, Germany

² Material Research Center for Energy Systems (MZE), Karlsruhe Institute of Technology (KIT), Karlsruhe, Germany

Corresponding author: philipp.quarz@kit.edu, nadine.zimmerer@kit.edu,

Hydrogen technology is one of the key elements of the energy revolution [1]. Via electrolyzers (excess) capacities from renewable energies can be stored chemically in a fuel, e.g. green hydrogen, and can be used on demand by using a fuel cell. Polymer electrolyte membrane water electrolyzers (PEM-WE) and polymer electrolyte membrane fuel cell (PEM-FC) are a promising approach because of their good partial load capacity and their simple stack design. [2]

The energy-converting reactions take place at the heart of the PEM-FC or PEM-WE, the catalyst coated membrane (CCM), consisting of a perfluorosulfonic acid (PFSA) membrane, e.g. NafionTM, and a catalyst layer coated on both sides. The catalyst layers must meet several specifications, such as a high reactive surface area, suitable porosity and a high number of multiphase boundaries [2]. The material and production of the respective CCMs of both systems, PEM-FC and PEM-WE, contribute decisively to the still high costs of the systems [3]. Therefore, there are two investigated approaches to optimize the production and the catalyst layer itself.

The first addresses the reduction of processing steps by coating the catalyst layers directly onto the PFSA membrane. In the production of CCM, direct membrane coating requires one fewer process step than the (industrially) established decal process and is therefore advantageous. However, the membrane direct coating poses a number of challenges including the solvent interactions and in particular swelling of the respective membranes used in contact with solvents from the catalyst inks [4]. These interactions cause the catalyst layer to form cracks. Understanding the mass transport happening during the CCM manufacturing via membrane direct coating helps adapting and optimising the existing manufacturing process to the new materials and process parameters needed. Adjustments in ink formulation and drying conditions are here focus of the investigation.

The second possibility for cost reduction aims at tailoring the microstructure of the catalyst layers. Many electrochemically active surfaces and so-called triple phase boundaries are necessary for the systems to function [2]. The number of these depends strongly on the microstructure of the catalyst layer. The microstructure is formed during the film solidification (drying step) [5-7]. For this reason, the investigation of the drying of the multicomponent ink is the focus of this approach including effects such as selectivity of the drying. During the drying of the catalyst inks (also on inert substrates), defects and cracks are formed in the film structure [8]. By linking drying parameters with electrode properties, the manufacturing process is to be further improved. The microstructure can also be further optimised by, for example, a multilayer-structured electrode design with multilayers of single layers with specifically tailored properties. Thus, gradients of porosity, catalyst loading and ionomer content can be achieved within the electrode.

In the approaches, both the material-specific and the process-related challenges are to be highlighted. The aim is to point out possible solutions for an optimisation of the cost-intensive fuel cell and electrolyser catalyst layers. With the investigation of the fundamental mechanism during the individual steps of the production chain, a deep understanding of the complete interdependent influenced processes is generated. Due to the different duties, the specific requirements between PEM-WE and PEM-FC are somewhat different. However, many of them are also similar and can be influenced to the same extent by the process, so that essential findings from PEM-FC can be transferred to PEM-WE and vice versa.

References

1. EU-Commission, Communication COM/2020/299 (2020).
2. U. Schelling, R. Zahoransky (Ed.), *Energietechnik 8. Auflage* (Springer Fachmedien, Wiesbaden, 2019).
3. U.S. DRIVE, Fuel Cell Technical Team Roadmap (2017).
4. M. B. Dixit, B. A. Harkey, F. Shen, K. B. Hatzell, J. Electrochem. Soc., 165, 264-271 (2018).
5. J. Kumberg, W. Bauer, J. Schmatz, R. Diehm, M. Tönsmann, M. Müller, K. Ly, P. Scharfer, W. Schabel, *Energy Technology*, Vol 9: 2100367 (2021).
6. S. Jaiser, M. Müller, M. Baunach, W. Bauer, P. Scharfer, W. Schabel, *Journal of Power Sources*, Vol. 318, 210-219 (2016).
7. J. Kumberg, M. Müller, R. Diehm, S. Spiegel, C. Wachsmann, W. Bauer, P. Scharfer, W. Schabel, *Energy Technology*, Vol 7: 1900722 (2019).
8. F. Scheepers, A. Stähler, M. Stähler, M. Carmo, W. Lehnert, D. Stolten, *J Coat Technol Res* (2019).

Particle migration in evaporating alcohol-water bimodal slurry films

Masato Yamamura

Department of Applied Chemistry, Kyushu Institute of Technology, Fukuoka 804-8550 Japan

Corresponding author: yamamura@che.kyutech.ac.jp

Abstract

We conducted the real-time photoluminescence spectroscopy to examine evolutions of small-on-top particle distributions. The slurry consisted of TiO₂ particles of 2 μm in average diameter and fluorescent polystyrene nanoparticles of 100 nm in diameter. The particles were dispersed in ethanol/water mixtures containing poly(-acrylic) acid as a binder. When the wet slurry coating was exposed to a laser beam of 532 nm in wavelength, the small particles emitted luminescence light with different intensities depending on the distribution in the thickness direction. The results revealed that the emission intensity increased in the ethanol-free slurry, whereas it initially decreased and then increased in the ethanol-rich liquid, indicating a suppressed migration of smaller particles via the ethanol addition. The final emission intensities of dried particulate films remained a low level at concentrations above the predicted pseudo-azeotrope composition.

1. Introduction

A thin liquid film coating containing a binary mixture of volatile solvents exhibits selective or non-selective evaporation, depending upon not only the thermodynamic equilibrium but also mass transfer resistances in the liquid and gas phases [1-3]. The drying becomes non-selective, i.e., a mass/molar ratio of two solvents maintains a constant value, by choosing a particular critical drying condition referred to as a dynamic azeotrope or pseudo-azeotrope [4-7]. For instance, ethanol-water mixtures show the pseudo-azeotrope at ethanol content of ~75 wt% when the solution evaporates at a constant temperature in ethanol-free dry airflow with a certain mass transfer coefficient. This value differs from the thermodynamic azeotrope of 96 wt% in ethanol content at 1 atm. Imposing a small compositional change near the pseudo-azeotrope composition alters which solvent selectively evaporates. When one solvent preferentially evaporates, another solvent component retains to be enriched near the evaporating surface, leading to local variations in composition-dependent surface tensions, diffusion coefficients, and solubility. An increase in the surface tension and a decrease in the diffusion coefficient can trigger the Marangoni instability and skinning, respectively, both of which are often detrimental to the final qualities of coating products. It is crucially important to predict the pseudo-azeotrope composition because it becomes a bifurcation point of compositional trajectories and thus the fate of the thin liquid films.

However, the roles of pseudo-azeotrope in particle dispersion coatings have received little attention. Let us consider an evaporating bimodal slurry coating consisting of large and small particles dispersed in a mixture of ethanol and water as the dispersing medium. Generally, the drying of dispersion coating is divided into two stages: the early stage, in which the total volume fraction of the particles (ϕ) is sufficiently low such that the particles or their aggregates are freely suspended in the liquid, and the late stage, in which ϕ reaches the critical packing volume fraction to form a packing layer of the particles across the thickness.

In the former, the diffusion and/or the heat transfer in the gas phase is the rate-limiting step dominated by the thermodynamic equilibrium at the descending gas-liquid interface. Unlike a single-solvent dispersion with a constant descending speed, the free surface motion of the ethanol-water suspension varies non-linearly with drying time because of non-ideal thermodynamic nature of the mixture. The water concentration and thus the partial vapor pressure of water increase when the initial ethanol composition is below the pseudo-azeotrope (PA) composition, resulting in a slower motion of free surface. On the other hand, the descending motion increases in speed in the opposite case of the initial ethanol composition above PA, in which ethanol retains in the liquid even it evaporates faster than water. When the descending motion of the surface is much faster than the thermal Brownian diffusion or the gravity-driven settling of the particles, the particles are accumulated under the free surface [8-10], resulting in a development of particle concentration gradients sometimes referred to as the top-down consolidation process.

In the late stage of evaporation, the receding interface is no longer flat but rather curved when it retreats into the particle packing, inducing the capillary pressure $\sim \gamma/r$ where γ and r represent the surface tension and the radius of meniscus curvature, respectively. The surface tension increases when the ethanol preferentially evaporates, whereas the ethanol-retaining evaporation reduces γ in the slurry. According to Luo et al. [11], the negative capillary pressures beneath the concave free surfaces initiate upward flows that transport smaller particles through interstitial spaces between larger particles, leading to a preferential migration of small particles on the dried coating surface. The physical model has been successfully supported by the recent in-situ photoluminescence microscopy [12-13] and the cryogenic broad ion beam slope-cutting and scanning electron microscopy (Cryo-BIB-SEM) [14]. Thus we expect that the water-retaining evaporation process would enhance the pressure-driven surface migration of small particles in the slurries with initial ethanol concentrations lower than the pseudo-azeotrope composition.

To explain the preferential surface migration of smaller particles, extensive models have been proposed by focusing on the difference in electrostatic repulsions between small and large particles [15], diffusiophoresis [16-18], cross diffusion [19-20], and normal stress [21], but, to the best of our knowledge, not previously on the roles of transient surface tensions and vapor

pressures below/above the pseudo-azeotrope composition. Indeed, most previous studies have been limited to the early evaporation stage of slurries containing a single solvent as a dispersing medium. Despite the recent progress in experimental techniques using ellipsometry [22], confocal scanning microscopy [23], GARField NMR imaging [24], atomic force microscopy (AFM) [24], cryogenic scanning electron microscopy (Cryo-SEM) [9-10, 14], photoluminescence microscopy [12-13], cross-sectional Raman spectroscopy [25], energy-dispersive x-ray spectroscopy (EDS) [26], and microbeam small-angle X-ray scattering (SAXS) [27], the precise mechanism behind preferential surface migration of smaller particles in bimodal solvent-mixture slurries remain unknown. In addition, many industrial coating slurries contain a mixture of two or more volatile solvents with different vapor pressures and surface tensions. Typical examples include mixtures of alcohol and water for fuel cell electrodes [28-30], alcohol and toluene for multi-layer ceramic capacitors [31-33], and terpineol and water for conductive inks [34]. It is important to understand the underlying physics of the particle consolidation process in order to design and optimize the practical multicomponent drying processes.

This study aims at utilizing the pseudo-azeotrope concept in drying alcohol–water bimodal suspensions to vary particle distributions across the thickness. We used real-time photoluminescence microscopy technique to investigate the preferential migration of small fluorescent latex particles in the presence of large non-emissive TiO_2 particles. The results revealed that the evolutions of small-on-top particle distributions was significantly hindered when we chose the initial alcohol concentration to exceed the predicted pseudo-azeotrope composition.

2. Experimental procedure

We used fluorescent polystyrene latex particles (micromer®-redF, micromod, Germany; diameter = 100 nm; zeta potential in water = -40 ± 5 mV) and nonemissive titanium dioxide particles (Kojundo Chemical Laboratory Co. Ltd, Japan; average diameter = 2.2 μm). The maximum excitation and emission wavelengths of the fluorescent particle are 552 and 580 nm, respectively. Polyacrylic acid (PA, Fujifilm Wako Pure Chemical Co. Ltd, Japan; average molecular weight of $M_w = 5,000$) was dissolved in mixtures of ethanol (Fujifilm Wako Pure Chemical Co. Ltd, Japan) and distilled water. All of the chemicals were used as received without further purification. The particles were added to the polymeric solution at particle volume fractions of 0.0688 and 1.94 vol% for latex and TiO_2 particles, respectively. The particle-to-binder mass ratio between TiO_2 and PA was fixed at 1:3 w/w, corresponding to the initial binder concentration of 25.2 wt%.

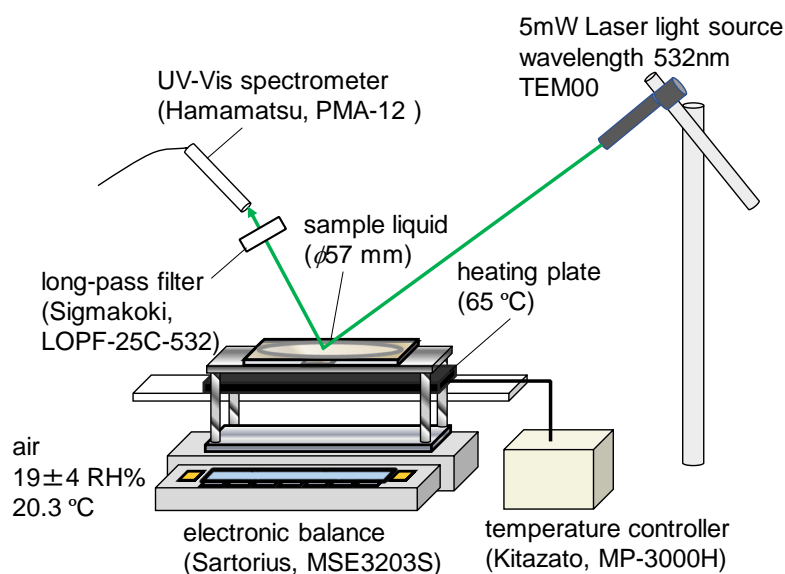


Figure 1 Experimental setup

Figure 1 shows a schematic of the drying apparatus. A TEM00-mode laser (LasirisTM Green, Coherent, USA; wavelength = 532 ± 1 nm) was incident to excite the fluorescent particles in slurries. A UV-Vis spectrometer (Hamamatsu, PMA-12) with a long-pass filter (Sigmakoki, LOPF-25C-532) was used to capture the emission spectra within 530-799 nm in wavelength from the sample at 20 s intervals. The slurry with a predetermined volume was cast onto the glass substrate by using a micropipette to coat a 420- μm -thick liquid film. The coated area was set at 25 cm^2 by gluing a 1.0-mm-thick duralumin shim onto the substrate. The substrate-bottom temperature was adjusted to 65 $^{\circ}\text{C}$ by using a heating plate (MP-3000H, Kitazato, Japan) placed beneath the coating at interspaces of less than 1 mm. Solvent loss was simultaneously measured in real time by using an electronic balance (Cubis MSE-3203S-0-00-DE, Sartorius, Japan) at a sampling rate of 1.0 Hz with an accuracy of 1 mg. The temperature and humidity of drying air were fixed at 20.3 $^{\circ}\text{C}$ and 19 \pm 4 RH%, respectively. All equipment was set up on a vibration isolation table and was covered with a black curtain to prevent exterior light from interfering with the measurements. A more detailed

experimental procedure is given elsewhere [12-13]. The drying conditions and the viscosities of the suspending medium were chosen so that $Pe > 200$ in order to ensure that the rate of film shrinkage (E) was orders of magnitude greater than that of the Brownian diffusion of particles predicted by the Stokes–Einstein diffusion coefficient (D), where the Peclet number is defined as $Pe = Eh_0/D$ and h_0 denotes the initial thickness. We also estimated the rate balance between sedimentation and evaporation for the sedimentation number, $Ns = U/E$, where U is the Stokes' settling velocity. We found $Ns = 0.5 \sim 2$ for the titania particle and $Ns < 10^{-5}$ for the latex particle at the initial ethanol volume fractions ranging between 0 and 55 vol%, indicating that the gravity-driven settling of latex particles was negligibly slow, whereas the settling speed of TiO_2 particle was almost comparable to that of film shrinkage because of the larger particle size and the higher solid density. Note that Pe and Ns depend on the initial solvent compositions because the partial vapor pressures in the slurry vary with the ethanol concentration.

3. Results and discussion

Figure 2a shows the typical time-evolutions in emission intensities at the wavelength of 580 ± 3 nm for two slurries at different initial concentrations of 0 and 91 vol% ethanol. The intensity showed a stepwise increase in the ethanol-free slurry, whereas it initially decreased, showed a minimum, and then increased to reach a higher level in the ethanol-rich slurry. The previously proposed emission models show that the intensity becomes higher than unity when the fluorescent particles are enriched near the evaporating surface, implying that the surface migration of smaller particles was hindered by adding alcohol with a lower surface tension. To further examine the effect of ethanol addition, we compared the final emission intensity of dried particulate films. As shown in Figure 2b, the final intensities remained a higher level at initial ethanol concentrations below a critical value. To explore the critical condition of the suppressed migration, we predicted the pseudo-azeotrope composition by solving the coupled mass balance equations for the two solvents. We simply assumed isothermal gas-diffusion-limited drying and negligible effects of particles and binder on the solvent activity. The results revealed that the initial ethanol volume fraction corresponding to the pseudo-azeotrope was found to be 83 vol%, indicating that the ethanol preferentially evaporates below this critical composition. This result shows a good consistent with our physical picture: the capillary-driven migration of small particles becomes significant in the particularly case when water retains to increase the surface tension, and hence the negative capillary pressure, in the slurry evaporated below the pseudo-azeotrope composition.

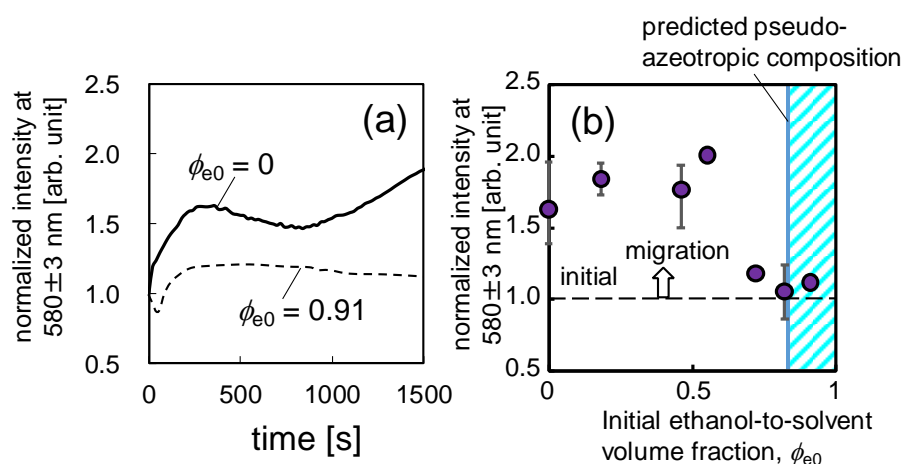


Fig. 2. (a) Time-evolutions in emission intensity of drying slurries. (b) Variations in the emission intensity of dried particulate films with different initial ethanol contents.

Acknowledgement

The author wishes to thank Erigo Goto for her technical assistance with the experiments. The author acknowledges the financial support from the Japan Society for the Promotion of Science (JSPS) KAKENHI (20H02507) Grant-in-Aid for Scientific Research B.

References

1. T. Riede, E. U. Schlünder, Selective evaporation of a ternary mixture containing one nonvolatile component with regard to drying processes. *Chemical Engineering and Processing*, **28**, 151-163 (1990).
2. M. Viduarre, J. Martinez, Continuous drying of a solid wetted with ternary mixtures. *AIChE Journal*, **43**, 681-692 (1997).
3. J. Martinez, F. Setterwall, Gas-phase controlled convective drying of solids wetted with multicomponent mixtures. *Chemical Engineering Science* **9**, 2235-2252 (1991).
4. F. Thurner, E.U. Schlünder, Progress towards understanding the drying of porous materials wetted with binary mixtures. *Chemical Engineering and Processing*, **20**, 9-25 (1989).
5. Y.S. Huang, K. Sundmacher, Z. Qi, E.U. Schlünder, Residue curve maps of reactive membrane separation. *Chemical Engineering Science*, **59**, 2863-2879 (2004).

6. F. Scheepers, A. Stähler, M. Stähler, M. Carmo, W. Lehnert, D. Stolten, Steering and in situ monitoring of drying phenomena during film fabrication. *Journal of Coatings Technology and Research*, **16**, 1213-1221 (2019).
7. M. Yamamura, Drying paths of phase-separating solution coatings exposed to humidity, *Journal of Coatings Technology and Research*, **19**, 15–23 (2022).
8. A.F. Routh, W.B. Zimmerman, Distribution of particles during solvent evaporation from films, *Chem Eng Sci.*, **59**, 2961–2968 (2004).
9. C.M. Cardinal, Y.D. Jung, K.H. Ahn, L.F. Francis, Drying regime maps for particulate coatings, *AIChE J.*, **56**, 2769-2780 (2010).
10. F. Buss, C.C. Roberts, K.S. Crawford, K. Peters, K.F. Francis, Effect of soluble polymer binder on particle distribution in a drying particulate coating, *J. Colloid Interface Sci.*, **359**, 112-120 (2011).
11. H. Luo, C. M. Cardinal, L. E. Scriven, L. F. Francis, Ceramic nanoparticle/monodisperse latex coatings. *Langmuir*, **24**, 5552-5561 (2008).
12. S. Lim, K. H. Ahn, M. Yamamura, Latex migration in battery slurries during drying. *Langmuir*, **29**, 8233–8244 (2013).
13. T. Tashima, M. Yamamura, Two-step migration of particles in evaporating bimodal suspension films at high Peclet numbers. *Journal of Coatings Technology and Research*, **14**, 965–970 (2017).
14. S. Jaiser, J. Kumberg, J. Klaver, J. L. Urai, W. Schabel, J. Schmatz, P. Scharfer. Microstructure formation of lithium-ion battery electrodes during drying - An ex-situ study using cryogenic broad ion beam slope cutting and scanning electron microscopy (Cryo-BIB-SEM). *Journal of Power Sources*, **345**, 97e107 (2017).
15. A.K. Atmuri, S.R. Bhatia, A.F. Routh, Autostratification in Drying Colloidal Dispersions: Effect of Particle Interactions, *Langmuir*, **28**, 2652 (2012).
16. R.P. Sear, P.B. Warren, Diffusiophoresis in nonadsorbing polymer solutions: The Asakura-Oosawa model and stratification in drying films, *Physical Review E*, **96**, 062602 (2017).
17. A. Fortini, I. Martín-Fabiani, J.L. De La Haye, P.-Y. Dugas, M. Lansalot, F. D’Agosto, E. Bourgeat-Lami, J.L. Keddie, R.P. Sear, Dynamic stratification in drying films of colloidal mixtures, *Phys. Rev. Lett.* **116**, 118301(2016).
18. E. Hooiveld, H.M. van der Kooij, M. Kisters, T.E. Kodger, J. Sprakel, J. van der Gucht, In-situ and quantitative imaging of evaporation-induced stratification in binary suspensions, *Journal of Colloid and Interface Science*, **630**, 666-675 (2023).
19. J. Zhou, Y. Jiang, M. Doi, Cross interaction drives stratification in drying film of binary colloidal mixtures, *Physical Review Letters*, **118**, 108002 (2017).
20. R. Tatsumi, O. Koike, Y. Yamaguchi, Y. Tsuji, Classification of drying segregation states by a generalized diffusion model, *J. Chem. Phys.* **153**, 164902 (2020).
21. J.H. Jeong, Y.K. Lee, K.H. Ahn, stratification mechanism in the bidisperse colloidal film drying process: evolution and decomposition of normal stress correlated with microstructure, *Langmuir*, **37**, 13712-13728 (2021).
22. A. Tzitzinou, J.L. Keddie, Film formation of latex blends with bimodal particle size distributions: consideration of particle deformability and continuity of the dispersed phase, *Macromolecules*, **33**, 2695-2708 (2000).
23. I. Nikiforow, J. Adams, M. Koenig, A. Langhoff, K. Pohl, A. Turshatov, D. Johannsmann, Self-stratification during film formation from latex blends driven by differences in collective diffusivity, *Langmuir*, **26**, 13162-13167 (2010).
24. Trueman, RE, Domingues, EL, Emmett, SN, Murray, MW, Keddie, JL, Routh, AF, Auto-stratification in drying colloidal dispersions: experimental investigations, *Langmuir*, **28**, 3420-3428 (2012).
25. H. Hagiwara, W.J. Suszynski, L.F. Francis, A Raman spectroscopic method to find binder distribution in electrodes during drying, *Journal of Coatings Technology and Research*, **11**(1), 11-17 (2014).
26. S. Jaiser, M. Muller, M. Baunach, W. Bauer, P. Scharfer, W. Schabel, Investigation of film solidification and binder migration during drying of Li-Ion battery anodes, *Journal of Power Sources*, **318**, 210 -219 (2016).
27. W. Liu, A. J. Carr, K. G. Yager, A. F. Routh, S. R. Bhatia, Sandwich layering in binary nanoparticle films and effect of size ratio on stratification behavior. *Journal of Colloid and Interface Science*, **538**, 209–217 (2019).
28. T. Mabuchi, S.-F. Huang, T. Tokumasu, Dispersion of Nafion ionomer aggregates in 1-propanol/water solutions: Effects of ionomer concentration, alcohol content, and salt addition, *Macromolecules*, **53**, 3273–3283(2020).
29. N. Kumano, K. Kudo, A. Suda, Y. Akimoto, M. Ishii, H. Nakamura, Controlling cracking formation in fuel cell catalyst layers, *Journal of Power Sources*, **419**, 219-228 (2019).
30. H. Ren, X. Meng, Y. Lin, Z. Shao, Microstructure formation mechanism of catalyst layer and its effect on fuel cell performance: Effect of dispersion medium composition, *Journal of Energy Chemistry*, **73**, 588-598 (2022).
31. J. Shibata, N. Murayama, H.-H. Lee, Dispersion of nano-sized BaTiO₃ particles in toluene-ethanol media using phosphate ester, *Resources Processing*, **59**, 125-130 (2012).
32. A.B.G. Simpson, J.A. Byrne, J.A.D. McLaughlin, M. Strawhorne, Effect of solids concentration on particle size distribution of deagglomerated barium titanate in stirred media mills, *Chemical Engineering Research and Design*, **93**, 287-292 (2015).
33. M. Yamamura, Sigmoidal temporal increase in shear viscosity of titania-toluene-ethanol colloidal suspensions, *Colloids and Surfaces A: Physicochemical and Engineering Aspects*, **675**, 132047 (2023).
34. M. Schneider, E. Koos, N. Willenbacher, Highly conductive, printable pastes from capillary suspensions, *Scientific Reports*, **6**, 31367 (2016).

Particle dynamics in coating and drying processes of particulate suspensions

Byoungjin Chun, Jinseong Yun, and Hyun Wook Jung

Department of Chemical and Biological Engineering, Korea University, Seoul 02841, Republic of Korea

Corresponding author: hwjung@grtrkr.korea.ac.kr

Complex liquids used in coating industries are often polydisperse particulate suspensions for making the targeted coating products. Particles uniformly distributed in the coating film are mostly desirable. However, such a situation is not always achievable even with a well-dispersed supply of raw materials. We would like to introduce recent results, based on mesoscale simulations, for particle motions in coating flow fields and vertical drying situations. Migration and segregation phenomena of bidisperse spherical particles were interpreted in Poiseuille and Couette flow regimes, respectively [1,2]. Also, stratification patterns (large-on-top or small-on-top) of bidisperse particles during vertical drying were compared through implicit/explicit solvent methods, depending on Peclet number [3]. Regarding the motion of non-spherical colloidal rods, it is found that the characteristics strain rate of the flow universally determines the orientational ordering of non-spherical colloidal rods in various shear and extensional flows [4]. By evaluating the degree of orientational alignment of rods along the flows, it has been observed that there is no significant difference between flow types, and the flow-induced ordering of rods dominantly depends on the variation of Pe_r (rotational Peclet number) up to moderate Pe_r . We are now trying to elucidate how motions of colloidal rods in confined channel flow deviate from Jeffery orbits, which represents the motion of elliptical particles freely suspended in a shear flow.

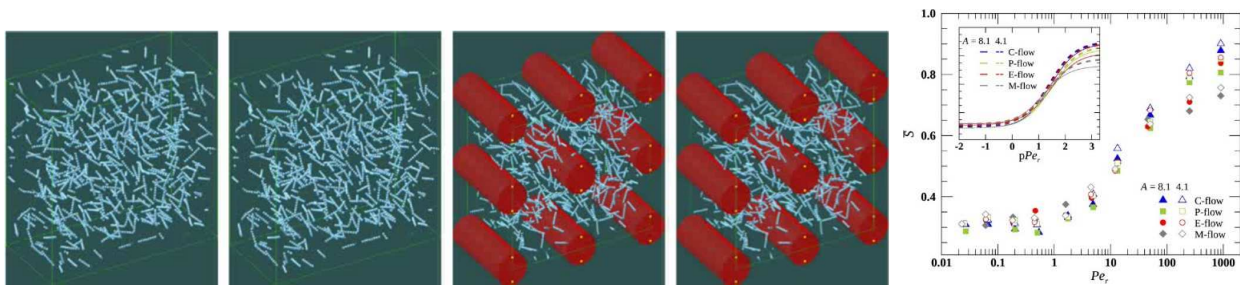


Fig. 1. Flow-induced orientational ordering of colloidal rods in shear and extensional flow fields [4].

References

1. B. Chun, J.S. Park, Y.-Y. Won, H.W. Jung, Shear-induced particle migration and segregation in non-Brownian bidisperse suspensions under planar Poiseuille flow, *J. Rheol.*, 63, 437-453 (2019).
2. B. Chun, H.W. Jung, Inertia- and shear-induced inhomogeneities in non-Brownian mono and bidisperse suspensions under wall-bounded linear shear flow, *Phys. Fluids*, 33, 053318 (2021).
3. J.S. Park, J. Yun, B. Chun, H.W. Jung, Mild stratification in drying film of colloidal mixtures. *Soft Matter*, 18, 3487-3497 (2022).
4. B. Chun, H.W. Jung, Universal flow-induced orientational ordering of colloidal rods in planar shear and extensional flows: dilute and semi-dilute concentrations, *J. Rheol.*, 67, 315-330 (2023).

The effect of the spatial variation of the evaporative flux on the deposition from a sessile droplet

Stephen K. Wilson, Hannah-May D'Ambrosio, Alexander W. Wray, Brian R. Duffy

Department of Mathematics and Statistics, University of Strathclyde, 26 Richmond Street, Glasgow G1 1XH, UK

Corresponding author: s.k.wilson@strath.ac.uk

The evaporation of sessile droplets plays a key role in a wide variety of practical contexts, including agricultural spraying, coating and painting, the preparation of chemical and biological assays, and inkjet printing. As a consequence, there have been extensive experimental, numerical, and theoretical investigations of this problem in recent years (see, for example, [1, 2]). In the present work a mathematical model for the effect of the spatial variation of the local evaporative flux on the evaporation of and deposition from a thin pinned particle-laden sessile droplet is formulated and solved. We then analyse the behaviour for a one-parameter family of local evaporative fluxes with the free parameter n (> -1) that exhibits qualitatively different behaviours mimicking those that can be obtained by, for example, surrounding the droplet with a bath of fluid such that the level of the bath coincided with the base of the droplet and/or confining the droplet within a chamber to suppress evaporation near the contact line [3, 4], or using a mask with one or more holes in it to achieve a desired pattern of evaporation enhancement and/or suppression [5, 6]. We show that when $-1 < n < 1$ (including the special cases $n = -1/2$ of diffusion-limited evaporation into an unbounded atmosphere and $n = 0$ of spatially-uniform evaporation), all of the particles are eventually advected to the contact line, and so the final deposit is a ring deposit at the contact line, whereas when $n > 1$ all of the particles are eventually advected to the centre of the droplet, and so the final deposit is at the centre of the droplet. In particular, we demonstrate that a singular (or even a non-zero) evaporative flux at the contact line is not an essential requirement for the formation of a ring deposit. In addition, we calculate the paths of the particles when diffusion is slower than both axial and radial advection, and show that in this regime all of the particles are captured by the descending free surface before eventually being deposited onto the substrate.

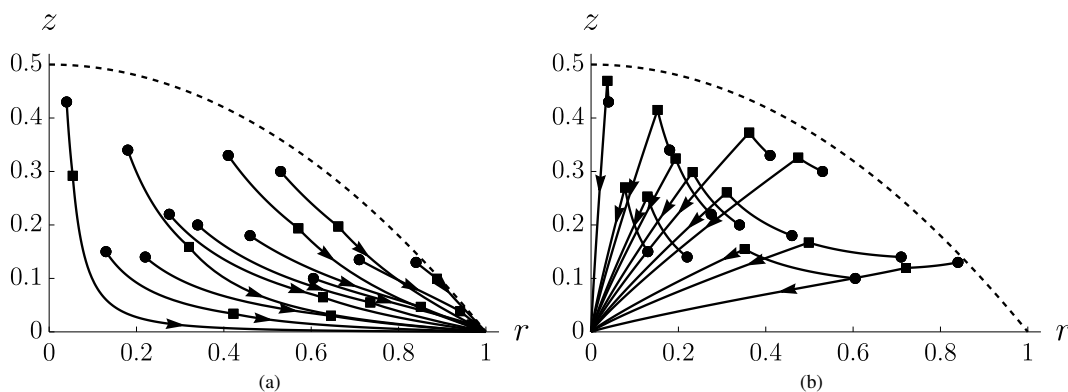


Figure 1: The paths of twelve representative particles for (a) $n = -1/2$ and (b) $n = 4$. The dots and the squares denote the initial position and the position of free-surface capture, respectively, of each particle. The dashed lines denote the initial free-surface profile.

References

- [1] S. K. WILSON AND B. R. DUFFY, Chapter 4 in *Drying of Complex Fluid Drops: Fundamentals and Applications* (eds. D. Brutin, K. Sefiane), Soft Matter Series No. 14, (Royal Society of Chemistry, London, 2022).
- [2] S. K. WILSON AND H.-M. D'AMBROSIO, *Annual Review of Fluid Mechanics* **55**, 481–509 (2023).
- [3] R. D. DEEGAN, O. BAKAJIN, T. F. DUPONT, G. HUBER, S. R. NAGEL, AND T. A. WITTEN, *Physical Review E* **62** (1), 756–765 (2000).
- [4] T. KAJIYA, D. KANEKO, AND M. DOI, *Langmuir* **24** (21), 12369–12374 (2008).
- [5] D. J. HARRIS, H. HU, J. C. CONRAD, AND J. A. LEWIS, *Physical Review Letters* **98** (14), 148301 (2007).
- [6] D. J. HARRIS, J. C. CONRAD, AND J. A. LEWIS, *Philosophical Transactions of the Royal Society A: Mathematical, Physical and Engineering Sciences* **367** (1909), 5157–5165 (2009).

Drops sliding down an inclined soft coating

Mathieu Oléron¹, Laurent Limat¹, Julien Dervaux¹, Matthieu Roché¹.

¹MSC, Matière et Systèmes Complexes, Université Paris Cité, CNRS, UMR 7057, Paris, France

Corresponding author: laurent.limat@u-paris.fr

Soft coating made with gels or polymers are often encountered in several applications, where static or dynamic wetting properties must be controlled (fog harvesting, anti-dew films, anti-condensation or anti-icing coatings...). We have investigated the shape and morphology of drops sliding down an inclined plate, coated with a viscoelastic gel [1]. We show that energy dissipation partition between liquid and solid controls the shape and stability of droplets sliding on the viscoelastic gel. When both phases dissipate energy equally, droplet dynamics is similar to that on rigid solids. When only the solid dissipates, we observe an apparent contact angle hysteresis, of viscoelastic origin, that in turn modifies the drop shape. We find excellent agreement between our data and a non-linear model of the wetting of gels of our own that also indicates the presence of significant slip [2]. Our work opens general questions on the dynamics of curved or singular contact lines [3] on rigid versus compliant substrates.

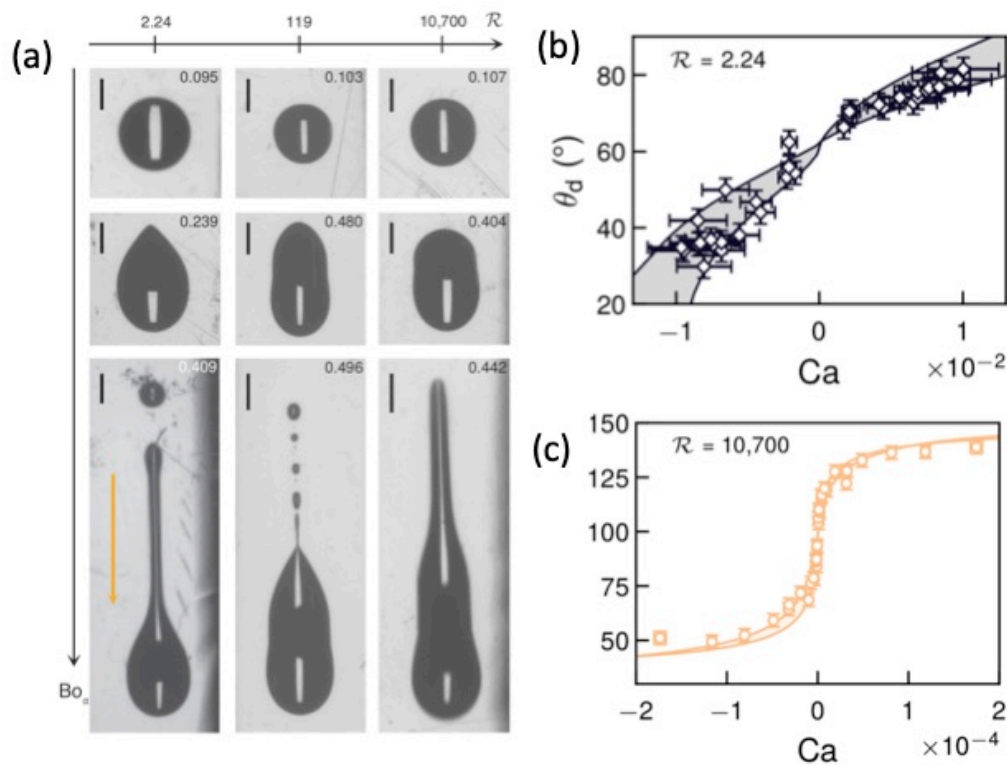


Fig. 1. (a) Typical shapes observed for liquid drops sliding down an incline, coated with a viscoelastic gel. The drop volume increases from top to bottom, while the deformability of the gel increases from left to right. (b) and (c): Advancing and receding contact angle measured at the front and rear of the drops, versus capillary number, for the two extreme cases of (a). An apparent hysteresis of purely viscoelastic origin develops for very soft gels. The continuous line represents our model, the coloured area reflecting uncertainties on the physical parameters.

References

1. M. Oléron, L. Limat, J. Dervaux, and M. Roché, *Morphology and stability of droplets sliding on soft viscoelastic substrates*, arXiv preprint arXiv:2304.04925
2. J. Dervaux, M. Roché, and L. Limat, *Soft Matter* **16**, 5157 (2020)
3. I. Peters, J. Snoeijer, A. Daerr, L. Limat, *Physical Review Letters*, 103 (11), pp. 114501 (2009)

Absolute/convective instability threshold for a liquid film over a moving substrate via linear stability analysis

Fabio Pino^{1,2}, Benoit Scheid², Miguel Alfonso Mendez¹

¹ Environmental and Applied Fluid Dynamics Department, von Karman Institute for Fluid Dynamics, Sint-Genesius-Rode, Belgium.

² Transfers, Interfaces and Processes (TIPs) laboratory, Université libre de Bruxelles, Brussels, Belgium

Corresponding author: fabio.pino@vki.ac.be

The linear stability properties of liquid film steady state solutions play an important role in many coating processes. Among the different stability analysis, the study of an instability's absolute or convective dynamics is pivotal for control and sensing applications [1]. In this work, we extend the knowledge of absolute/convective instability regions of falling liquid film [2, 3] calculating the threshold for a two-dimensional liquid film over a moving substrate coming out of a liquid bath via linear stability analysis of the Navier-Stokes equations.

An instability is absolute or convective, depending on the growth rate of the zero group velocity mode. To find this growth rate, we ran a spatio-temporal analysis, mapping the complex wavenumber space into the complex frequency space via Chebyshev-Tau spectral method and Rayleigh quotient iteration. We determined the absolute/convective threshold for Landau-Levich-Derjaguin (LLD) dip-coating problem [4], depending on the Kapitza (Ka) and the Reynolds (Re) numbers. Moreover, we investigate the space of non-dimensional liquid film heights \hat{h} and Re numbers for four fluids with $Ka \in (4, 553, 4300, 11525)$.

We found that the threshold between absolute (shadowed area) and convective (white area) in the $Ka - Re$ space (see Fig.1a) presents an exponential power-law growth region with a $5/9$ exponent dependency, for $Re \gtrsim 10$ and a minimum value, at $Ka = 16.63$ and $Re = 3$, below which the instabilities are always convective. In addition, in the $\hat{h} - Re$ space, we found a window of absolute instability around the LLD liquid film height ($\hat{h} = 1$) (see Fig.1b) with a minimum value in the thin film solution range ($\hat{h} < 1$) and a maximum for $\hat{h} \approx \sqrt{3}$ for the four fluids.

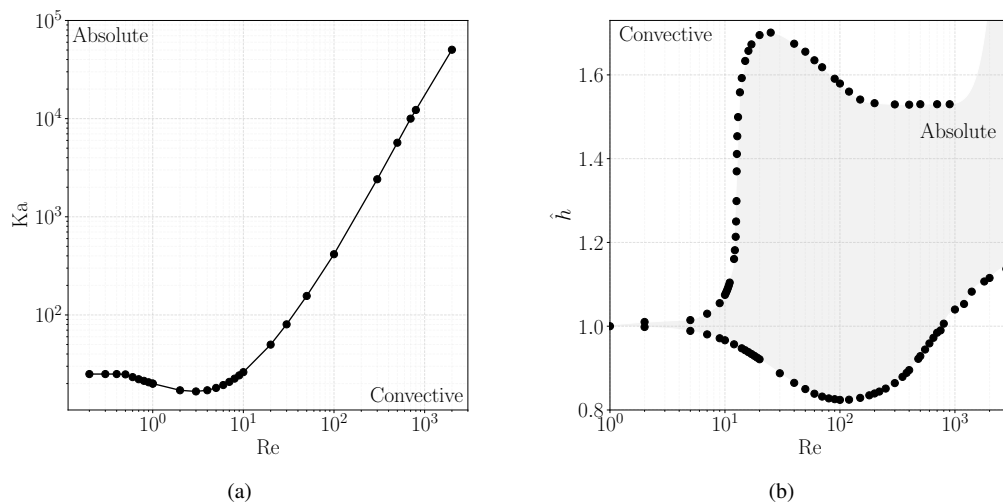


Figure 1: Absolute/convective threshold in $Ka - Re$ space for ($\hat{h} = 1$) and in the $\hat{h} - Re$ space for liquid zinc with $Ka = 11525$ (b).

References

- [1] PIER, BENOÎT, *Open-loop control of absolutely unstable domains*, (Proceedings of the Royal Society of London. Series A: Mathematical, Physical and Engineering Sciences, 2003).
- [2] F. PINO, B. SCHEID, AND M.A. MENDEZ., *Absolute/convective instability threshold in inverted falling film through linear stability analysis*, (AIP Conference Proceedings, 2022).
- [3] SCHEID, BENOIT, NICOLAS KOFMAN, AND WILKO ROHLFS., *Critical inclination for absolute/convective instability transition in inverted falling films.*, (Physics of fluids 28.4, 2016).
- [4] LANDAU, LEVICH AND LEVICH, B., *Dragging of a liquid by a moving plate*, (Dynamics of curved fronts, 1988).

Bilayer Couette and Film Flow over a Profiled Substrate

Markus Scholle¹, Philip H. Gaskell², Sara Ismail–Sutton², Marcel Mellmann³

¹ Institute for Flow in Additively Manufactured Porous Media (ISAPS), Heilbronn University, Heilbronn

² Department of Engineering, Durham University, Durham

³ Casculate, Kaiserslautern

Corresponding author: markus.scholle@hs-heilbronn.de

1 Problem formulation

1.1 Physical modelling and notations

Steady, shear– and gravity–driven bilayer [1] flow over a stationary, rigid periodically patterned substrate (given by $x_2 = b(x_1)$), as illustrated in Fig. 1, and involving two immiscible liquids (Newtonian, dynamic viscosity η and incompressible, density ρ), one lying above the other, is explored. Both are analysed in terms of internal flow structure and interface disturbance. In the case of the Couette flow, the confining substrates

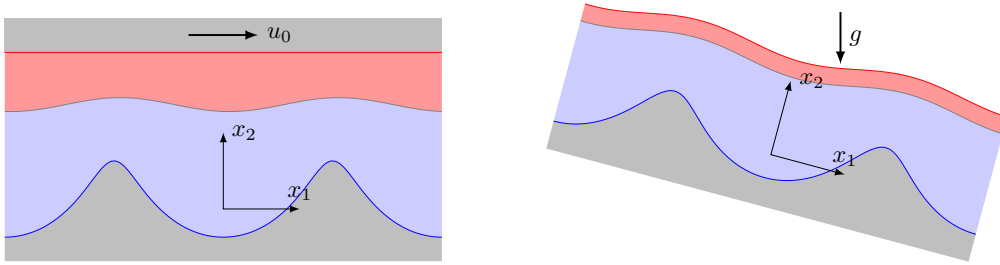


Figure 1: Bilayer, shear–driven Couette (left) and gravity–driven film (right) flow over topography.

are in parallel alignment, the upper, planar rigid one moves with constant speed u_0 ; for the film flow case the upper boundary is a free–surface $x_2 = f_2(x_1)$ whose shape has to be solved for in addition, like the liquid layer separating interface.

Tensor notation with Einstein’s summation convention is used throughout. Accordingly, for an assumed velocity field, u_i , the continuity equation is simply:

$$\partial_i u_i = 0; \quad (1)$$

the corresponding momentum balance can be expressed as:

$$\partial_j [\rho u_j u_i - T_{ji} + \rho V \delta_{ij}] = 0, \quad (2)$$

with $T_{ij} = -p \delta_{ij} + \eta [\partial_i u_j + \partial_j u_i]$ denoting the associated stress tensor and $V = g [x_2 \cos \alpha - x_1 \sin \alpha]$ the specific potential energy.

1.2 Mathematical modelling

1.2.1 Potential–based variational formulation

As is wellknown [2], Eq. (1) is fulfilled identically by introducing a stream function vector Ψ_k such that:

$$u_i = \varepsilon_{ijk} \partial_j \Psi_k; \quad (3)$$

in an analogous way, Eq. (2) can be fulfilled identically by introducing a tensor potential, a_{kq} , for the momentum flux density leading to:

$$\rho u_j u_i - T_{ji} + \rho V \delta_{ij} = \varepsilon_{ikl} \varepsilon_{j pq} \partial_k \partial_p a_{lq} \partial_l \partial_p a_{kq} \quad (4)$$

the meaning of which is discussed in [3], in terms of an analogy with Maxwell's theory where the vector potential appears for the magnetic flux density. Among the most striking advantages of the use of potentials in Maxwell theory is the self-adjoint form achieved. The same is realised for viscous flow by using potentials according to (3) and (4), allowing the following Lagrangian [3] to be found:

$$\ell = \rho \bar{a}_{ij} u_i u_j + 2 [\eta u_j - \partial_j \Phi] \partial_i \bar{a}_{ij} + \frac{1}{2} \varepsilon_{ilk} \varepsilon_{jpk} \partial_l \bar{a}_{ij} \partial_p \bar{a}_{kq}, \quad (5)$$

where the tensor potential is, according to $a_{ij} = \bar{a}_{ij} + 2\Phi\delta_{ij}$, decomposed into a traceless part, \bar{a}_{ij} and an isotropic part with a scalar potential Φ ; the velocity field is expressed in terms of the stream function vector via Eq. (3). The Euler–Lagrange equations resulting by variation of the action integral:

$$\delta \iiint_V \ell(\psi_i, \partial_n \psi_i) dV = 0, \quad (6)$$

with respect to \bar{a}_{ij} and Φ , reproduce the tensor field equation (4) by linear combination; whereas variation with respect to Ψ_m and Φ provides gauging conditions for the potentials [3].

The above 3D formulation is adapted for 2D flow by taking $\Psi_k = \psi\delta_{k3}$ and $\bar{a}_{i3} = 0$ as specific choices for the current function vector and the tensor potential, respectively. The Euler–Lagrange equations varied with respect to a_{11} and a_{12} are thus:

$$\frac{\rho}{2} [(\partial_2 \psi)^2 - (\partial_1 \psi)^2] = \partial_1 (\eta \partial_2 \psi - \partial_1 \Phi) + \partial_2 (\eta \partial_1 \psi + \partial_2 \Phi), \quad (7)$$

$$\rho \partial_1 \psi \partial_2 \psi = \partial_2 (\eta \partial_2 \psi - \partial_1 \Phi) - \partial_1 (\eta \partial_1 \psi + \partial_2 \Phi). \quad (8)$$

It can be found in [4] how the 2D Navier–Stokes equation for steady flow is recovered from (7) and (8).

1.2.2 Boundary and interface conditions

On expressing the velocity in terms of the stream function, the no-slip/no-penetration conditions at the profiled substrate take the form of Dirichlet– and Neumann–conditions:

$$\psi(x_1, b(x_1)) = 0, \quad (9)$$

$$n_i \partial_i \psi(x_1, b(x_1)) = 0. \quad (10)$$

Similarly, the conditions at the internal interface and bounding free-surface in the case of gravity-driven flow, related to the continuity of the velocity field and to the kinematic condition determining their shape are:

$$[[\psi]] = 0, \quad (11)$$

$$[n_i \partial_i \psi]_{\pm} = 0, \quad (12)$$

respectively; the double square bracket indicates the jump at the interface/free-surface: $[[\dots]] := [\dots]_2 - [\dots]_1$, with $[\dots]_{1,2}$ denoting the limit of the respective expression approached from above (subscript 2) or below (subscript 1).

A key features of this potential-based first integral approach, is a greatly simplified and utilitarian form of the dynamic condition at an internal interface or free-surface (with n_i denoting the normal vector their), namely:

$$[[\partial_i \Phi]] = \frac{\sigma}{2} n_i + \frac{[[\rho]]}{2} \int V dx_i, \quad (13)$$

for the gradient of the scalar potential [4]. This simplified reformulation of the dynamic condition is arguably the decisive advantage of the potential-based first integral approach.

2 Solution methods

For the case of Stokes flow, two different methods of solution are adopted; the inertia terms are zero, in which case and with reference to left hand sides of (7) and (8), the following linear PDEs are required to be solved:

$$\partial_1 (\eta \partial_2 \psi - \partial_1 \Phi) + \partial_2 (\eta \partial_1 \psi + \partial_2 \Phi) = 0, \quad (14)$$

$$\partial_2 (\eta \partial_2 \psi - \partial_1 \Phi) - \partial_1 (\eta \partial_1 \psi + \partial_2 \Phi) = 0. \quad (15)$$

The first method, based on the long-wave approximation, is purely analytic; the second is semi-analytic, leading to an advantageous problem reduction. For validation/comparison purposes, solutions of a FE discrete form of the classical Navier–Stokes equations were also generated.

2.1 Analytical method

Invoking the long-wave (lubrication) approximation, based on the assumptions that (i) the flow velocity u_1 in the direction of flow dominates compared to the velocity in the cross-flow direction, u_2 , while (ii) gradients in the cross-flow direction are dominant compared to those in direction of flow, namely $\partial_1^2 \psi \ll \partial_2^2 \psi$, simplifies the field equation (15) to the integrable form $\partial_2 [\eta u_1 - 2\partial_1 \Phi] = 0$, which following integration yields:

$$2\partial_1 \Phi = \eta u_1 + F_1(x_1), \quad (16)$$

with integration function $F_1(x_1)$. This can be substituted into equation (14), resulting again in an integrable form, the integration of which is:

$$2\partial_2 \Phi = 3\eta u_2 + F_1'(x_1)y + F_2(x_1), \quad (17)$$

giving rise a second integration function $F_2(x_1)$. After elimination of the potential Φ by computing $\partial_2(16) - \partial_1(17)$ and further integration steps, one finally obtains the following analytical solution for the stream function:

$$\eta\psi = F_1''(x_1)\frac{x_2^3}{6} + F_2'(x_1)\frac{x_2^2}{2} + F_3(x_1)x_2 + F_4(x_1). \quad (18)$$

The integration functions $F_1(x_1), \dots, F_4(x_1)$ are obtained by inserting the above solution into the boundary and interface conditions. This procedure is explained in detail in [5] for a monolayer film flow and applied to bilayer Couette flow in [6].

2.2 Complex Variable (CV) method

The following semi-analytic method [7], is comprised of an analytic reduction in dimension (from 2D to 1D) followed by a discrete approach for finding the final solution. Representing the field equations (14) and (15) in terms of the complex variable:

$$\xi := x_1 + ix_2, \quad (19)$$

together with its complex conjugate, $\bar{\xi}$, leads to the complex equation:

$$\frac{\partial^2}{\partial \xi^2} [\Phi + i\eta\psi] = 0, \quad (20)$$

which is integrable. By direct twofold integration and considering periodicity of the stream function, the following general solution [7] is obtained:

$$\Phi + i\eta\psi = iA(\bar{\xi} - \xi)\xi + B(3\bar{\xi} - \xi)\xi^2 + 2R(\xi) + (\bar{\xi} + \xi)Q(\xi), \quad (21)$$

containing two periodic holomorphic functions $Q(\xi), R(\xi)$ and constants A, B , which have to be determined via the boundary and interface conditions. The latter are discretised by a spectral method, i.e. by representing Q and R as Fourier series, leading to an algebraic set of equations. This equation set is nonlinear but can be linearised in the case of weak curvature of the interface separating the two layers and at the free surface, enabling them to be conveniently solved via iteration; the methodology was implemented within Python.

2.3 FE discretisation

For validation and comparison purposes, a standard Galerkin FE discretisation of the classical Navier–Stokes equations was undertaken and, as above, implemented within Python; further details are available in [6, 8].

3 Results and Discussion

Since monolayer flow is just a special case of a bilayer flow, both types of flow have been considered. As an example of what is achievable, Fig. 2 provides a set of sample solutions for bilayer Couette flow over harmonic corrugations given by:

$$b(x) = -a \cos x, \quad (22)$$

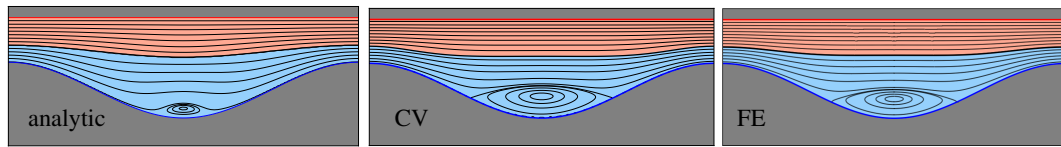


Figure 2: Streamline flow patterns for bilayer Couette flow, as predicted by the analytic (left), semi-analytic (middle) and FE (right), methods of solution.

with amplitude $a = 0.5$. The average film thicknesses of the individual layers are $h_1 = 0.7$ and $h_2 = 0.6$. The viscosity ratio is $\eta_1/\eta_2 = 2$, with $\rho_1/\rho_2 = 1$, while interface tension is neglected, $\sigma = 0$.

Flow separation is observed to occur in all cases; while the results obtained analytically, as described in section 2.1, embody the main features of the flow, those obtained using the CV method, section 2.2, compare almost identically with the corresponding FE solution. Note, the latter require significantly more computational time to achieve. Despite the observed deviations of the analytical solution from the FE results, it serves a valuable quick diagnostic tool for pin-pointing regions of parameter space exhibiting interesting behaviour, and its value should not be underestimated; also for much smaller amplitudes of the bottom contour, improved comparative accuracy is observed.

The CV method as presented has its weakness, in that if the amplitude of the corrugations is larger than 0.5, the Fourier series diverges, as known from prior investigations [9, 10]. However, this shortcoming can be satisfactorily addressed and overcome by various strategies: in the work of Adler [10] a Padé approximation is used as a replacement for the divergent Fourier series; in [9] the Fourier discretisation only applies to the boundary values of the functions $Q(\xi)$ and $R(\xi)$, while the functions themselves are reconstructed from their boundary values via Cauchy's integral formula.

4 Concluding remarks

The potential-based first integral approach provides a promising basis for the development of highly efficient analytical and semi-analytical solution methods for the exploration of lubrication like flow problems and related thin-film coating flows. Its major benefits are the existence of a variational principle and a considerably simplified form of the dynamic interface condition to a Dirichlet/Neumann form.

The model problem presented here, with an a priori unknown interface location that forms part of the solution, is solved by a purely analytic approach based on invoking the Lubrication approximation, and by a semi-analytic CV approach with spectral discretisation. A numerical FE discretisation of the governing continuity and Navier-Stokes equation has been implemented and solved for validation/comparison purposes. The semi-analytic CV and FE solutions are found to be practically indistinguishable, yet the former can be obtained in a mere fraction of the time.

References

- [1] A. A. ABDALLA, S. VEREMIEIEV, and P. H. GASKELL, *Chemical Engineering Science* **181**, 215–236 (2018).
- [2] G. K. BATCHELOR, *An Introduction to Fluid Dynamics*, Cambridge Mathematical Library (Cambridge University Press, 2000).
- [3] M. SCHOLLE, P. H. GASKELL AND F. MARNER, *Journal of Mathematical Physics* **59** (4), 043101 (2018).
- [4] F. MARNER, P. H. GASKELL AND M. SCHOLLE, *Physical Mesomechanics* **17**(4), 341–348 (2014).
- [5] M. SCHOLLE, P. H. GASKELL, and F. MARNER, *Fluids* **4**(2), 82 (2019).
- [6] M. SCHOLLE, M. MELLMANN, P. H. GASKELL, L. WESTERKAMP AND F. MARNER, *Multilayer modelling of lubricated contacts – a new approach based on a potential field description*, DOI: 10.1007/978-3-030-60124-9_16 (Springer Tracts in Mechanical Engineering, 2021).
- [7] F. MARNER, P. H. GASKELL AND M. SCHOLLE, *Journal of Mathematical Physics* **58**(4), 043102 (2017).
- [8] M. MELLMANN, *Simulation dünner Filme mit freien Oberflächen und Phasengrenzen mittels eines iterativen FE-Verfahrens*, Master's thesis, Heilbronn University, 2020.
- [9] M. SCHOLLE, A. WIERSCHEM AND N. AKSEL, *Acta Mechanica* **168**(3), 167–193 (2004).
- [10] A. E. MALEVICH, V. V. MITYUSHEV AND P. M. ADLER, *Acta Mechanica* **182**(3-4), 151–182 (2006).

Weakly non-parallel stability of a condensing film flow

Simeon Djambov¹, François Gallaire¹

¹ Laboratory of Fluid Mechanics and Instabilities, École Polytechnique Fédérale de Lausanne, 1015 Lausanne, Switzerland
Corresponding author: simeon.djambov@epfl.ch

A quiescent, saturated vapour condenses onto a uniformly cooled, inclined plate and forms a laminar, incompressible, gravity-driven film flow of a Newtonian liquid of constant material properties (fig. 1). We make the problem dimensionless by rescaling all distances with a characteristic length H_N , to be determined; we use a Nusselt velocity scale, a hydrostatic pressure scale, and recast the temperature field from 0 on the wall to 1 on the interface. The system is governed by the incompressible Navier–Stokes and heat equations

$$\nabla \cdot \mathbf{u} = 0, \quad (1)$$

$$Re(\partial_t \mathbf{u} + \mathbf{u} \cdot \nabla \mathbf{u}) = -\nabla p + \mathbf{f} + \nabla^2 \mathbf{u}, \quad (2)$$

$$Pe(\partial_t T + \mathbf{u} \cdot \nabla T) = \nabla^2 T, \quad (3)$$

where \mathbf{u} is the two-dimensional velocity field, p is the pressure, and T is the temperature; $\mathbf{f} = \hat{\mathbf{x}} - \cot \theta \hat{\mathbf{y}}$ is the gravity forcing. The Reynolds number $Re = \rho^2 g \sin \theta H_N^2 / \mu^2$ compares inertial and viscous effects and the Péclet number $Pe = \rho g \sin \theta H_N^3 / (\mu \kappa) = Pr Re$ is the ratio of thermal advection to thermal diffusion, related to the Reynolds number through the Prandtl number Pr .

No-slip and no-penetration conditions, as well as a constant temperature are imposed at the substrate, $y = 0$. We consider conditions, in which the phase change takes place in a quasi-equilibrium. Hence the temperature of the interface is constant and equal to the saturation condensation temperature. Further, we perform our analysis in the framework of the one-sided model, whereby we consider the vapour phase as mechanically passive [1]. The liquid–vapour interface, $y = h(x)$, is thus free of tangential stress and undergoes a curvature-induced jump in the normal stress, $We \partial_{xx}^2 h / (1 + (\partial_x h)^2)^{3/2}$. The Weber number $We = \gamma / (\rho g \sin \theta H_N^2)$ compares capillary to hydrostatic pressures.

The set of governing equations is completed by the kinematic boundary condition of the free surface, or equivalently the mass conservation equation

$$\partial_t h + \mathbf{u} \cdot \nabla [h - y]|_{y=h} = -\frac{Ja}{Pe} \nabla T \cdot \nabla [h - y]|_{y=h}, \quad (4)$$

where $Ja = c_p(T_\infty - T_w) / h_{lv}$ is the Jakob number, which measures the ratio of sensible to latent heats.

For most liquids of interest, including water, the steady basic flow is to a very good approximation the one derived by Nusselt (1916) [2]. The flow fields are all adiabatically slaved to the film thickness $h_0(x)$ and

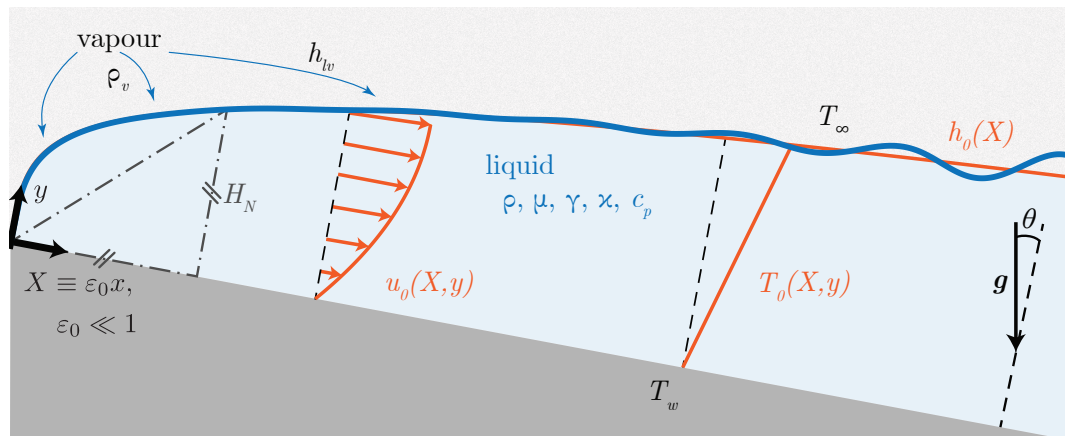


Figure 1: Sketch of the problem at hand. The basic flow is depicted in orange.

involve a half-parabolic velocity, linear pressure, and linear temperature profiles in the wall-normal direction

$$h_0(x) = x^{1/4}, \quad (5)$$

$$\mathbf{u}_0(x, y) = y(h_0(x) - y/2)\hat{\mathbf{x}} - h'_0(x)y^2/2\hat{\mathbf{y}}, \quad (6)$$

$$p_0(x, y) = \cot \theta(h_0(x) - y), \quad (7)$$

$$T_0(x, y) = y/h_0(x), \quad (8)$$

where we have chosen a length scale such that $Pe = 4Ja$,

$$H_N = \left(\frac{4\mu\kappa c_p(T_\infty - T_w)}{\rho g \sin \theta h_{lv}} \right)^{1/3}. \quad (9)$$

This choice can be geometrically interpreted as the equality of the streamwise position with the film thickness at that position (see fig. 1).

We seek to establish the system's linear response to a harmonic forcing of real angular frequency ω . We are interested in the onset of Kapitza waves on the condensing film's surface [3]. The problem's well-posedness is ensured by the convective nature of the Kapitza instability. The basic flow's slow dependence on the streamwise coordinate, $h'_0(x \rightarrow \infty) \rightarrow 0$, enables the use of the Wentzel–Kramers–Brillouin–Jeffreys (WKBJ) formalism [4]. The linear perturbations take the form

$$\mathbf{q}(x, y, t) \sim A(X)\tilde{\mathbf{q}}(y; X) \exp \left[i \left(\varepsilon_0^{-1} \int_{X_0}^X k(\omega; X') dX' - \omega t \right) \right] + \text{c.c.}, \quad (10)$$

where the local eigenfunctions $\tilde{\mathbf{q}} = (\tilde{\mathbf{u}}, \tilde{p}, \tilde{T}, \tilde{h})$ contain the state variables and $X \equiv \varepsilon_0 x$ is the slow streamwise coordinate with $\varepsilon_0 \ll 1$, which is a measure of the basic flow's weak non-parallelism. The local complex wave number $k(\omega; X')$ is associated to the frequency ω , at the streamwise section X' ; its negative imaginary part is the local spatial growth rate. It is computed from the linearised governing equations at leading order in ε_0 , *i.e.* over a quasi-parallel slice of the basic flow. The slowly-varying, complex envelope function $A(X)$ smoothly stitches the local spatial stability analyses. It is obtained from a solvability condition at first order in ε_0 , where the slow evolution of both the basic flow and of the local spatial dispersion relations are taken into account. Imposing $A(X_0) = 1$ as initial condition, describes a localised forcing with the local eigenfunction $\tilde{\mathbf{q}}(y; X_0)$. The geometry of the problem lacks a proper inlet and X_0 is the arbitrary position, where a disturbance could force the system.

Indeed, as regards the system's local linear stability, a unique spatial branch, associated to downstream-propagating waves, becomes unstable (fig. 2a). Compared to the classical Kapitza instability of an isothermal, uniform film flow, where destabilising inertia competes against the stabilising effects of gravity and capillarity, the condensing film flow is additionally locally stabilised by the phase change: as thinner liquid layers promote heat transfer, eq. (8), vapour tends to condense more in the perturbation's troughs rather than on the crests, thus damping perturbations. Nevertheless, since the basic film thickness grows, eq. (5), inertia experienced by perturbations increases downstream and after a critical distance x^c , Kapitza waves can develop. Note that the wavelength of the first locally linearly unstable perturbation is much smaller than the basic flow evolution length scale at the same location, for the example of fig. 2a $k^* \approx 4 \times 10^{-3} \gg 4 \times 10^{-5} \approx h'_0(x)/h_0(x) = 0.25x^{-1}$. This is systematically the case and makes the weakly non-parallel approach suitable. Marginal stability is attained for considerably higher local Reynolds numbers $Re_x = Reh_0^3(x)$ than for the non-condensing case. Increasing the Jakob number Ja , *i.e.* a cooler plate, requires a thicker film for the onset of instability. However, this also makes the basic flow thicken – and hence, reach local linear instability – faster, *i.e.* in a shorter dimensional distance (fig. 2b).

Finally, in order to predict the linearly prevalent frequency, we consider the amplification of locally present noise. The gain is defined as the squared modulus of the linear perturbation, eq. (10),

$$G^2(L, X_0; \omega) = |A(L)|^2 \exp \left[-2 \int_{X_0}^L k_i(\omega; X') dX' \right], \quad (11)$$

where k_i is the imaginary part of the wave number, *i.e.* the negative local spatial growth rate. It consists in an accumulation of the local growth rates, corrected for the weak non-parallelism by the WKBJ amplitude (presented separately in fig. 3 for $X_0 = 1$). Upstream of the critical distance x^c , all perturbations are damped. Higher frequencies are subject to more severe attenuation and over a longer distance, but tend to grow faster

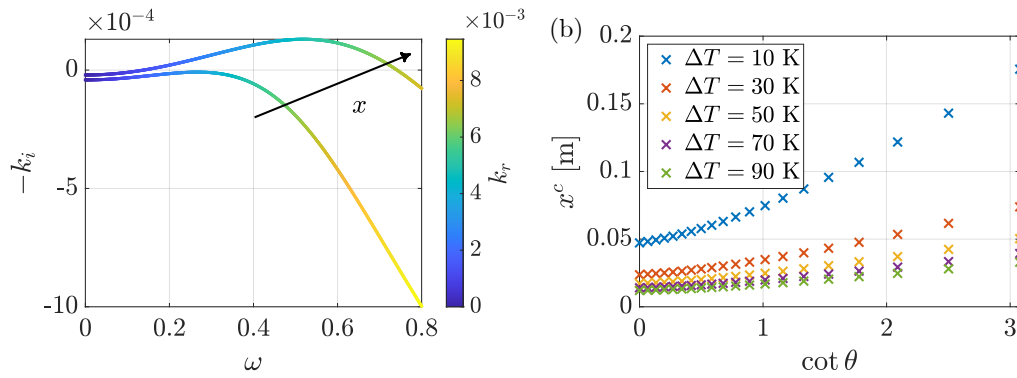


Figure 2: (a) $\theta = \pi/4$, $Ja \approx 0.02$, $We \approx 8 \times 10^4$, $Pr \approx 7$. Examples of stable and unstable spatial dispersion relations at streamwise sections $x = \{6 \times 10^3, 1.2 \times 10^4\}$ (in dimensional quantities, for water, condensing on an incline of $\pi/4$ with an imposed cooling of 10 K, these scale to around 7 and 14 cm; the film is around 100 and 120 μm thick). (b) Dimensional critical distance as a function of the inclination angle θ for several imposed temperature differences $\Delta T \equiv T_\infty - T_w$, material properties of water.

afterwards. The weakly non-parallel correction remains inferior to 1, which captures the non-optimal projection of perturbations on the local eigenfunctions of following slices. It also exhibits a non-monotonic behaviour, which indicates the presence, although minor, of non-parallel instability mechanisms, overlooked by the local stability analyses. Remark the radical difference in scale of the ordinates; the accumulation of local spatial growth rates is by far the main contribution to the gain.

The competition, which would settle the linear frequency selection, has two aspects: on the one hand, larger frequencies take longer to become unstable, while on the other hand, once unstable, they tend to grow faster. Figure 4 presents the gain, eq. (11), as a function of plate length L and frequency ω with a forcing location X_0 , optimised for each frequency. This optimal forcing location is found at the minimum of the gain, as in this way perturbations can avoid the upstream damping region, while benefiting from the longest possible region of sustained growth. It is almost equal to the critical streamwise distance for local linear instability x^c , only slightly modulated by the amplitude $|A(L)|$. Before this minimum, *i.e.* before perturbations can start growing, the maximum attainable gain is 1, resulting from a forcing located at the position of interest itself.

After setting a threshold for nonlinear saturation (in other words, an external perturbation amplitude, assuming nonlinearities kick in for amplitudes equal to one), our analysis results in a prediction for the Kapitza waves frequency. For example, $G_{\text{sat}}^2 = 10^{10}$ is first reached by a forcing of angular frequency 0.88. In dimensional quantities, for water, condensing on an incline of $\pi/4$ with an imposed cooling of 10 K, waves of frequency 11 Hz should saturate after around 46 cm. If the threshold is higher, *e.g.* thanks to lower ambient noise levels,

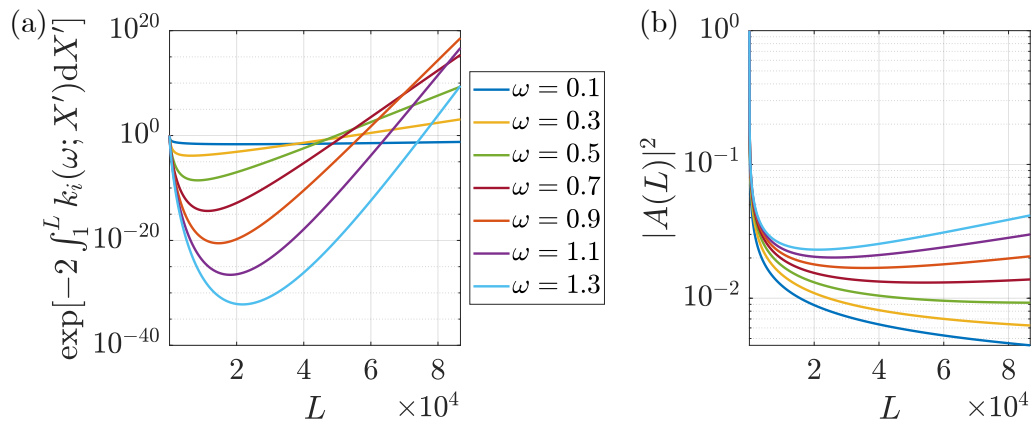


Figure 3: $\theta = \pi/4$, $Ja \approx 0.02$, $We \approx 8 \times 10^4$, $Pr \approx 7$, $X_0 = 1$. (a) Leading-order spatial gain. (b) WKBJ amplitude. The legend is common for both panels.

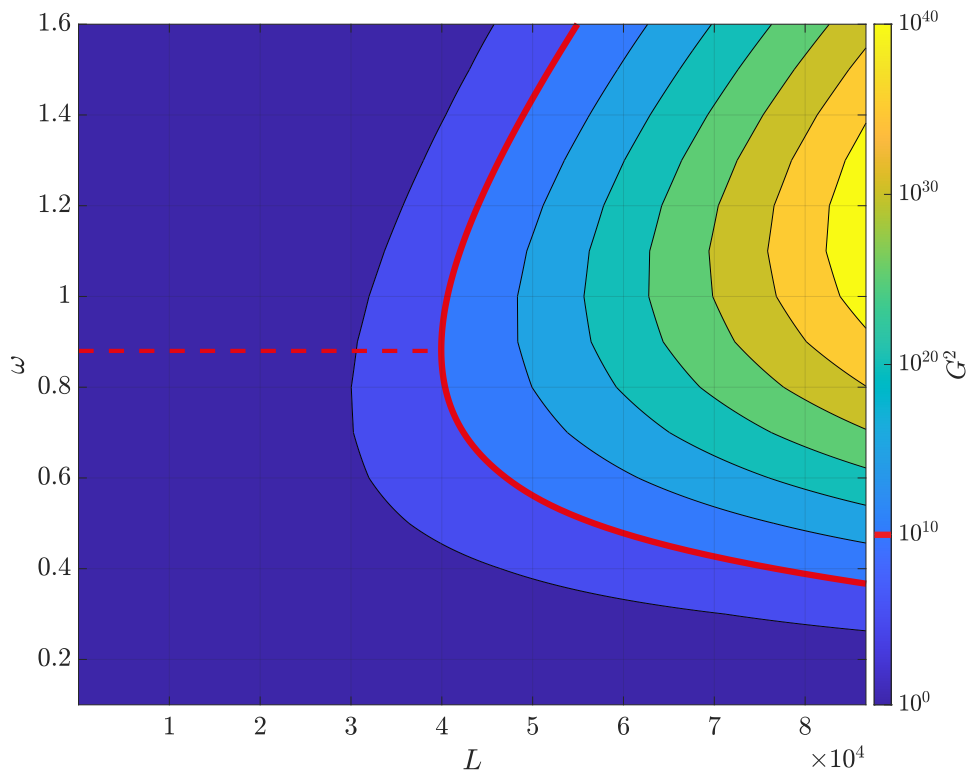


Figure 4: $\theta = \pi/4$, $Ja \approx 0.02$, $We \approx 8 \times 10^4$, $Pr \approx 7$. Optimal locally-forced gain as a function of plate length and frequency. The red solid line follows an isoline of $G^2 = 10^{10}$.

the predicted most amplified frequency increases.

Thereafter, a more realistic, spatially-distributed forcing can be considered in order to eventually improve the prediction. Our analysis can also be extended to other weakly non-parallel flows, for example the rain-fed film flow, which thickens as $x^{1/3}$.

References

- [1] A. ORON, S. H. DAVIS, AND S. G. BANKOFF, *Rev. Mod. Phys.* **69**(3), 931–980 (1997).
- [2] W. NUSSELT, *Z. Ver. Dtsch. Ing.* **60**(27), 541–546 (1916).
- [3] P. L. KAPITZA, *Zh. Eksp. Teor. Fiz.* **18**, 3–18 (1948).
- [4] P. HUERRE AND M. ROSSI, Hydrodynamic instabilities in open flows, *Hydrodynamics and nonlinear instabilities* / C. Godrèche and P. Manneville, (Cambridge University Press, 1998).

Condensation-induced self-patterning of a thin clayey layer. Impact on painted caves.

Jérôme Martin¹ and Frédéric Doumenc^{1,2}

¹ FAST Laboratory, Université Paris-Saclay, Orsay, France.

² UFR 919, Sorbonne Université, Paris, France

Corresponding author: martin@fast.u-psud.fr

The granular material lying on the humid walls of underground cavities can self-organize to form a wide variety of patterns, called vermiculations (see Ref.[1] and Fig1a). Understanding the formation of vermiculations is a major challenge in the context of the preservation of painted caves [2-3]. Indeed, vermiculations induce, during their formation, a migration of the pigments constituting the paintings. We address this challenging issue through the coupling of rheological characterization of the granular material collected on wall caves, and laboratory experiments reproducing mass transfert and chemical evolutions encountered in cave environments.

The rheological study showed that the granular material lying on cave walls forms a granular paste that behaves as a yield stress fluid [4]. The yield stress is due to colloidal interactions between clay particles present in the material. It depends on the chemical compositions of the water film present on the walls.

In order to reproduce vermiculations in laboratory, we carried out experiments on a thin layer (150 μm thick) of the clayey paste coated on a limestone substrate. These experiments demonstrated that self-patterning could be triggered by condensation. Under certain physicochemical conditions, condensation reduces the material yield stress to zero. This solid-to-liquid transition of the paste layer results in the paste flow and the formation of band structures (Fig. 1b) [5]. A systematic parametric study provides various scenarios leading to the formation of vermiculations, in line with the physicochemical properties of the clay present in the granular paste [4].

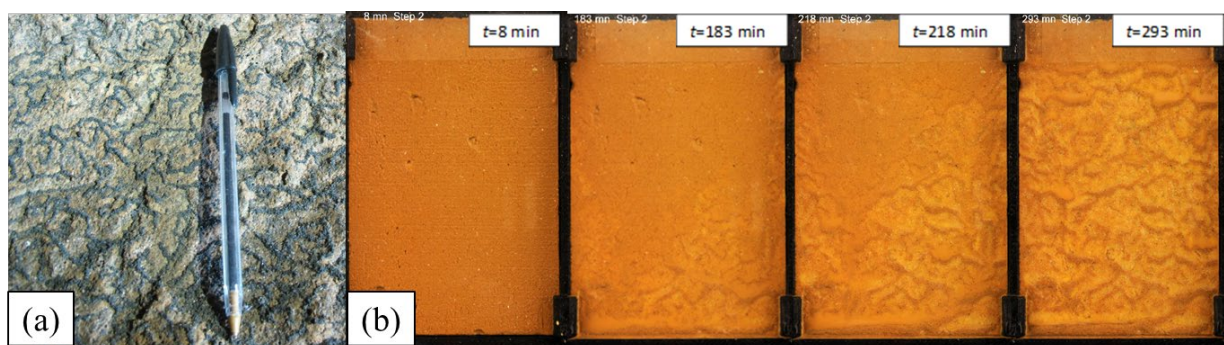


Fig. 1. (a) Vermiculations in the cave of Maillol (Dordogne, France). (b) Laboratory reproduction of vermiculations induced by condensation, on a limestone rock of 80×55 mm initially coated with a 150 μm thick layer of granular material collected in the cave of Maillol. The time elapsed since the initiation of condensation is indicated at the top left of each picture. .

References

1. A. Bini, M. Cavalli Gori, S. Gori, *Int. J. Speleol.*, **10**, 11-33 (1978).
2. J. Clottes, *Gallia préhistoire*, **24**, 525-570 (1981).
3. P. Freydier, E. Weber, J. Martin, P.Y. Jeannin, B. Guerrier, F. Doumenc, *Int. J. Speleol.*, **50**, 289-299 (2021).
4. P. Freydier, J. Martin, B. Guerrier, P.Y. Jeannin, F. Doumenc, *Rheologica Acta*, **58**, 675-685 (2019).
5. J. Martin, F. Doumenc, *Europhysics Letters*, **138**, 1301 (2022).

High and low fidelity models to understand the physics of air-knife coating

David Barreiro-Villaverde^{1,2}, Anne Gosset³, Marcos Lema¹ and Miguel A. Mendez²

¹ University of A Coruña, CITIC Research, Spain

² Environmental and Applied Fluid Dynamics, von Karman Institute, Sint-Genesius-Rode, Belgium

³ University of A Coruña, Campus Industrial de Ferrol CITENI, Spain

Corresponding author: david.barreiro1@udc.es

We combine high and low fidelity numerical techniques to analyze the undulation mechanism in air-knife coating, mostly governed by the two-way coupling between the planar gas jets and the coating film¹. This work focuses on improved similarity conditions with respect to the metallurgical process of galvanization, employing water as a working fluid. The high-fidelity model implements a Volume of Fluid (VOF) technique for the two-phase problem and Large Eddy Simulation (LES) for the treatment of turbulence in the gas jet. The low fidelity model consists in an Integral Boundary Layer (IBL) film model previously validated for the study of three-dimensional coating films on upward moving substrates^{2,3}. The present study extends the validation to air-knife coating, in which pressure gradients and shear stresses at the interface play an important role in the control of the film thickness and its smoothness. Multiscale modal analysis is applied to detect the flow structures responsible for the undulation in these flow conditions, paying special attention to the differences with respect to highly viscous liquids such as dipropylene glycol, studied in previous works.

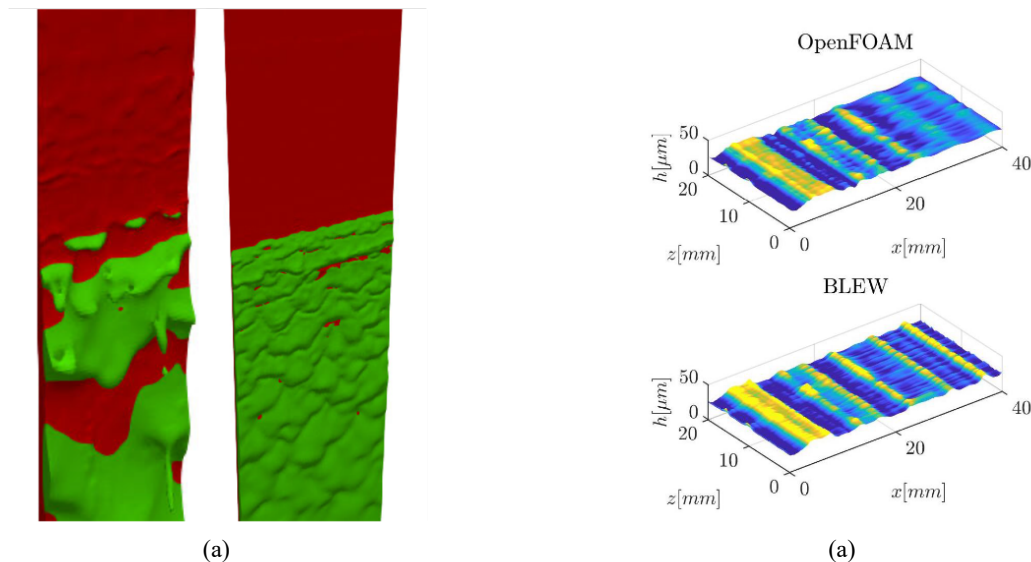


Fig. 1. 3D reconstruction of the liquid film with dipropylene glycol and water (a), and qualitative comparison between the undulation patterns obtained with the CFD simulations (OpenFOAM) and IBL model (BLEW) (b).

References

1. D. Barreiro-Villaverde, A. Gosset, and M. A. Mendez, *Physics of Fluids* **3** (2021).
2. M.A. Mendez, A. Gosset, B. Scheid, M. Balabane, and J.-M. Buchlin, *Journal of Fluid Mechanics* **911** (2021)
3. T. Ivanova, F. Pino, B. Scheid, M. A. Mendez, *Physics of Fluids* **1** (2021).

Analysis of edge formation in intermittent slot coating process

Sanghun Jee and Hyun Wook Jung

Department of Chemical and Biological Engineering, Korea University, Seoul 02841, Republic of Korea

Corresponding author: hwjung@grtrkr.korea.ac.kr

Slot coating is commonly used in industrial fields such as lithium-ion secondary batteries, fuel cells, and flat panel displays. As a pre-metered process, the precise control of coating thickness is possible by the relation of flow rate and web speed [1]. Recently, the importance of the intermittent pattern slot coating process, which has several advantages in the post-treatment stage after coating process, is being emphasized [2]. In the pattern slot coating process, however, it is rather difficult to control edges of a coating patch under flow startup and stop conditions. During the production of continuous discrete coating patches, the level control of start (leading) and end (trailing) edges should be performed, taking into account the liquid rheological properties and the residue residing on die lips after end operation [2].

In this study, the relationship between the die residual volume and flow directional edges was scrutinized through two-dimensional CFD simulations for intermittent flows in coating bead region. By performing CFD simulation in various conditions, we observed that the die residual volume shows an increasing trend as Capillary number (Ca) increases, and emerges only above a certain Ca threshold value ($Ca = 0.1$). End edge length (L_E) shows an opposite behavior in comparison to that of die residual volume with respect to Ca , and the presence of the die residual volume itself causes the difference between start edges of coating patches.

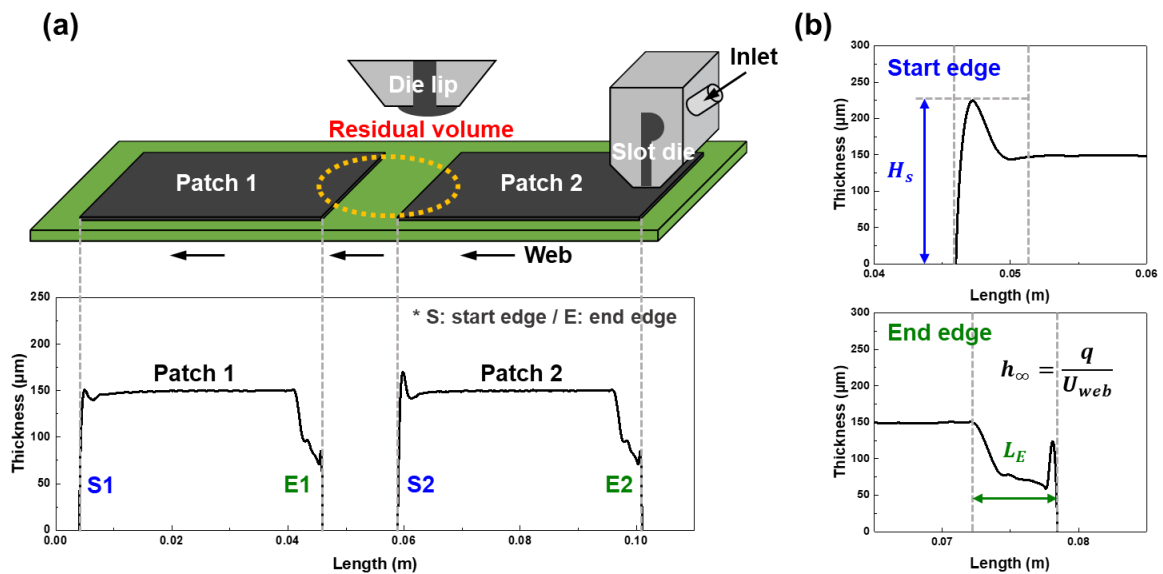


Fig. 1. (a) Overall process of intermittent slot coating and (b) parameters at start/end edges.

References

1. Park, J. S., Yoo, T., Chun, B., Lee, K. Y., & Jung, H. W., *J. Coat. Tech. Res.*, **19**, 35-47 (2022)
2. Diehm, R., Weinmann, H., Kumberg, J., Schmitt, M., Jurgen, F., Scharfer, P., & Schabel, W., *Energy Technol.*, **8**, 1900137 (2020)

About the production of catalyst layers for PEM-fuel cells and PEM-electrolysis

Philipp Quarz^{1,2}, Nadine Zimmerer^{1,2}, Philip Scharfer^{1,2}, Wilhelm Schabel^{1,2}

¹ Thin Film Technology (TFT), Karlsruhe Institute of Technology (KIT), Karlsruhe, Germany

² Material Research Center for Energy Systems (MZE), Karlsruhe Institute of Technology (KIT), Karlsruhe, Germany

Corresponding author: philipp.quarz@kit.edu, nadine.zimmerer@kit.edu,

Hydrogen technology is one of the key elements of the energy revolution [1]. Via electrolyzers (excess) capacities from renewable energies can be stored chemically in a fuel, e.g. green hydrogen, and can be used on demand by using a fuel cell. Polymer electrolyte membrane water electrolyzers (PEM-WE) and polymer electrolyte membrane fuel cell (PEM-FC) are a promising approach because of their good partial load capacity and their simple stack design. [2]

The energy-converting reactions take place at the heart of the PEM-FC or PEM-WE, the catalyst coated membrane (CCM), consisting of a perfluorosulfonic acid (PFSA) membrane, e.g. NafionTM, and a catalyst layer coated on both sides. The catalyst layers must meet several specifications, such as a high reactive surface area, suitable porosity and a high number of multiphase boundaries [2]. The material and production of the respective CCMs of both systems, PEM-FC and PEM-WE, contribute decisively to the still high costs of the systems [3]. Therefore, there are two investigated approaches to optimize the production and the catalyst layer itself.

The first addresses the reduction of processing steps by coating the catalyst layers directly onto the PFSA membrane. In the production of CCM, direct membrane coating requires one fewer process step than the (industrially) established decal process and is therefore advantageous. However, the membrane direct coating poses a number of challenges including the solvent interactions and in particular swelling of the respective membranes used in contact with solvents from the catalyst inks [4]. These interactions cause the catalyst layer to form cracks. Understanding the mass transport happening during the CCM manufacturing via membrane direct coating helps adapting and optimising the existing manufacturing process to the new materials and process parameters needed. Adjustments in ink formulation and drying conditions are here focus of the investigation.

The second possibility for cost reduction aims at tailoring the microstructure of the catalyst layers. Many electrochemically active surfaces and so-called triple phase boundaries are necessary for the systems to function [2]. The number of these depends strongly on the microstructure of the catalyst layer. The microstructure is formed during the film solidification (drying step) [5-7]. For this reason, the investigation of the drying of the multicomponent ink is the focus of this approach including effects such as selectivity of the drying. During the drying of the catalyst inks (also on inert substrates), defects and cracks are formed in the film structure [8]. By linking drying parameters with electrode properties, the manufacturing process is to be further improved. The microstructure can also be further optimised by, for example, a multilayer-structured electrode design with multilayers of single layers with specifically tailored properties. Thus, gradients of porosity, catalyst loading and ionomer content can be achieved within the electrode.

In the approaches, both the material-specific and the process-related challenges are to be highlighted. The aim is to point out possible solutions for an optimisation of the cost-intensive fuel cell and electrolyser catalyst layers. With the investigation of the fundamental mechanism during the individual steps of the production chain, a deep understanding of the complete interdependent influenced processes is generated. Due to the different duties, the specific requirements between PEM-WE and PEM-FC are somewhat different. However, many of them are also similar and can be influenced to the same extent by the process, so that essential findings from PEM-FC can be transferred to PEM-WE and vice versa.

References

1. EU-Commission, Communication COM/2020/299 (2020).
2. U. Schelling, R. Zahoransky (Ed.), *Energietechnik 8. Auflage* (Springer Fachmedien, Wiesbaden, 2019).
3. U.S. DRIVE, Fuel Cell Technical Team Roadmap (2017).
4. M. B. Dixit, B. A. Harkey, F. Shen, K. B. Hatzell, *J. Electrochem. Soc.*, 165, 264-271 (2018).
5. J. Kumberg, W. Bauer, J. Schmatz, R. Diehm, M. Tönsmann, M. Müller, K. Ly, P. Scharfer, W. Schabel, *Energy Technology*, Vol 9: 2100367 (2021).
6. S. Jaiser, M. Müller, M. Baunach, W. Bauer, P. Scharfer, W. Schabel, *Journal of Power Sources*, Vol. 318, 210-219 (2016).
7. J. Kumberg, M. Müller, R. Diehm, S. Spiegel, C. Wachsmann, W. Bauer, P. Scharfer, W. Schabel, *Energy Technology*, Vol 7: 1900722 (2019).
8. F. Scheepers, A. Stähler, M. Stähler, M. Carmo, W. Lehnert, D. Stolten, *J Coat Technol Res* (2019).

Drying of slurry for manufacturing of battery electrodes: microfluidic studies of binder migration

Djibrilla Mounkaila Noma¹ and Jean-Baptiste Salmon¹

¹ *Laboratory of the Future (LOF) UMR 5258, CNRS, Solvay, University of Bordeaux, Pessac, France*

Corresponding author: djibrilla.noma-ext@solvay.com

During manufacturing of battery electrodes, the wet processing is confronted with some problems such as microstructural defects due to the drying process [1,2]. These defects not only affect the microstructure in terms of adhesion, but can also impair the electrochemical performance of the cells.

In our research, we studied the drying of slurry for manufacturing of battery electrodes (anodes). One of the challenges is to understand the role and impact of the migration of polymeric and colloidal additives during the drying process, both on the evaporation kinetics of the manufacturing process, but also on the microstructure.

For this purpose, the migration of binders (SBR: Styrene-Butadiene-Rubber and CMC: CarboxyMethylCellulose) is experimentally investigated with microfluidic approaches [3]. The system consists of microfluidic chips in a PDMS block. By using pervaporation of water through the PDMS, we are able to obtain a solidification front along the channel. Thus, we observed for SBR, the existence of different regions downstream of the front. First, an area characterized by shear bands with cracking, as discussed in previous research work [4]. This is followed by an area of delamination and then a completely dry region. To understand these observations, we used Raman spectrometry to probe the content of the different zones. Similar experiments have been carried out for CarboxyMethylCellulose. Finally, experiments are underway to determine the mutual diffusion coefficient of these binders, using infrared transmittance.

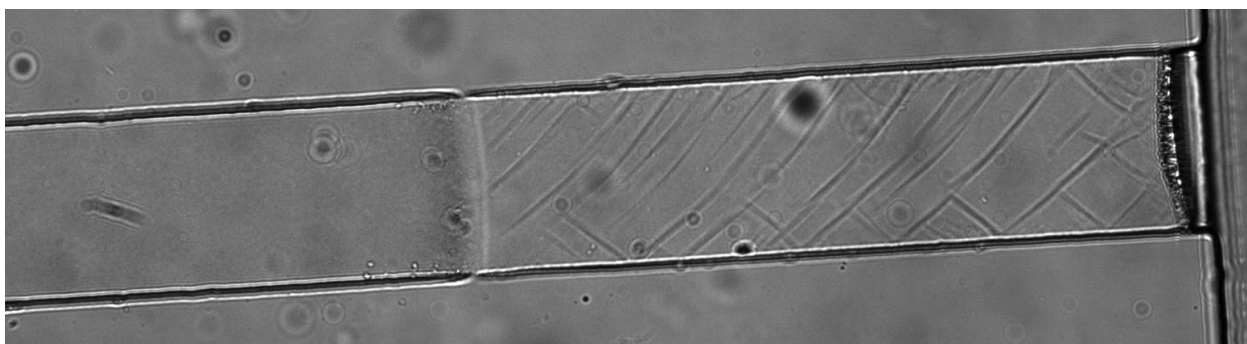


Fig. 1. Microscope image of a solidification front.

References

1. Jaiser, Stefan, et al. "Experimental investigation into battery electrode surfaces: The distribution of liquid at the surface and the emptying of pores during drying." *Journal of colloid and interface science* 494 (2017): 22-31.
2. Hawley, W. Blake, and Jianlin Li. "Electrode manufacturing for lithium-ion batteries—Analysis of current and next generation processing." *Journal of Energy Storage* 25 (2019): 100862.
3. Bacchin, Patrice, Jacques Leng, and Jean-Baptiste Salmon. "Microfluidic evaporation, pervaporation, and osmosis: from passive pumping to solute concentration." *Chemical Reviews* 122.7 (2021): 6938-6985.
4. Routh, Alexander F. "Drying of thin colloidal films." *Reports on Progress in Physics* 76.4 (2013): 046603.

Investigation of microstructure formation and pore emptying in relation to drying conditions and particle properties

Linus Janning, Julian Klemens, David Burger, Philip Scharfer, Wilhelm Schabel

Thin Film Technology (TFT), Material Research Center for Energy Systems (MZE), Karlsruhe Institute of Technology (KIT), Karlsruhe, Germany

Corresponding author: linus.janning@googlemail.com

During processing of slurry-based battery electrodes, one challenge is the migration of the binder during drying and microstructure formation. The migration takes place mainly during the so-called pore emptying of the formed capillary network and leads to the inhomogeneous distribution of the binder. This results, for example, in a reduction of the adhesion force and an increase of the ionic as well as electrical resistances due to fast drying. By changing influencing parameters and measuring the resulting electrode properties, it is possible to deduce the microstructure formation and the progress of binder migration. Some influencing parameters such as the drying rate, the heat- and mass transfer coefficient and the effect of different particle morphologies have already been investigated in the literature but are not fully understood mechanistically [1-3]. There are, for example, material systems that show no or a lower degree of binder migration even though they were produced under identical conditions (Fig. 1). This work is intended to provide a basic understanding of the occurrence and reduction of binder migration.

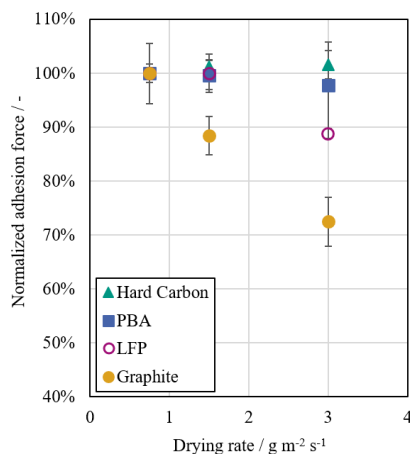


Fig. 1. Adhesion force measurements of different active materials for lithium-ion and sodium-ion batteries. The adhesion force is normalized to the adhesion force at the lowest drying rate investigated

Findings on microstructure formation and the influence of process conditions as well as slurry properties on the pore emptying of battery electrodes will be comparatively analyzed. A study is presented linking the influence of specifically selected drying conditions and slurry properties with drying curves, pore emptying and properties of the dry electrode.

As a systematic approach, the distinct influences of drying rate, film temperature and composition are investigated by measurements of adhesion force and linked to the investigation of the drying process by means of gravimetric measurements of drying curves and optical investigation of the drying through a glass substrate. The evolution of the pore structures as well as the contact area and structure of the dry coating on glass are quantitatively evaluated. The study will be linked to data for different active material systems with other particle morphologies and particle sizes to extend the understanding of microstructure formation and binder migration for new materials as well.

This work was funded by the Deutsche Forschungsgemeinschaft (DFG, German Research Foundation) under Germany's Excellence Strategy – EXC 2154 – Project number 390874152 (POLiS Cluster of Excellence) and contributes to the research performed at CELEST (Center for Electrochemical Energy Storage Ulm Karlsruhe) and MZE (Material Research Center for Energy Systems).

References

1. S. Jaiser, et al., P. Scharfer, W. Schabel, Impact of drying conditions [...], *Drying Technology* **35**, 1807-1817 (2017).
2. J. Kumberg, et al., P. Scharfer, W. Schabel, Reduced Drying Time of Anodes [...], *Energy Technology* **9**, 2100367 (2021).
3. A. Altvater, et al., P. Scharfer, W. Schabel, (Near-) Infrared Drying of Lithium-Ion Battery Electrodes [...], *Energy Technology* **4**, 2200785 (2023).

Mass transport through battery electrode coatings during post-drying and humidity management

Philipp Barbig, Thilo Heckmann, Philip Scharfer, Wilhelm Schabel

Thin Film Technology (TFT), Material Research Center for Energy Systems (MZE), Karlsruhe Institute of Technology (KIT), Karlsruhe

Corresponding author: thilo.heckmann@kit.edu

For competitive battery cells, an important prerequisite is energy savings in the cell production. An essential cost factor in the production process of Lithium-ion batteries poses the moisture management and post drying. In this process, adsorbed moisture from the air desorbs from the compounds of the battery according to the dew-point temperature, pressure, temperature, and heat- and mass-transfer coefficients of the post dryer.[1] Literature has revealed a connection between electrochemical performance and the remaining moisture content.[2] If not sufficiently reduced prior to cell assembly, the adsorbed moisture reacts with the electrolyte during the operation of the battery cell, which leads to its degeneration. Therefore, the mass transport processes during the vacuum post-drying step need to be understood completely, to control and adjust the moisture in the compounds of the battery cost-efficiently. A precise and comprehensive analysis of the mass transport within the multi-component and porous electrodes via experiments allows for process optimization of the moisture management.

The focus of this study lies on the mass transport in the structure of an electrode and its influence on the diffusion as water desorbs from the porous media at different pressures. The electrode structure consists of various components that affect the mass transport at different length scales (e.g., gas phase mass transport with Knudsen and Stefan diffusion). These mass transport mechanisms respond differently to system parameters such as pressure and temperature. This circumstance is exploited to draw conclusions about the governing mass transport mechanism. A magnetic suspension balance measures the desorption curves at defined constant pressures and temperatures. The simulation of the experiments considers this desorption at the different scales and validates the physical models utilized to describe the process.

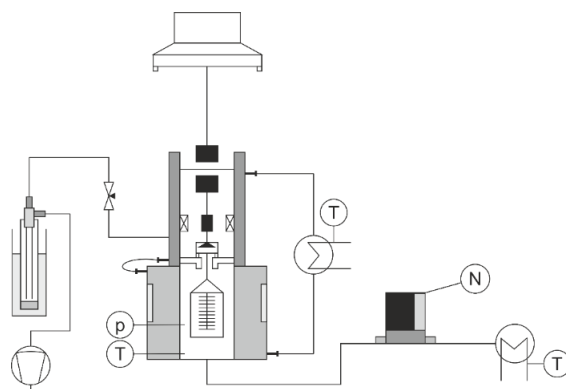


Figure 1: Experimental set up to investigate mass transport phenomena at defined pressure, temperature, and relative humidity.

This work contributes to the research performed at CELEST (Center for Electrochemical Energy Storage Ulm Karlsruhe) and the Material Research Center for Energy Systems (MZE). The authors would like to acknowledge financial support of the Federal ministry of Education and Research (BMBF) via the ProZell cluster project “Epic” (Grant No. 03XP0295A).

References

1. J. Eser, et al., P. Scharfer and W. Schabel, Moisture Adsorption Behaviour [...], *Energy Technology* **8**, 1801162 (2020)
2. M. Stich, et al., A. Bund, Drying and moisture resorption behaviour of [...], *Journal of Power Sources* **364**, 84-91 (2017)

Multi-component drying of electrolyte solvents from porous electrodes and separators for recycling processes of lithium-ion batteries

L. Lödige^{1,2}, T. Heckmann^{1,2}, P. Scharfer^{1,2}, W. Schabel^{1,2}

¹ Thin Film Technology (TFT)

² Material Research Center for Energy Systems (MZE)

Karlsruhe Institute of Technology (KIT), Karlsruhe, Germany

Corresponding author: lukas.loedige@kit.edu

The successful development of a sustainable and rapidly growing lithium-ion battery (LIB) market requires efficient recycling technologies for end-of-life batteries. A promising process approach in terms of recovery yield and quality of battery materials combines mechanical comminution and separation steps with hydrometallurgical treatment of the active material powder removed from the conductor foils. [1] During the comminution of the LIB cells, a mixture of liquid organic solvent electrolytes with the conductive Lithium (Li) salt diluted therein is released. The electrolyte solvents represent a large proportion of material costs and have a detrimental influence on the recovery rate in subsequent process steps. [2, 3] Therefore, these solvents have to be removed from the crushed material by drying towards low residual solvent contents, with the possibility of recovery and reuse in cell production.

From an economic and ecological point of view, the optimization of the drying time and conditions is of major interest. For this purpose, in this study the multi-component drying process is investigated in order to develop a deep understanding. On the one hand, the complexity is increased in particular by the presence of a multi-component mixture with mutual interactions of the individual components as well as their different thermodynamic and material transport properties. On the other hand, the precise consideration of the influence of the porous structure and the adsorption and absorption behavior of the comminuted material on the drying kinetics is a challenging task that requires further efforts. [4] Drying experiments are conducted to obtain data and information about the mass transport kinetics in a material system with overlaying diffusion and sorption mechanisms. Various measurement techniques capture (component-specific) drying curves and quantify the electrolyte solvents before and during drying. [5, 6, 7] First results on the dependence of drying kinetics on process conditions will be presented. The experimental results are condensed into a predictive simulation model of critical process times and the optimization as a function of the drying boundary conditions imposed by the process parameters during drying, resulting in energy and costs reductions. In the end, the findings gained about the drying in the LIB recycling can be used for the improvement of existing and the development of innovative industrial scale plants.

[1] Marshall, Jean; Gastol, Dominika; Sommerville, Roberto; Middleton, Beth; Goodship, Vanessa; Kendrick, Emma (2020): Disassembly of Li Ion Cells—Characterization and Safety Considerations of a Recycling Scheme. In: *Metals* 10 (6), S. 773. DOI: 10.3390/met10060773.

[2] Harper, Gavin; Sommerville, Roberto; Kendrick, Emma; Driscoll, Laura; Slater, Peter; Stolkin, Rustam et al. (2019): Recycling lithium-ion batteries from electric vehicles. In: *Nature* 575 (7781), S. 75–86. DOI: 10.1038/s41586-019-1682-5.

[3] Schmuch, R. et al. (2018) Performance and cost of materials for lithium-based rechargeable automotive batteries. *Nat. Energy* 3, 267–278.

[4] Kumberg, Jana; Baunach, Michael; Eser, Jochen; Altvater, Andreas; Scharfer, Philip; Schabel, Wilhelm (2021): Investigation of Drying Curves of Lithium-Ion Battery Electrodes with a New Gravimetric Double-Side Batch Dryer Concept Including Setup Characterization and Model Simulations. In: *Energy Technology* 9, 2000889. DOI: 10.1002/ente.202000889

[5] Jaiser, Stefan; Friske, Anatolij; Baunach, Michael; Scharfer, Philipp; Schabel, Wilhelm (2017): Development of a three-stage drying profile based on characteristic drying stages for lithium-ion battery anodes. In: *Drying Technology* 35:10, 1266-1275. DOI: 10.1080/07373937.2016.1248975

[6] Eser, Jochen; Deichmann, Birthe; Wirsching, Tobias; Merklein, Lisa; Müller, Marcus; Scharfer, Philip; Schabel, Wilhelm (2020): Diffusion kinetics of water in graphite anodes for Li-ion batteries. In: *Drying Technology* 40:6, 1130-1145. DOI: 10.1080/07373937.2020.1852568

[7] Eser, Jochen; Wirsching, Tobias; Weidler, Peter; Altvater, Andreas; Börnhorst, Tobias; Kumberg, Jana; Schöne, Gerrit; Müller, Marcus; Scharfer, Philip; Schabel, Wilhelm (2020): Moisture Adsorption Behavior in Anodes for Li-Ion Batteries. In: *Energy Technology*, 8, 1801162. DOI: 10.1002/ente.201801162

Acknowledgements:

This work contributes to the research performed at CELEST (Center for Electrochemical Energy Storage | Ulm & Karlsruhe) and Material Research Center for Energy Systems (MZE). The authors would like to acknowledge financial support of the Federal ministry of Education and Research (BMBF) via the greenBatt cluster-project “LOWVOLMON” (Grant number: 03XP0354C).

CFD simulation of slot-die coating for single- and multilayered lithium-ion battery electrodes in OpenFOAM

A. Hoffmann^{1,2}, S. Spiegel^{1,2}, T. Heckmann^{1,2}, P. Scharfer^{1,2}, W. Schabel^{1,2}

¹Thin Film Technology (TFT), Karlsruhe Institute of Technology (KIT), Karlsruhe, Germany

²Material Research Center for Energy Systems (MZE), KIT, Karlsruhe, Germany

Corresponding author: alexander.hoffmann@kit.edu

The slot-die coating process is a widely used method for producing wet-processed lithium-ion battery electrodes. This technique allows for processing a broad range of liquids with respect to rheological and other properties while maintaining a high level of quality in terms of the homogeneity of the wet film height distribution across the coating width. However, despite the apparently straightforward application method, several scientific questions about the process remain unresolved. For example, in single-layer coatings, the coating edges, whose geometry strongly depends on the process conditions, are worth mentioning [1–3]. Furthermore, the flow conditions in the liquid bridge between the substrate and the die lips are critical to the stability of the coating. Therefore, detailed information about the flow profiles for different positions and orientations of the slot die and potentially optimized geometries of the die lips is of great interest. These questions can also be extended to multilayer coatings, where, in addition to the above-mentioned relationships, it should be noted that the general coating stability cannot be calculated by simple analytical or iterative models, as the equations become highly non-linear [4].

To investigate these issues, a computational fluid dynamics (CFD) model is employed [5]. The single-layer model in OpenFOAM serves as the basis, encompassing the slot-die coating process in two and three dimensions for shear-thinning fluids, using the volume-of-fluid method with a Cross-Power-Law approach. Additionally, special features are included, such as dynamic mesh refinement, which works in 2D and 3D in this case, in contrast to the standard method. Furthermore, the processing power of each processor is monitored and, if necessary, redistributed to minimize overall computational time and requirements. Moreover, the wetting behavior is described using a specially developed boundary condition to avoid unphysical air entrainment that occurs at the dynamic contact line. In Figure 1, rendered simulation data for single-layer coatings are shown in 2D and 3D.

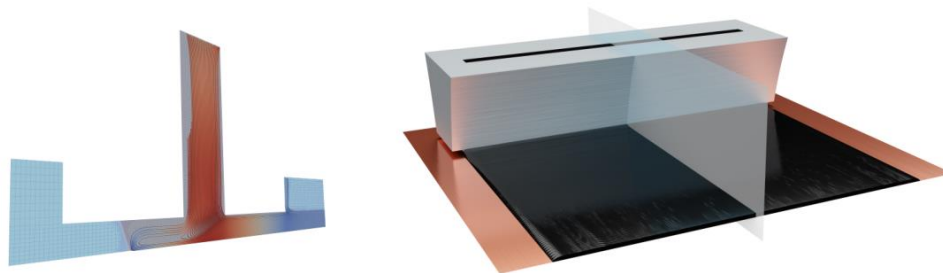


Figure 1: Rendered simulation data from 2D (left) and 3D (right) simulations for single-layer coatings.

In the next step, the model was extended to multilayer coatings. This allows for the simulation-based investigation of two- and three-dimensional effects that lead to defects, whose root causes are experimentally challenging to measure and require significant experimental effort. Additionally, fundamental insights into the stability of multilayer coatings can be derived and compared with experimental observations.

This work contributes to the research performed at CELEST (Center for Electrochemical Energy Storage Ulm Karlsruhe) and Material Research Center for Energy Systems (MZE) and is funded by the BMBF under Project ID 03XP0242C (Sim4Pro).

Keywords

slot die, coating, multilayer, CFD, OpenFOAM, dynamic mesh refinement, wetting behaviour

References

- 2016 - Schmitt et al.: A half-empirical model to predict heavy edges in slot die coating
- Spiegel, S., Hoffmann, A., Klemens, J., Scharfer, P., Schabel, W.: Optimization of edge quality in the slot-die coating process of high-capacity lithium-ion battery electrodes. *Energy Tech* (2022). <https://doi.org/10.1002/ente.202200684>
- Spiegel, S., Heckmann, T., Altvater, A., Diehm, R., Scharfer, P., Schabel, W.: Investigation of edge formation during the coating process of Li-ion battery electrodes. *J Coat Technol Res* (2022). <https://doi.org/10.1007/s11998-021-00521-w>
- Schmitt, M., Raupp, S., Wagner, D., Scharfer, P., Schabel, W.: Analytical determination of process windows for bilayer slot die coating. *J Coat Technol Res* (2015). <https://doi.org/10.1007/s11998-015-9701-4>
- Hoffmann, A., Spiegel, S., Heckmann, T., Scharfer, P., Schabel, W.: CFD model of slot die coating for lithium-ion battery electrodes in 2D and 3D with load balanced dynamic mesh refinement enabled with a local-slip boundary condition in OpenFOAM. *J Coat Technol Res* (2022). <https://doi.org/10.1007/s11998-022-00660-8>

Data-driven modeling-based design of dual-shim configuration for uniform coating of non-Newtonian liquids in the PEMFC slot coating process

Donguk Kim, Jin Seok Park and Hyun Wook Jung

Department of Chemical and Biological Engineering, Korea University, Seoul 02841, Republic of Korea

Corresponding author: hwjung@grtrkr.korea.ac.kr

Slot coating processes have been widely utilized in many industries such as lithium-ion secondary batteries and fuel cells due to their ability to rapidly produce functional coating films with uniform thickness. As a pre-metered coating method, the coating thickness through the slot coating process can be simply determined by the mass balance between the flow rate and web speed, irrespective of the properties of the liquid being used [1]. Optimal design of the manifold within the slot die is necessary to ensure uniform flow distribution of coating liquid in the cross-web direction at the die exit [2,3]. Also, the shims or spacers can be modified to achieve coating uniformity, not replacing the slot die with specialized manifold geometry [4]. In the slot coating process for a proton exchange membrane fuel cell (PEMFC), a somewhat careful shim design is required due to the severe shear-thinning property of coating liquids under low flow rate conditions. Therefore, in this study, an optimal "dual-shim" configuration was designed for the uniform coating flow in a practical PEMFC slot coating process. Non-Newtonian PEMFC coating liquids were applied to the three-dimensional CFD simulations for interpreting internal die flows. While dual-shim configuration is an effective strategy for uniform coating, optimizing shim geometry for practical applications can be challenging due to the complexity of design parameters. Consequently, a data-driven modeling approach was implemented to improve the dual shim configuration for the given system. A neural network trained using sets of CFD simulation data was able to predict the outlet velocity profile of a dual-shim configuration and, moreover, find the optimal dual-shim configuration that can satisfy the velocity deviation criterion.

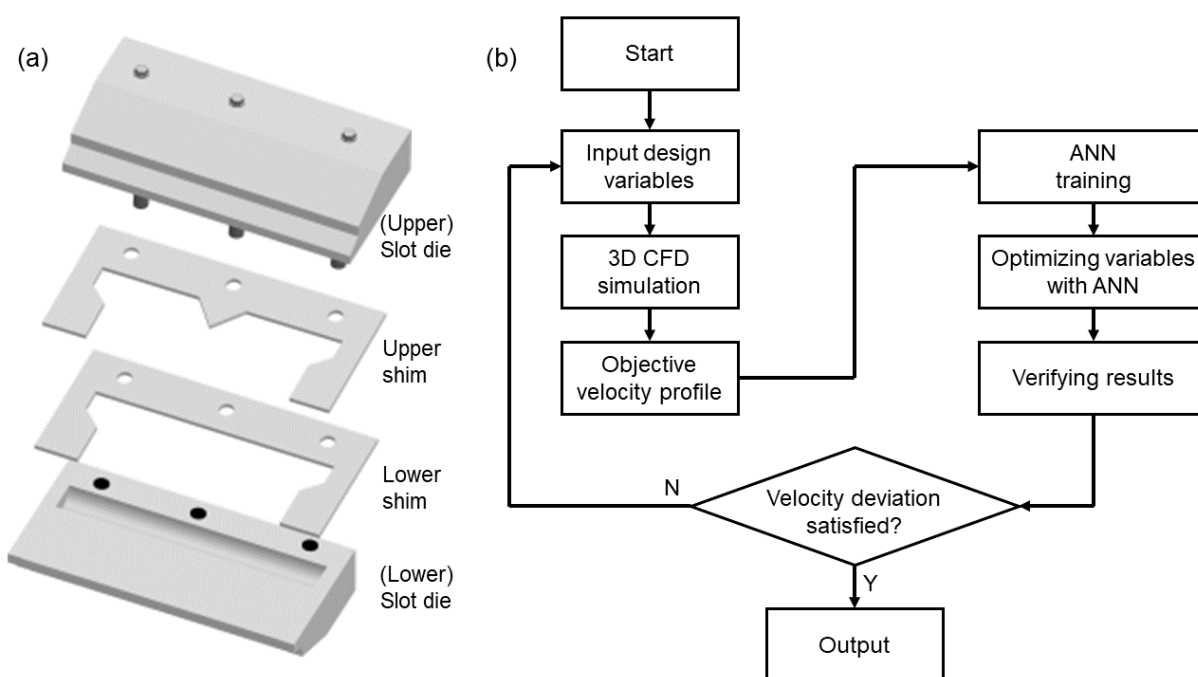


Fig. 1. (a) Schematic diagram on dual shim configurations and (b) flowchart of the optimal die design process.

References

1. Kistler S. F. and Schweizer P. M., *Liquid film coating: scientific principles and their technological implications*, (Springer, Berlin, 1997)
2. Sartor L., *Slot coating: Fluid mechanics and die design*, PhD thesis, University of Minnesota (1990)
3. Lee S. H., Koh H.J., Shim S. H., Jung H. W. and Hyun J. C., *An optimal die design for the coating uniformity of non-Newtonian liquids in slot coating process*, *Korean Chemical Engineering Research*, 49(3), 314-319 (2011)
4. Jin G. L., Ahn W. G., Kim S. J., Nam J., Jung H. W. and Hyun J. C., *Effect of shim configuration on internal die flows for non-Newtonian coating liquids in slot coating process*, *Korea-Australia Rheology Journal*, 28, 159-164 (2016)

Multi-stage drying of battery electrodes and comparison of drying process and energy efficiency with NIR and laser energy input

Julian Borho^{1,2}, Andreas Altvater^{1,2}, Philip Scharfer^{1,2}, Wilhelm Schabel^{1,2}

¹ Thin Film Technology (TFT), Karlsruhe Institute of Technology (KIT), Karlsruhe, Germany

² Material Research Centre for Energy Systems (MZE), Karlsruhe Institute of Technology (KIT), Karlsruhe, Germany

Corresponding author: julian.borho@kit.edu

Lithium-ion batteries are omnipresent in a multitude of applications, although further optimization is required concerning energy and power density as well as production costs and process efficiency. In the manufacturing process, the drying step is crucial and often speed-determining, since the selected drying conditions and parameters have a significant influence on the quality of the final cell. High drying rates lead to an increasingly inhomogeneous component distribution, which causes, for e.g., a reduction of the adhesion strength between active material and collector foil and a decreased cell performance. Isothermal drying tests indicate that the effect of binder migration is less marked at high film temperatures and low heat transfer coefficients. [1] To increase the film temperature, radiation-based energy input, such as with near infrared radiation (NIR) or laser (vertical-cavity surface-emitting laser, VCSEL), can be used. Here, heat and mass transfer are decoupled from each other to a certain extent, whereby higher film temperatures are achieved than with convective drying. Drying experiments performed with NIR confirm these considerations. [2] The relations between energy input, film temperature and electrode properties must be further investigated in order to develop a complete comprehension of the process, also taking economic aspects into account.

The study addresses the investigation of multi-stage drying of battery electrodes using NIR, with the objective of further understanding the role of film temperature and achieving a reduction in drying time without compromising electrode quality. Therefore, drying experiments were conducted on aqueous graphite-based anodes, whereby the energy input was selectively adjusted to defined drying stages, such as film shrinkage or the beginning of pore emptying (Fig. 1, left). To evaluate the distribution of the components, the dried electrodes were analyzed by determining the adhesive force. Moreover, pore emptying during drying was observed. The results show that a significant reduction in drying time can be achieved when the defined drying stages are complied with, without a negative effect on the adhesive strength of the electrode. It is also revealed that the film temperature is relevant for electrode properties in each phase of the drying process. To evaluate the efficiency of radiation-based energy input and its applicability to the industrial drying process, the efficiencies of drying with NIR and VCSEL are compared, and advantages and disadvantages regarding handleability and homogeneity of both methods are discussed.

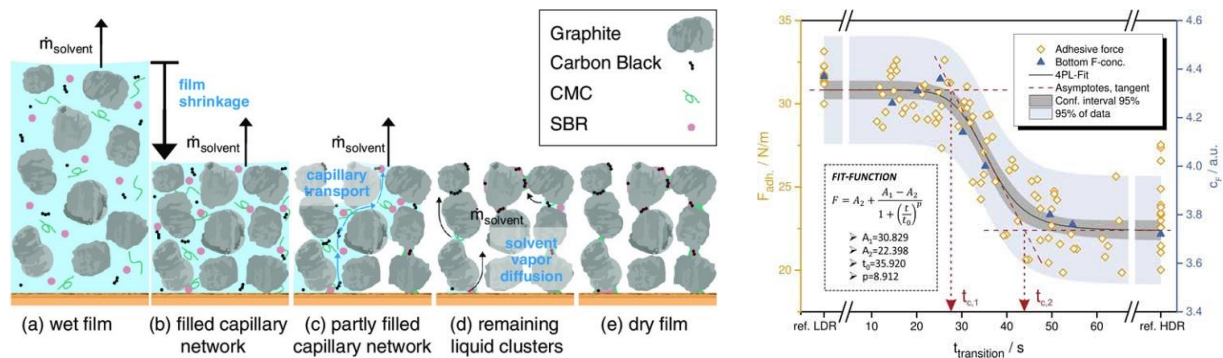


Fig. 1: Schematic illustration of the drying process of an aqueous anode (left) and the dependency of adhesion and binder concentration at the interface between active layer and current collector on transition time from high to low drying rates (right) [1, 3].

This work contributes to the research performed at CELEST (Center for Electrochemical Energy Storage Ulm Karlsruhe) and the Material Research Center for Energy Systems (MZE). The authors would like to acknowledge financial support of the Federal ministry of Education and Research (BMBF) via the ProZell cluster project “Epic” (Grant No. 03XP0295A) and the InZePro cluster project “InMiTro” (Grant No. 03XP0345).

References

1. J. Kumberg, et al., P. Scharfer and W. Schabel, Drying of Lithium-Ion Battery [...], *Energy Technology*, **7**, 1900722 (2019).
2. A. Altvater, et al., P. Scharfer and W. Schabel, (Near-) Infrared Drying [...], *Energy Technology*, 2200785 (2022).
3. S. Jaiser, et al., P. Scharfer and W. Schabel, Development of a three-stage [...], *Drying Technology*, **35**(5), 1266-1275 (2017).

Simulation study on cooperative motion of particles in a quasi-two-dimensional colloidal glass-forming liquid

Jinseong Yun, Byoungjin Chun and Hyun Wook Jung

Department of Chemical and Biological Engineering, Korea University, Seoul 02841, Republic of Korea

Corresponding author: hwjung@grtrkr.korea.ac.kr, byoungjin.chun@gmail.com

Colloidal suspensions of hard spheres exhibit exponential increases in viscosity and relaxation time as the packing fraction increases, eventually changing to a colloidal glass beyond a certain packing fraction [1,2]. Although these macroscopic properties provide insight into the dynamics of dense colloidal systems, they cannot fully offer information at the particle level. Near the glass transition, the particle is trapped in a "cage" formed by neighboring particles, and after a long period, particles in some regions escape the cage and exert string-like cooperative motion. This behavior is known as dynamical heterogeneity, where a system at different regions relaxes at different rates [2,3]. Such cooperative motion plays a crucial role in inducing glassy relaxation. It is challenging to quantify and analyze the cooperative motion of particles in glassy samples due to dynamical heterogeneity. Introducing local disturbances to a system can help observe the characteristics of glassy dynamics [4].

In this study, we designed a quasi-2D colloidal system employing hybrid lattice Boltzmann and molecular dynamics simulations [5,6], taking into account the hydrodynamic interactions. We scrutinized both the self-diffusion and pair diffusion of particles in relation to their packing fraction. Our results showed that above a certain packing fraction, the cooperative motion of particles was induced, and the size of these cooperative groups increased with increasing the packing fraction. To quantify the cooperative motion of particles, we perturbed the system at the particle level by applying a probing force to the center of the system, clarifying nonlinear dynamic behavior as a function of packing fraction. The packing fraction at which the maximum response was observed coincided with the packing fraction at which cooperative motion first appeared, meaning the onset of transition to a glassy system.

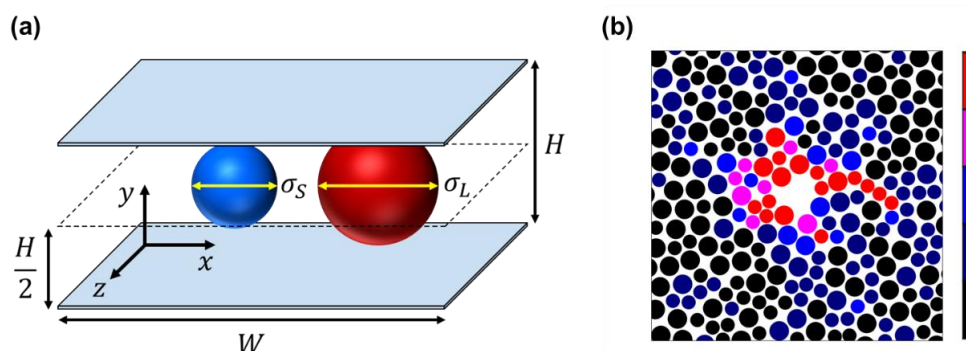


Fig. 1. (a) Schematic illustration of a quasi-2D system of a colloidal suspension. (b) Simulation snapshot immediately after applying the probing force to the center of the system. The color bar represents the displacements of the particles.

References

1. Binder, K., Kob, W., Glassy materials and disordered solids: An introduction to their statistical mechanics. (World scientific, 2011).
2. Hunter, G. L., Weeks, E. R., The physics of the colloidal glass transition. *Rep. Prog. Phys.*, **75**(6), 066501 (2012).
3. Weeks, E. R., Weitz, D., Properties of cage rearrangements observed near the colloidal glass transition. *Phys. Rev. Lett.*, **89**(9), 095704 (2002).
4. Li, B., Lou, K., Kob, W., Granick, S., Anatomy of cage formation in a two-dimensional glass-forming liquid. *Nature*, **587**(7833), 225-229 (2020).
5. Ahlrichs, P., Dünweg, B., Simulation of a single polymer chain in solution by combining lattice Boltzmann and molecular dynamics. *J. Chem. Phys.*, **111**(17), 8225-8239 (1999).
6. Lobaskin, V., Dünweg, B., A new model for simulating colloidal dynamics. *New J. Phys.*, **6**, 54-54 (2004).

Towards an optimized electrode production - Recent approaches in flexibility and efficiency

J. Mohacsi^{1,2}, K. Ly^{1,2}, P. Scharfer^{1,2}, W. Schabel^{1,2}

¹ Thin Film Technology (TFT), Karlsruhe Institute of Technology (KIT), Karlsruhe, Germany

² Material Research Center for Energy Systems (MZE), KIT, Karlsruhe, Germany

Corresponding author: jonas.mohacsi@kit.edu and kevin.ly@kit.edu

Lithium-ion batteries have become a crucial aspect of our daily lives owing to their high energy and power density. As electro-mobility gains momentum, lithium-ion batteries are expected to play a pivotal role in this domain. However, the automotive industry and battery research face several challenges in meeting the demand for higher performance, cost efficiency, and safety. This poster focuses on two different approaches to optimize electrode production in terms of flexibility and efficiency.

While current production systems for battery cells churn out standardized high-quality cells, they lack the necessary adaptability to meet changing customer requirements or production conditions, such as varying materials or formats. To address this issue, one approach aims to develop a flexible manufacturing process that can accommodate different formats, materials, and quantities. The project's primary focus is the development of a fully automated battery production system that uses a single sheet batch process based on robot cells. By placing the production modules in microenvironments, the production process can take place under controlled air conditions, ensuring optimal quality control.

When it comes to state-of-the-art electrodes, the drying process is one of the most expensive steps in the production process. Another approach aims to reduce solvent content during electrode processing, thus increasing the cost-efficiency of battery manufacturing. By reducing the solvent content and utilizing granules in battery paste manufacturing, the storage stability of produced electrode pastes can be extended to several weeks, allowing for greater production flexibility and decoupling of paste and electrode production. To fully understand the drying process, it's essential to investigate the influence of highly concentrated particulate granular systems on the process. Factors such as pore structure, film consolidation, and binder migration have a significant impact on the drying process, and in-depth fundamental studies will be conducted to elucidate these phenomena.

Acknowledgements:

This work contributes to the research performed at CELEST (Center for Electrochemical Energy Storage Ulm Karlsruhe) and Material Research Center for Energy Systems (MZE). The authors would like to acknowledge financial support of the Federal ministry of Education and Research (BMBF) via the InZePro cluster-projects "AgiloBat2" (Grant number: 03XP0369A) and "GranuProd" (Grant number: 03XP0344C).

Experimental characterization of the rivulets in a liquid film down an inclined plane

Sofia Fraga Ludeiro¹, Marcos Lema², David Barreiro-Villaverde², Anne Gosset¹

¹ University of A Coruña, Campus Industrial de Ferrol, CITENI, Spain

² University of A Coruña, CITIC Research, Spain

Corresponding author: anne.gosset@udc.es

When subjected to mass forces (gravity or centrifugal), or shear stress (due to a tangential airflow or surface tension gradient), a continuous liquid film is susceptible to separate into rivulets. This topic covers a broad range of applications, from the most academic test cases (film flowing down an incline plane) to more industrial applications (spin coating, icing on aerodynamic surfaces, surface cooling in industrial processes...), in which the presence of rivulets affects the surface of heat and mass exchange between the substrate, the liquid and the ambient. This poster focuses on the experimental characterization of the breakup of a liquid film along an incline into rivulets.

In this flow configuration, the advancing contact line is sensitive to transverse perturbations, due to surface irregularities for example, which may perturb the contact angle. Most references in literature deal with constant volume flows, in which a given volume of fluid is released on the surface, and the resulting film thins with time. We can cite the studies of Silvi and Dussan¹, de Bruyn², Veretennikov et al.³ and Hocking et al.⁴. These authors underline the existence of two main types of rivulet patterns: with highly wetting fluids, sawtooth rivulets are found, while with partially wetting fluids, they take the shape of fingers with parallel sides. As for constant flux flows, characterized by auto-similar velocity profiles within the film, only one study is reported, from Johnson et al.⁵. No systematic experimental study was published since them, and theoretical and numerical analysis still use this database for validation, for example in ⁶ and ⁷. This work intends at reproducing and extending this database with a wider range of fluids and flow conditions. A light absorption technique is used for the characterization of the thickness distribution, and image processing techniques for the determination of the relevant parameters. In particular, the rivulet wavelength and width, as well as the film thickness at breakup will be presented as a function of the capillary and Reynolds numbers. They will be confronted to the empirical correlations proposed by Johnson et al.⁵.

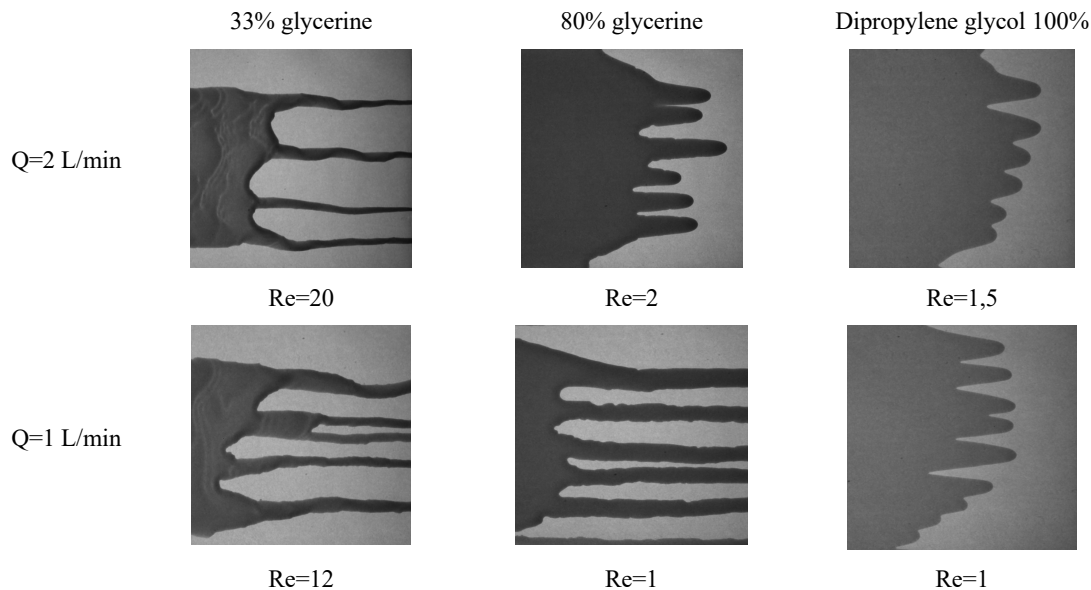


Fig. 1. Visualization of the rivulet patterns in different conditions and for different fluids.

References

1. N. Silvi and E. B. Dussan V, *Phys. of Fluids* **28(1)**, 5–7 (1985).
2. L. M. Hocking, W. R. Debler, and K. E. Cook, *Phys. of Fluids* **11(2)**, 307–313 (1999).
3. I. Veretennikov, A. Indeikina, and H.-C. Chang, *J. Fluid Mech.* **373**, 81–110 (1998).
4. J. R. de Bruyn, *Physical Review A* **46(8)**, R4500 (1992).
5. M. Johnson, R. A. Schluter, M.J. Miksis, and S. G. Banko, *J. Fluid Mech.* **394**, 339–354 (1999).
6. L. Kondic and J. Diez, *Phys. Fluids* **13**, 3168 (2001).
7. J. Lallement, P. Trontin, C. Laurent and P. Villedieu, AIAA 2018-3012, Atmospheric and Space Environments Conf., Atlanta (GA, USA) (2018).

Transient deformation and swelling of paper by aqueous co-solvent solutions

C.-L. Wong¹, S. Wang¹, S. Karimnejad¹, M. G. Wijburg¹, H. Mansouri² and A. A. Darhuber¹,

¹ Fluids & Flows Group, Department of Applied Physics, Eindhoven University of Technology, The Netherlands

² Canon Production Printing, Venlo, The Netherlands

Corresponding author: A.A.Darhuber@tue.nl

Inkjet printing inks frequently contain polar liquids of low volatility such as glycerol or poly(ethylene glycols) in addition to the main solvent water. As can be seen in Fig. 1, The deposition of these liquids on paper sheets induces swelling of the cellulose fibers, which leads to an overall, anisotropic deformation of the sheet. We characterized the corresponding strain components by means of a grid projection method and white light interferometry. For pure water, most of the hydroexpansion strain vanishes again after drying is complete. However, for aqueous solutions of non-volatile co-solvents, a large fraction of the deformation persists after the water has evaporated. Because swelling occurs only after liquid enters the cellulose fibers, monitoring the dynamics of expansion provides insight into the pore-fiber distribution of co-solvents. The corresponding timescales of pore-fiber transport strongly depend on the co-solvent concentration, as a sufficient quantity of water is needed to plasticize the fiber walls.

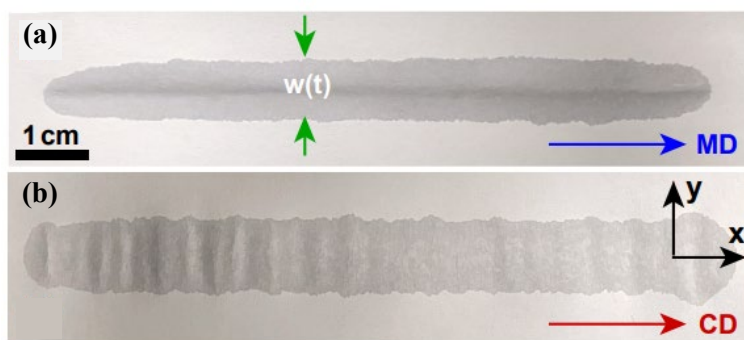


Fig. 1. Top-view photographs of wet zones deposited via substrate motion in the (a) machine direction (MD) and (b) cross-machine direction (CD). The gray-scale modulations point at the presence of wrinkles that are oriented in the MD. They are caused by anisotropic expansion of the paper sheet which induces a buckling instability.

While the expansion in the cross machine direction (CD) was found to be on order of 2.5%, it amounts to approximately 40% in the thickness direction. Pure water gives rise to a persistent CD expansion strain of about 0.3% after drying, which rises up to 2.4% for solutions of non-volatile co-solvents that remain in the paper after the water has evaporated.

We found that the expansion strain not only depends on the quantity of co-solvent deposited, but also on the history of the sample, e.g. the initial co-solvent concentration in the solution. We ascribe this history dependence to the sensitivity of the co-solvent transport through the fiber walls to the concentration of water, which is needed to plasticize the fiber walls before molecules of larger molecular weight can pass through swiftly [1,2].

References

1. M. G. Wijburg, S. Wang and A. A. Darhuber, *Colloids Surf. A Physicochem. Eng. Asp.*, **656**, 130268 (2023).
2. C.-L. Wong, S. Wang, S. Karimnejad, M. G. Wijburg, H. Mansouri and A. A. Darhuber, *Soft Matter*, **19**, 1202-1211 (2023).

Quantifying the coating layer shape in finite depth dip coating

Jisoo Song¹, Jaewook Nam¹

¹ Microfluidics and Coating Process Laboratory, Seoul National University, Republic of Korea
Corresponding author: jaewooknam@snu.ac.kr

Dip coating is a "simple old way"[1] of applying a liquid layer onto a substrate by immersing the object into a bath of fluid and then withdrawing it. Most studies on dip coating have focused on systems where a long substrate, such as a slab or cylinder, is pulled out from the bath in its length direction. In such systems, coating layers have simple geometries; the substrate profiles are flat, and the coating layer profiles can be represented as a single-valued function over the substrate profile. On the other hand, industrial dip coating processes often involve irregular geometries, and these processes are usually designed based on empirical knowledge. However, with the increasing need for thin and uniform coating layers with complex rheological properties, there is a growing demand to systematically analyze these processes. For this, understanding the relationship between process conditions and the shape of the coating layer is crucial, which requires reliable indicators to quantify the coating layer shape. Popular indicators, such as surface roughness and conformality, are traditionally measured using the local thickness of the coating layer in the direction normal to the substrate surface. Unfortunately, the local thickness is not easily defined in systems with irregular geometries.

In this work, we focus on the dip coating process with a small immersion depth. We refer to the process as "finite depth dip coating" to distinguish it from the coating of long films or wires. Finite depth dip coating is characterized by the presence of the lower edge of the substrate in the system. The lower edge introduces significant irregularities to the coating layer geometry, which complicates difficult to define local thickness. One irregularity is that the substrate profile is no longer flat but inherently curved. If the profile contains a concave region, local thickness in surface-normal direction may not be defined there. In addition, if sharp corners exist on the substrate profile, local thickness cannot be continuously defined. Another irregularity is that the coating layer profile can have an overhang. During the withdrawal of the substrate, a capillary bridge forms between the substrate and the coating bath. The bridge then ruptures through pinch-off dynamics, leaving residual fluid hanging under the substrate. Capillary force induces flow from the residue into the rest of the coating layer, which often causes the residue to buckle and form an overhang due to instability. When an overhang exists, surface-normal thickness cannot be uniquely determined. Because of these irregularities, traditional measures for the layer shape cannot be generally applied. New definitions, which do not rely on local thickness and thus can be applied to arbitrary geometries, are required.

In order to quantify the coating layer shape in finite depth dip coating, we developed general definitions of conformality and surface roughness. Our definitions are based on dynamic time warping (DTW), which is a similarity measure between two series of data. To measure conformality, we discretized the substrate profile and the coating layer profile, and computed the optimal pairs of points using DTW. We refer to this conformality as C_{DTW} . To measure surface roughness, we first defined an ideal coating layer profile and then calculated the DTW distance between it and the actual coating layer profile. We refer to this roughness as R_{DTW} . Since DTW can be computed between any arbitrary series, our method can be applied to any coating layer, regardless of its irregular features.

To evaluate the performance of the measures we developed, we analyzed the formation of external electrodes on multi-layer ceramic capacitors (MLCC) by dip coating. During the process, a cuboid MLCC chip is partially immersed into metal paste to deposit the fluid onto its edges[2]. A variety of pastes with different rheological properties are used, and the shape of the coating layer varies accordingly. Using our method, we quantified the shapes of the coating layers at equilibrium and compared the results to the rheological property data. The two set of data showed a similar classification, verifying that our method can be used to find the relationship between the process conditions and the layer shapes.

In conclusion, we have developed general measures that extend traditional layer shape indicators into arbitrary geometry. This provides a systematic way to quantify the quality of the coating layer from finite depth dip coating. Furthermore, our method can be applied to any other process involving a layer with irregular geometry.

References

- [1] SCRIVEN, L. E., *Journal of Materials Chemistry* **121**, 717 (1988).
- [2] HONG, KOOTAK, ET AL., *Journal of Materials Chemistry C* **7**(32), 9782-9802 (2019).

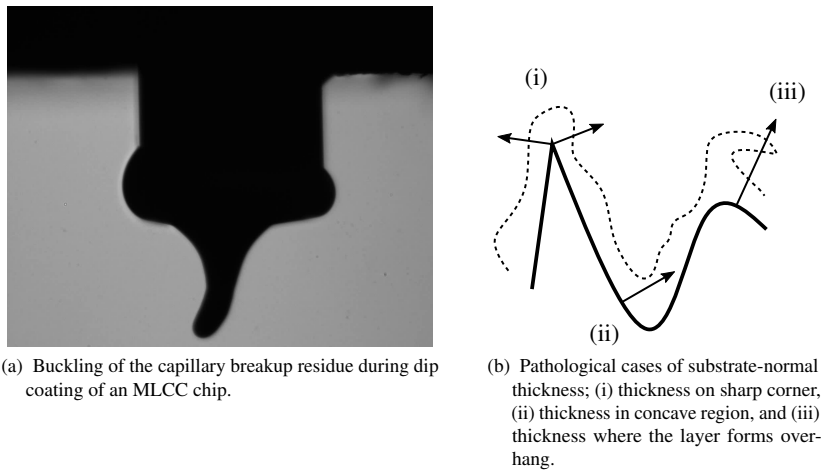


Figure 1: Examples of irregular geometry of the coating layer and its effect on defining substrate-normal thickness.

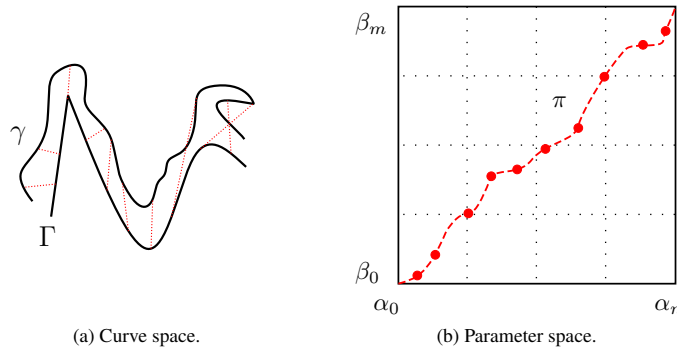


Figure 2: Schematic figure of dynamic time warping (DTW) between curves. Curves Γ and γ in curve space are discretized to series $(\Gamma(\alpha_0), \dots, \Gamma(\alpha_n))$ and $(\gamma(\beta_0), \dots, \gamma(\beta_m))$. Computing the DTW distance is equivalent to finding the weighted shortest path π in parameter space. Dashed lines in (a) represent point pairs, whose counterparts are drawn as red circles in (b).

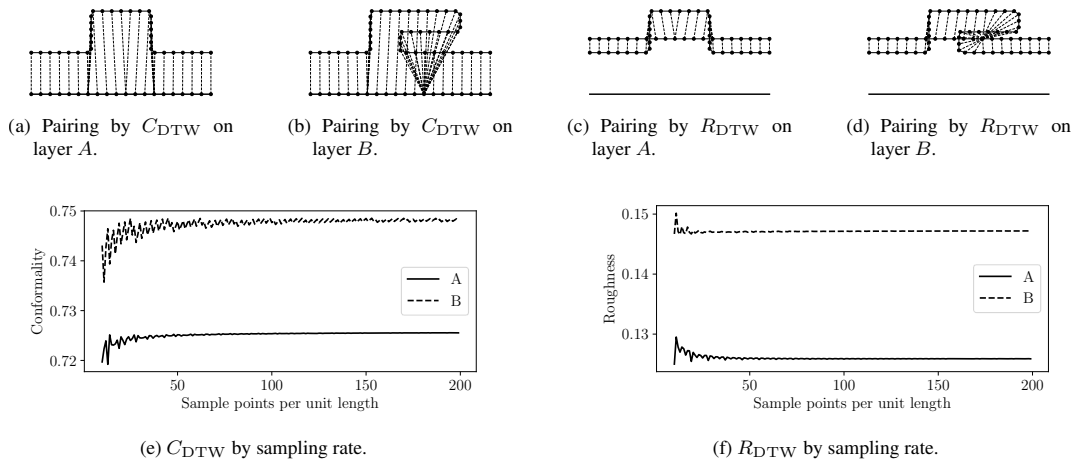


Figure 3: C_{DTW} and R_{DTW} of layer A without overhang and layer B with overhang. Both layers have the same volume.

Simplified model for stable operating condition of thick-film battery electrode slot coating

Jihwan Yoon¹, Kyengmin Min¹, Sangho Oh¹ and Jaewook Nam¹

¹ School of Chemical and Biological Engineering, Seoul National University, Seoul, 08826, Korea

Corresponding author: jaewooknam@snu.ac.kr

The slot coating method is widely employed for manufacturing thick electrode films required for high-capacity secondary batteries [1,2]. Given the rapid evolution of battery electrodes, it has become increasingly important to predict the operating conditions required for a stable process. These conditions, known as stable operating conditions, are necessary to prevent significant coating defects. The conditions include web speed (u), coating liquid wet thickness (h_{∞}), and coating gap (H_0), as depicted in Fig. 1a and 1b. Notably, the thick electrodes are coated as a wet film over half of the coating gap, referred to as a thick-film.

In this study, we investigated the stable operating conditions of thick-film slot coating based on dimensional analysis. To identify these conditions, we conducted a lab-scale slot coating experiment using a model fluid that simulates slurry viscosity [3,4]. The model fluid enabled us to rapidly screen for stable operating conditions. We validated the experimental results further based on an analytic model, numerical method, and machine learning [5].

However, the stable operating condition did not necessarily result in a uniform wet thickness profile, as shown in Fig. 1b. To address this issue, we analyzed the coating uniformity of battery model slurry for various coating gaps. As depicted in Fig. 1c, we examined a simplified relationship between coating uniformity and coating gap. This relationship allowed us to achieve a uniform wet thickness profile, as demonstrated in Fig. 1d.

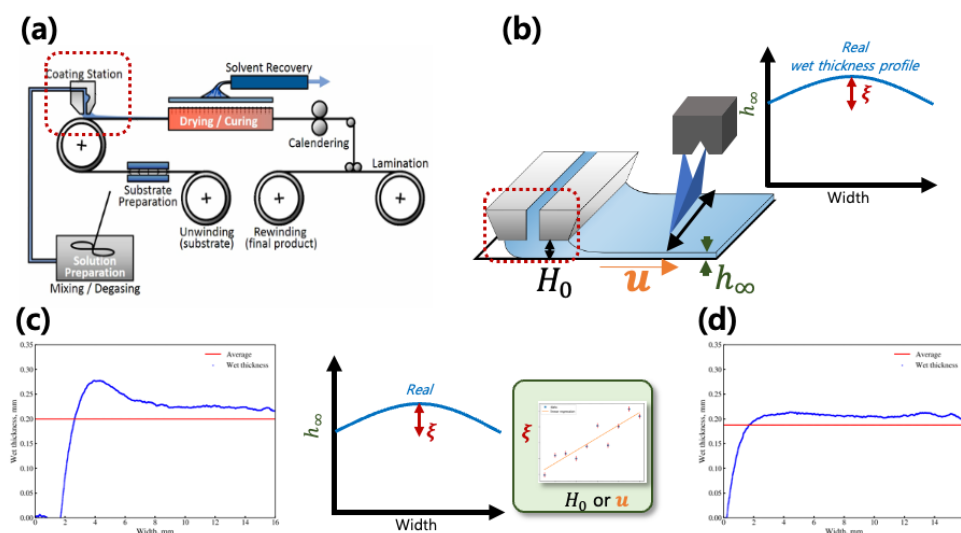


Fig. 1. Schematic of (a) the process flow diagram (PFD) of the entire slot coating process, including a series of unit processes such as the coating station; (b) the detection of coating uniformity under stable operating conditions of the coating station; (c) the coating thickness profile and an analysis of the relationship between the profile and operating conditions; and (d) the desired coating thickness profile, which is the target of model prediction for optimal operating conditions.

References

1. Bitsch, B., Dittmann, J., Schmitt, M., Scharfer, P., Schabel, W., & Willenbacher, N. (2014). A novel slurry concept for the fabrication of lithium-ion battery electrodes with beneficial properties. *Journal of Power Sources*, 265, 81-90.
2. Spiegel, S., Heckmann, T., Altvater, A., Diehm, R., Scharfer, P., & Schabel, W. (2021). Investigation of edge formation during the coating process of Li-ion battery electrodes. *Journal of Coatings Technology and Research*, 1-10.
3. Ishii, M., & Nakamura, H. (2022). Influence of molecular weight and concentration of carboxymethyl cellulose on rheological properties of concentrated anode slurries for lithium-ion batteries. *JCIS Open*, 6, 100048.
4. Lee, M., Jung, H., Lee, M., Kwak, H., & Nam, J. (2022). Model fluid for coating flows of Li-ion battery anode slurry. *Journal of Materials Science*, 57(38), 17935-17945.
5. Niri, M. F., Reynolds, C., Ramírez, L. A. R., Kendrick, E., & Marco, J. (2022). Systematic analysis of the impact of slurry coating on manufacture of Li-ion battery electrodes via explainable machine learning. *Energy Storage Materials*, 51, 223-238.

"A journey into cosmetic coatings through mascara deposition »

O. Sonneville-Aubrun, L. Lukyanova, L. Mineau, S. Rose, F. Giron, JY. Fouron

L'Oréal R&I

Mascaras are part of make-up routines. They are used to widen the eyes by highlighting the eyelashes. They consist in the deposition of a pasty material on eyelashes with a brush to form a thick, homogeneous, and long-lasting coating.

To better understand and control the deposition of mascara on eyelashes, a set of tests has been set up from rheological and structure characterizations of the bulk to mascara transfer properties on different substrates through different pathways.

Classical mascaras appear as complex fluids characterized by a high consistency at rest (between 10^3 and 10^5 Pa) as well as a marked solid behavior. They present inhomogeneous flow under stress. CLSM was used to observe mascaras' mesostructure using different fluorescent dyes. Images show fatty aggregates with different sizes and connectivity dispersed in an aqueous matrix. Their lamellar structure was revealed using cryoSEM at high magnification. The density and size of the lamellae vary between formulas studied. No link between structure and rheology could be established at this stage.

The transfer of mascara was studied on different substrates, from dip coating on glass slides or needles to applications on hair via a robotic platform with different applicators from model tools or brushes. Differences in coating thickness have been observed for the mascaras tested with different rankings depending on the transfer mode. In all cases the coating thickness seems to be limited by the solid behavior of the mascaras.

To end, an exploration with other complex fluids has been done to compare with classical mascara. Large dynamic of coating thickness could be observed depending on the fluids.

Cracking, stratification and instabilities in drying of colloidal dispersions

Alex Routh

Department of Chemical Engineering & Biotechnology, University of Cambridge

Drying of colloidal dispersions is ubiquitous in domestic and natural settings, with examples being paint films and river beds. Other biological examples include blood and bacterial colonies. Over the past 25 years there has been much research into the structures formed during the drying process. In this talk I will discuss the findings with regards the morphology of dried surfaces, the reasons films crack and also how different particles distribute throughout a film.



European Coating Symposium 2023

12-15 Sep 2023 Paris (France)

Air Entrapment during Coating of Viscous Fluids

H. Benkreira

Advanced Materials Engineering R & KT Centre,

Department of Chemical Engineering, University of Bradford, UK

Presenting author email address: H.Benkreira@bradford.ac.uk

Air bubbles are the menace of the liquid film coating industry causing expensive waste particularly in the high technology of battery coating where both the slurries and the substrate are very expensive and difficult if not impossible to recycle. Air bubbles trapped in a coating feed originate mainly from mixing with poor degassing and inadequate pumping from the feed vessel to the coating head. Coating at high speed also leads to air entrainment, the result of dynamic wetting failure at the junction air/liquid/substrate. Here we are considering a different problem that of the possibility of tiny air bubbles being entrapped at low speeds (well below the air entrainment limit) in a perfectly degassed coating. The problem is how do these bubbles (observed before drying-so cannot be considered dryer related) originate in certain coating flows, slot coating for example?

This presentation addresses this important problem both theoretically and with the aid of experimental data in various coating flow configurations.



Hydrodynamics of Short Curtain Coating

Fateh Rabehi¹, Matthieu Roché², Sandra Lerouge³, Laurent Limat⁴

Saint-Gobain designs, produces and distributes materials for the home and everyday life. The surface of these materials is often treated with thin liquid coatings (paint, silver, etc.) in order to obtain specific aesthetic and functional properties. A widely used technique for coating a substrate with a treatment layer (or coating) with well controlled properties is based on the formation of a vertical liquid curtain, under which the substrate moves (Figure 1-a and 1-b). However, the accessible thickness range is limited by the stability losses of the curtain, or by the entrainment of the surrounding gas between the deposited layer and the moving substrate surface.

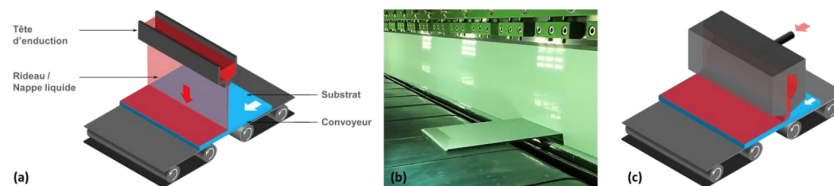


Figure 1: (a) Diagram of the standard curtain deposition process ; (b) Photograph of a wood plate passing through a paint curtain in the standard curtain process ; (c) Diagram of the short curtain deposition process.

Recent developments show that laminar coating (or slot-die coating) is the most reliable deposition process for overcoming the limitations of liquid sheet deposition¹. In this system, the liquid to be deposited emerges from a coating head placed at a distance of the order of a few hundred microns from the substrate surface, forming a meniscus rather than a curtain. However, this configuration can be problematic on rigid substrates that have height variations of the same order of magnitude as the working distance, leading to deposit inhomogeneities and even risks of collision with the coating head. In the case of the curtain, pressurising the liquid leaving the coating head could make it possible to avoid these problems, while maintaining the reliability of laminar coating. Indeed, the head can then be placed at a millimetre or centimetre distance from

¹fateh.rabehi@etu.u-paris.fr, Matter and Complex Systems

²matthieu.roche@univ-paris-diderot.fr, Matter and Complex Systems

³sandra.lerouge@univ-paris-diderot.fr, Matter and Complex Systems

⁴laurent.limat@univ-paris-diderot.fr, Matter and Complex Systems

the substrate surface (Figure 1-c). This "short curtain" mode of operation is not well known. The aim of this project is to establish a predictive description of these flows, by combining experiments, numerical simulations and theoretical work. The aim of this project is to understand how these centimetric curtains are deposited on the surface of a substrate as a function of substrate velocity.

Multiscale numerical modeling of antibubbles combining CFD and lubrication approach.

Omer Atasi¹, Dominique Legendre² and Benoit Scheid¹

¹TIPs, Fluid Physics Unit, Université Libre de Bruxelles, B-1050 Bruxelles, Belgium

²Institut de Mécanique des Fluides de Toulouse, Université de Toulouse, CNRS, Toulouse, France

Corresponding author: Omer.Atasi@ulb.be

An antibubble is a thin spherical shell of air surrounded by liquid [1,2]. It has attracted attention as a mean to studying the drainage and dissolution dynamics of an air film and deducing its rheological properties. The dynamics of this thin film can be described satisfactorily by the lubrication equation, assuming that the antibubble has a spherical shape and not considering the flow around and inside the antibubble (see for instance [2]). The reason for the latter assumption is the difficulty of describing the large-scale physics that occurs around the antibubble (fluid flow, deformation) on the centimeter scale, and the thin-film drainage that occurs on the submicron scale. In this study, we develop a numerical method that can capture the physics occurring at both scales. The method is based on the Level-set method in which an additional lubrication equation for the film thickness is solved in a Eulerian framework. We show that the method can describe gravitational drainage of the thin film as well as the large-scale flow and dissolved gas concentration field in the liquid (see Fig 1). We then show the effect of antibubble deformation and air dissolution on the film drainage process at the submicron scale and on the antibubble dynamics at the macroscopic scale.

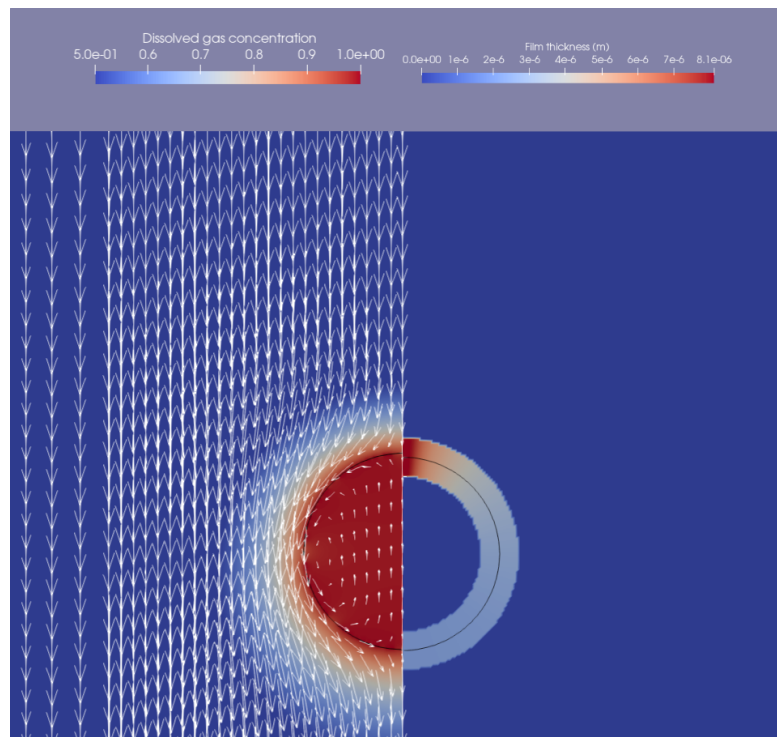


Fig. 1. Snapshot of the multiscale simulation showing a rising antibubble with radius $R = 7$ mm. The black lines in the right and left panels show the interface between the innermost phase (phase 1) of the antibubble and the outer liquid (phase 3). The thin film between phase 1 and phase 3 is implicitly taken into account by solving the lubrication equation governing its evolution using Eulerian method. The arrows in the left-hand panel show fluid velocity in the antibubble reference frame for the inner and the outer liquid phases. As the antibubble rises, the air film dissolves. The concentration of dissolved gas is shown in the color map (left panel). In the right-hand panel, the colors show the film thickness distribution (in the micrometer range, as indicated by the scale bar) and a pocket of gas forming at the apex of the antibubble. These simulations can capture the physics at centimeter and submicron scales at the same time. Note that the value of the Peclet number has been arbitrarily chosen low to reduce computational effort. The method is currently being validated to simulate more realistic values of the Peclet number.

References

- 1) S. Dorbolo, E. Reyssat, N. Vandewalle and D. Quéré. « Aging of an Antibubble ». *Europhysics Letters* **69** (6): 966-70. <https://doi.org/10.1209/epl/i2004-10435-7>.
- 2) B. Scheid, S. Dorbolo, L. R. Arriaga and E. Rio. « Antibubble Dynamics: The Drainage of an Air Film with Viscous Interfaces ». *Physical Review Letters* **109** (26)e: 264502. <https://doi.org/10.1103/PhysRevLett.109.264502>.

Three-dimensional damping of defects on coating films

David Barreiro-Villaverde^{1,2}, Anne Gosset³, Marcos Lema¹ and Miguel A. Mendez²

¹ University of A Coruña, CITIC Research, Spain

² Environmental and Applied Fluid Dynamics, von Karman Institute, Sint-Genesius-Rode, Belgium

³ University of A Coruña, Campus Industrial de Ferrol, CITENI, Spain

Corresponding author: david.barreiro1@udc.es

Coatings often feature interfacial defects due to disturbances during the deposition process which, if they persist until solidification, worsens the product quality. This work investigates the stability of a thin liquid film dragged by a vertical substrate moving against gravity, a flow configuration found in a variety of coating processes. The receptivity of the liquid film to three-dimensional disturbances is discussed with Direct Numerical Simulations (DNS), an in-house non-linear Integral Boundary Layer (IBL) film model^{1,2}, and Linear Stability Analysis (LSA). The thin film model, successfully validated with the DNS computations, implements a pseudo-spectral approach for the capillary terms that allows for investigating non-periodic surface tension dominated flows. The combination of these numerical tools allows for describing the mechanisms of capillary and non-linear damping and identifying the instability threshold of the coating processes. The results show that transverse modulations can be beneficial for the damping of two-dimensional waves within the range of operational conditions considered in this study, typical of air-knife and slot-die coating.

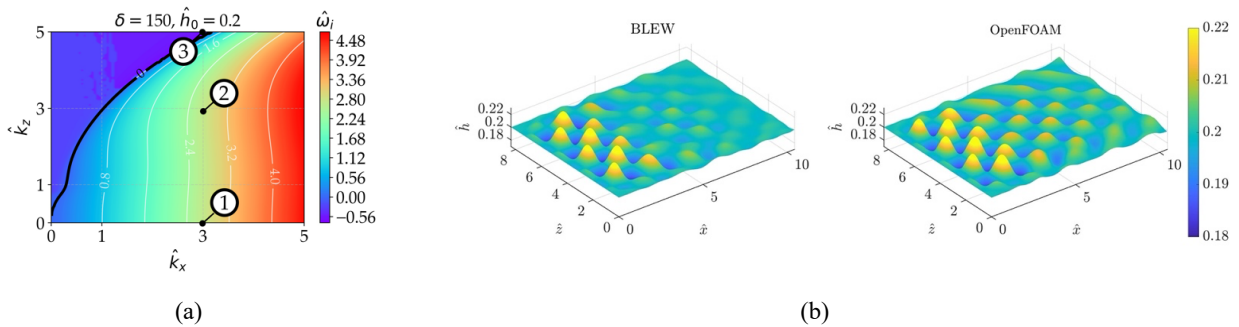


Fig. 1. (a) Contour plot of the amplification factor ω_i as a function of the stream and span-wise wavenumber obtained with LSA, and (b) snapshot of the film evolution predicted by the IBL solver (BLEW) and DNS computations (OpenFOAM) for the case labeled as 2 in (a).

References

1. M.A. Mendez, A. Gosset, B. Scheid, M. Balabane, and J.-M. Buchlin, *Journal of Fluid Mechanics* **911** (2021)
2. T. Ivanova, F. Pino, B. Scheid, M. A. Mendez, *Physics of Fluids* **1** (2021).

Simultaneous multilayer coating for battery electrodes and numerical simulations with model material systems

A. Hoffmann^{1,2}, S. Spiegel^{1,2}, P. Scharfer^{1,2}, W. Schabel^{1,2}

¹ Thin Film Technology (TFT), Karlsruhe Institute of Technology (KIT), Karlsruhe, Germany

² Material Research Center for Energy Systems (MZE), KIT, Karlsruhe, Germany

Corresponding author: alexander.hoffmann@kit.edu

In battery production, simultaneous multilayer slot-die coating is a promising method for both improving product properties and increasing the production efficiency in terms of reduced cost. With multi-layered configurations, different materials can be distributed along the film height resulting in a graded electrode whose electrochemical, electrical, mechanical or thermal properties can benefit from the synergistic effects of the individual materials [1–5]. These can lead to improved adhesion properties, reduced passive material contents, higher charging rates, better safety or improvements in energy and power density. Furthermore, influence can be exerted on the subsequent process steps, as for example Kumberg et al. [6] showed significantly reduced drying times as a result of multi-layered electrode structures. Another practical advantage of this method is the ability to retrofit in existing plants, in the best case, leading to an increase in productivity. However, the implementation is highly dependent on the coating fluids and process used. In case of batteries, shear-thinning slurries raise the level of complexity due to the variable viscosity.

This study outlines the basic investigations to apply the multilayer coating to battery electrodes. In this context, the coating defects for multilayers and their influencing variables are examined in more detail. This is done by means of a systematic, experimental parameter study. Focus is set on the rheological and thermodynamic properties of the coating fluids in the individual layers as well as the influence of the wet-film-height ratio. To enable a more targeted investigation, model material systems are used to map the rheology of the coating fluids. In order to increase visibility of coating defects in both layers of the coating, tailored dyes are added to the material systems.

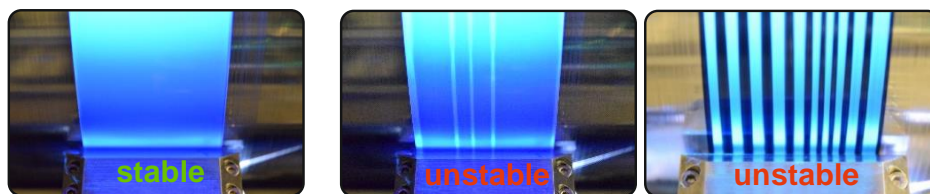


Figure 1: Dyed multilayer coatings at a stable operating point (left) and unstable operating points with defects (right).

Finally, mathematical methods to simulate the process are discussed. Different levels of complexity are considered, ranging from a high-resolution CFD simulation to simplified Navier-Stokes equations and further simplified geometric solution methods based on the velocity fields and the associated flow pressures.

This work contributes to the research performed at CELEST (Center for Electrochemical Energy Storage Ulm Karlsruhe) and Material Research Center for Energy Systems (MZE) and is funded by the Federal Ministry of Education and Research (BMBF) under Project ID 03XP0402B (ForeCast).

Keywords

slot-die, coating, multilayer, simultaneous, electrode production

References

1. Naoki Imachi, Yasuo Takano, Hiroyuki Fujimoto, Yoshinori Kida,* and Shin Fujitani*: 154 Layered Cathode for Improving Safety of Li-Ion Batteries. *Journal of The Electrochemical Society*, A412-A4116 (2007)
2. Liu, D., Chen, L.-C., Liu, T.-J., Chu, W.-B., Tiu, C.: Improvement of Lithium-Ion Battery Performance by Two-Layered Slot-Die Coating Operation. *Energy Technol.* (2017). <https://doi.org/10.1002/ente.201600536>
3. Huang, C., Young, N.P., Zhang, J., Snaith, H.J., Grant, P.S.: A two layer electrode structure for improved Li Ion diffusion and volumetric capacity in Li Ion batteries. *Nano Energy* (2017). <https://doi.org/10.1016/j.nanoen.2016.11.043>
4. Golmon, S., Maute, K., Dunn, M.L.: A design optimization methodology for Li+ batteries. *Journal of Power Sources* (2014). <https://doi.org/10.1016/j.jpowsour.2013.12.025>
5. Diehm, R., Kumberg, J., Dörrer, C., Müller, M., Bauer, W., Scharfer, P., Schabel, W.: In Situ Investigations of Simultaneous Two-Layer Slot Die Coating of Component-Graded Anodes for Improved High-Energy Li-Ion Batteries. *Energy Technol.* (2020). <https://doi.org/10.1002/ente.201901251>
6. Kumberg, J., Bauer, W., Schmatz, J., Diehm, R., Tönsmann, M., Müller, M., Ly, K., Scharfer, P., Schabel, W.: Reduced Drying Time of Anodes for Lithium-Ion Batteries through Simultaneous Multilayer Coating. *Energy Technol.* (2021). <https://doi.org/10.1002/ente.202100367>

Coating thickness analysis in slot coating process of the battery slurry

Kyengmin Min¹, Jiwhan Yoon¹, Jaewook. Nam^{1*}

¹ School of Chemical and Biological Engineering, Seoul National University, Seoul, 08826, Korea

Corresponding author: jaewooknam@snu.ac.kr

Slot coating is one of the most used coating methods in the industry. Especially in battery manufacturing, the coating of cathode and anode material called “battery slurry” is being actively researched because of its importance in the industry.

One of the issues that need to be addressed in the battery coating process is the “heavy edge” phenomenon. This is caused by the coating solution, in this case, the battery slurry, being dewetted after being coated, driving the edge to inflate relatively compared to its center. If a heavy edge occurs, the final product, the battery, will have an uneven thickness, requiring the removal of that portion, which can be critical to the product yield. Thus, we aim to find the conditions associated with the occurrence of heavy edges and explore ways to reduce them.

This study will present the experimental result of the coating thickness profile with various processes conditions. The data acquired by the laser profile sensor will then be analyzed to show the impact of coating gap, web speed, flowrate and die-lip length. We will select several parameters to evaluate the coating performance quantitatively in context of coating thickness.

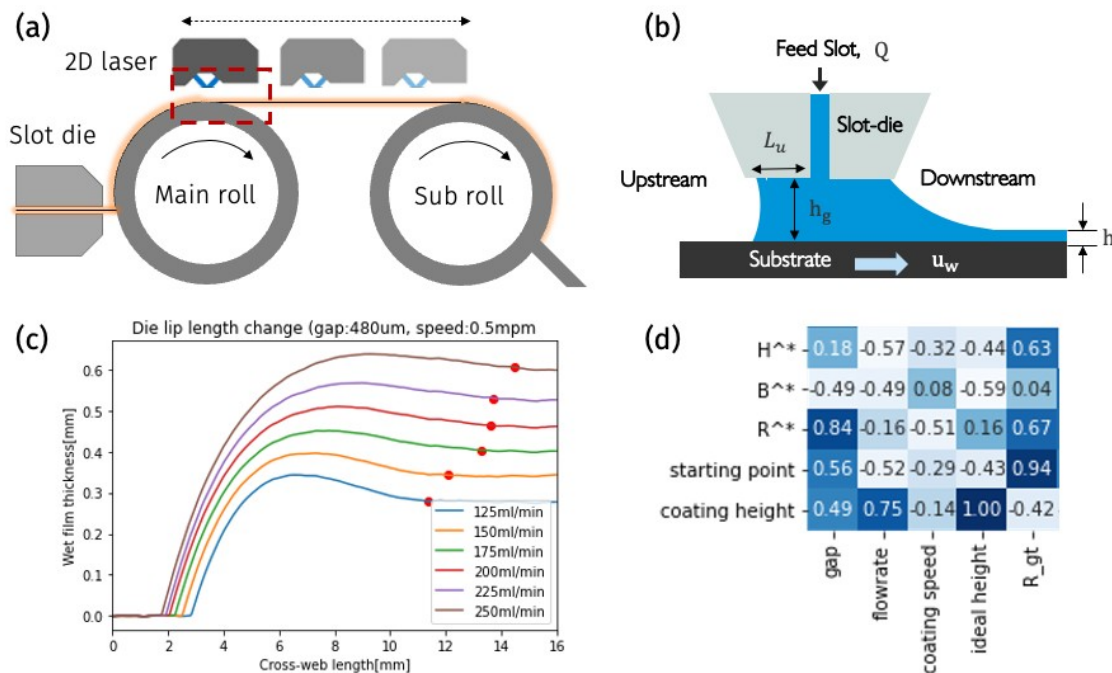


Fig. 1. (a) Schematic of the experimental setup for the research, which is composed of roll-to-roll slot coating machine and 2D laser sensor; (b) process parameters used for the experiment; (c) actual profiles acquired for different process parameters and (d) correlations between different process and edge parameters.

References

- Schmitt, M., Scharfer, P. & Schabel, W. Slot die coating of lithium-ion battery electrodes: investigations on edge effect issues for stripe and pattern coatings. *J Coat Technol Res* **11**, 57--63 (2014).
- Diehm, Ralf, et al. "Edge Formation in High-Speed Intermittent Slot-Die Coating of Disruptively Stacked Thick Battery Electrodes." *Energy Technology* 8.2 (2020): 1900137.
- Spiegel, Sandro, et al. "Optimization of Edge Quality in the Slot-Die Coating Process of High-Capacity Lithium-Ion Battery Electrodes." *Energy Technology* 11.5 (2023): 2200684.

A new concept for an energy- and cost-efficient battery electrode production - Drying investigation of a highly-concentrated granule-based system

K. Ly^{1,2}, D. Burger^{1,2}, L. Lödige^{1,2}, E. Wiegmann³, A. Kwade³, P. Scharfer^{1,2}, W. Schabel^{1,2}

¹ Thin Film Technology (TFT), Karlsruhe Institute of Technology (KIT), Karlsruhe, Germany

² Material Research Center for Energy Systems (MZE), KIT, Karlsruhe, Germany

³ Institute of Particle Technology (iPAT), TU Braunschweig (TU-BS), Braunschweig, Germany

Corresponding author: kevin.ly@kit.edu

Lithium-ion batteries have become an indispensable part of modern life. Due to their high energy and power density, lithium-ion batteries are expected to be used primarily in the field of electromobility in the future. The desire for higher performance, cost efficiency and safety poses various challenges for the automotive industry and battery research.

The drying process of battery electrodes has an enormous influence on the electrode quality. It determines electrode characteristics and most importantly cell performance. The major problem during drying is the migration of binder to the electrode surface, resulting in an inhomogeneous binder-distribution throughout the film.

As for state of the art electrodes, drying is one of the most cost-intensive process steps. A new approach for reducing the solvent content in electrode-processing and therefore increasing the cost-efficiency for the battery manufacturing process will be investigated in this work. By reduction of solvent content and the usage of granules in battery-paste manufacturing, the storage stability of the produced electrode pastes is several weeks. This leads to a decoupling of paste and electrode production and a significant increase in production flexibility.

In terms of the drying step it is essential to investigate the influence of the highly-concentrated particulate granular system on the drying process. Especially, the influence on pore structure, film consolidation and binder migration is crucial for understanding the drying process. For this purpose, a series of fundamental studies will be conducted. This work presents the experimental methods for the investigation of the drying behavior under defined process conditions. These are mainly gravimetric drying tests and investigations by means of cryo-SEM for the elucidation of the pore emptying mechanism, as well as investigations with a magnetic suspension balance for the disclosure of the sorption behavior. First results of the drying investigations will be presented.

Acknowledgements:

This work contributes to the research performed at CELEST (Center for Electrochemical Energy Storage Ulm Karlsruhe) and Material Research Center for Energy Systems (MZE). The authors would like to acknowledge financial support of the Federal ministry of Education and Research (BMBF) via the InZePro cluster-project "GranuProd" (Grant number: 03XP0344C).

Cleaning station for slot dies

Harald Doell¹

¹ TSE Troller AG, Murgenthal, Switzerland

Corresponding author: harald.doell@tse-coating.ch

(Harald Döll as the Technical Director of TSE Troller AG is mainly involved in the optimization of the coating dies as well as feasibility studies with customers for coating of new products and commissioning of both, pilot and production dies)

Keywords: slot die coating, optimized cleaning, battery slurries, medicated transdermal patches

Premetered coating in the slot format is an attractive method to apply single or multilayer structures of functional layers to continuously running substrates.

One of the largest advantages of the slot coating process is that the fluid circulates in a closed system without exposing solvent to the atmosphere, except of the coated film itself. In some fields with hazardous solvents or other ingredients the coating station with the slot die can be integrated in inert atmosphere.

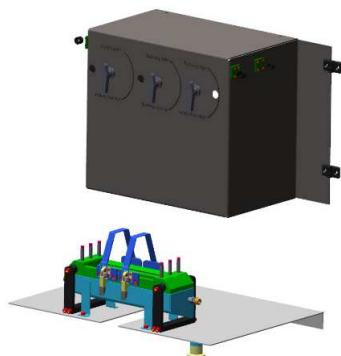
When the coating process is terminated the entire system needs to be cleaned in order to avoid remaining residues of coating fluid inside the die. In case of water-based fluids often the slot die can be flushed with water and the mixture of clear water and coating fluid is collected in a separate pan and then to be drained. The contact with the fluid is not hazardous and operators can use simple personal protective equipment PPE.

In case of solvent-based fluids such as battery slurries the contact with the solvents must be avoided and especially in applications for medicated transdermal patches including medical agents the safety regulations require a non-contact policy.

For such processes a special cleaning station for different size slot dies was designed. In the picture below a station with a 900mm wide slot die is shown. The granite stone table on the cleaning station allows the exact assembly of the slot die after the cleaning procedure.

After the coating run the slot die has to be closed first, the feed port and the slot will be covered to avoid spillage of fluid. Then the die shall be moved from the coating to the cleaning station and inserted upside-down into a sealed collection pan. The sealing also avoids that solvent or coating fluid can be spilled. The two connections in the transport side plates on the sides of the slot die will be connected with feeding hoses and the centre feed port will be linked to the central hose.

The drain port of the collection pan will be connected to a waste container, in which the fluid can be collected. In some cases a second container could be used for recirculation mode. A pulsating pump can be used to flush the cleaning agent / solvent into the die and on the operating board the path for the flow of the solvent can be selected and varied between inlet through the centre or through one or both bleed ports on the sides and the mix of fluids drains through the pan into the container. In some cases also a central flushing system can be connected to the cleaning station as well.



The design of the cleaning station can vary between different slot die sizes from rather narrow to wide dies, and the shape of the slot die holder is depending on the die itself and can be designed for single and dual layer slot dies.

On the left side a CAD- model of a cleaning station for a narrow single layer lot die is shown.

Stress and Fracture During the Drying of Aqueous Particulate Coatings

Annie Moorhead¹, Lorraine F. Francis¹

¹*Chemical Engineering and Materials Science Department, University of Minnesota, Minneapolis*

Corresponding author: lfrancis@umn.edu

In the processing of particulate materials, such as fuel cell catalyst layers and battery electrodes, controlling fracture is essential. These films begin as liquid dispersions of particles that are deposited onto substrates and then dried into coatings. During drying, capillary pressures arise due to the liquid menisci within the pores of the particle network. Prior work has demonstrated that tensile stress occurs within a coating due to these capillary pressures, coupled with constrained shrinkage from the coating adhering to the substrate [1,2]. When the thickness of the coating is above the Critical Cracking Thickness (CCT), tensile stress during drying may lead to the formation of cracks [2]. Stresses in drying coatings have been measured with cantilever beam deflection [1]. However, the scope of the technique is often limited to crack free coatings. Additionally, prior research has shown that drying uniformity must be preserved for accurate stress measurement [1]. The present work provides guidance on interpreting stress data for uniformly drying and cracking coatings using cantilever beam deflection. This work compares stress development and drying in silica coatings and zinc oxide coatings and shows the effects of cracking on the stress measurement data [3].

References

1. K. K. Price, Y. Wu, A. V. McCormick, and L. F. Francis, [Stress Development in Hard Particle Coatings in the Absence of Lateral Drying,] *Journal of the American Ceramic Society*, **98**, 2214–2222 (2015).
2. R. C. Chiu, and M. J. Cima, [Drying of Granular Ceramic Films: II, Drying Stress and Saturation Uniformity,] *Journal of the American Ceramic Society*, **76**, 2769–2777 (1993).
3. A. Moorhead, and L. F. Francis, [article in review]. (2023).

Mass transport and drying-induced stresses in charged colloidal dispersions

A. Bouchaudy¹, C. Loussert¹, S. Dehaeck², B. Sobac², J.B. Salmon¹

¹ CNRS, Solvay, LOF, UMR 5258, Univ. Bordeaux, F-33600 Pessac, France

² TIPs Lab, Université libre de Bruxelles, 1050 Brussels, Belgium

Corresponding author: jean-baptiste.salmon-exterieur@solvay.com

We have investigated the drying of droplets of charged silica dispersions squeezed between two circular glass wafers separated by $\simeq 200 \mu\text{m}$ spacers, see Figure 1. These experiments, combined with *in situ* measurements of concentration fields using Mach-Zehnder interferometry, help us to investigate the colloid mass transport during the drying dynamics [2]. Our experiments provide the evidence that mass transport within the drop can be described by a purely diffusive process for some range of parameters for which buoyancy-driven convection is negligible. We were then able to extract from these experiments the collective diffusion coefficient of the dispersion $D(\varphi)$ over a wide concentration range $\varphi = 0.24\text{--}0.5$, i.e., from the liquid dispersed state to the solid glass regime above $\varphi_c \simeq 0.32$. The measured values of $D(\varphi) = 5\text{--}12D_0$ are significantly larger than the estimate D_0 given by the Stokes–Einstein relation, thus highlighting the important role played by the colloidal interactions in such dispersions

We have also developed a setup to continuously measure stresses induced by the drying of the charged colloidal dispersion [1]. This setup is based on a precision scale working with an electromagnetic force compensation technique that provides accurate measurements of forces, while allowing simultaneously controlled evaporation rates, *in situ* microscopic observations of the confined drop, and quantitative estimates of normal stresses. Stress measurements show the occurrence of large tensile stresses during drying, well-before the solidification evidenced by the invasion of the porous colloidal material by air. The combined measurements of solid deformation and concentration profiles show that these stresses are due to the formation of the solid glass at $\varphi_c \simeq 0.32$, which further undergoes drying-induced shear deformations up to the colloid close-packing, as also supported by large deformation poroelastic modeling. Above all, our results highlight the importance of repulsive colloidal interactions in the build-up of mechanical stresses during drying.

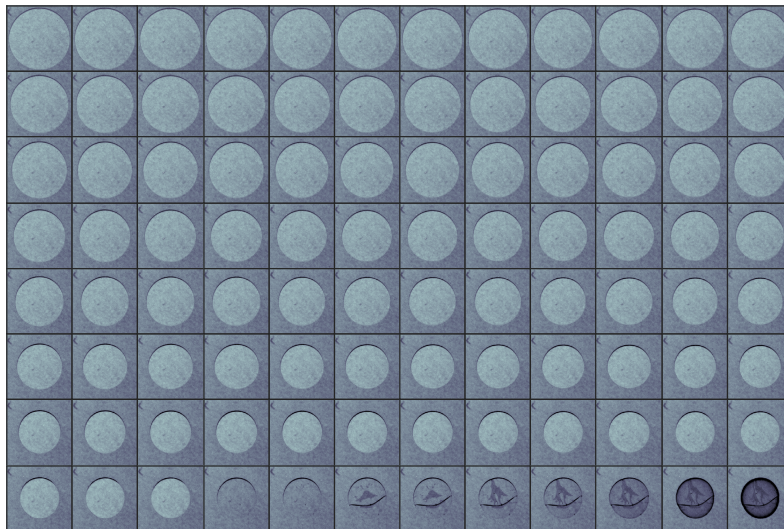


Figure 1: Time series of snapshots showing the drying of a confined drop of a charged colloidal dispersion until its complete solidification. The initial diameter of the drop is 3 mm.

References

- [1] A. BOUCHAUDY AND J.-B. SALMON, *Soft Matter* **15**, 2768–2781 (2019)
- [2] B. SOBAC, S. DEHAECK, A. BOUCHAUDY, AND J.-B. SALMON, *Soft Matter* **16**, 8213–8225 (2020)

Formation of glassy skins in drying polymer solutions

Laurence Talini¹ and François Lequeux²

¹ *Surface du Verre et Interfaces, CNRS, Saint-Gobain, Aubervilliers, France*

² *Sciences et Ingénierie de la Matière Molle, ESPCI Paris, PSL Research University, Sorbonne Université, Paris, France*

Corresponding author: francois.lequeux@espci.fr

When a complex fluid dries, a layer of concentrated solute may build up at its interface with air. The formed skin can be at the origin of fracture or buckling of the sample and it is therefore crucial to predict its apparition time and thickness. However, resolution of the associated diffusion equation is not straightforward since it involves a moving boundary condition, and, in the past decade, several works have examined ways to handle it [1,2]. In solutions of amorphous polymers, an additional difficulty is introduced by the concentration dependence of the mutual diffusion coefficient of solvent and polymer, which, in particular, strongly decreases in the vicinity of glass transition in solvent content. Consideration of the diffusion equation with a singular diffusion coefficient has been limited to scaling law analysis [3] and numerical resolutions [4].

We introduce a new approach to solve the problem of glassy skin formation at the surface of drying polymer solutions. As previously suggested [1], we use a Lagrangian scheme to handle the moving boundary condition; in addition, we demonstrate that analytical solutions to the diffusion equation can be found by using a simple approximation, which applies to any diffusion equation. We first show by considering different cases that the approximated solutions differ by less than 15% from numerical resolutions. We further focus on an evaporating polymer solution in realistic conditions, and we study the influence of the variations of the diffusion coefficient on skin formation.

We show that the apparition time of the skin weakly depends on the exponent characterizing the decrease of the diffusion coefficient, whereas its thickness varies by several orders of magnitude for exponents spanning the same range (see Fig. 1).

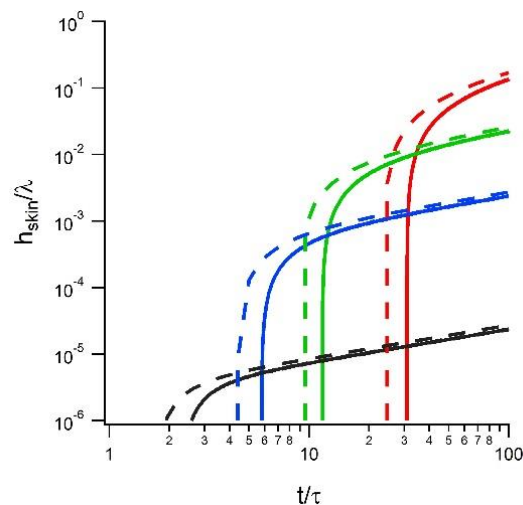


Fig. 1. Thickness of the skin formed at the surface of an evaporating polymer solution as a function of time for differently varying diffusion coefficients. The decrease of the diffusion coefficient at increasing polymer concentration is stronger from right to left. The approximated solutions (dashed lines) are shown with numerical resolutions (full lines). Thickness and time are normalized by respectively characteristic length and time of the evaporation problem.

We also show that the skin thickness slowly increases with time since it varies with the square root of time. Counter intuitively, when the diffusion coefficient very strongly decreases in the vicinity of glass transition, the formed skin may be and remain very thin throughout drying, limiting its macroscopic consequences.

References

1. L. Luo, F. Meng, J. Zhang, and M. Doi, *Chinese Phys. B* **25**, 076801 (2016).
2. M. G. Hennessy, C. J. W. Breward, and C. P. Please, *SIAM J. Appl. Math.* **76**, 1711–1736, (2016).
3. P.G. de Gennes, *Eur. Phys. J. E* **7**, 31–34 (2002).
4. K. Ozawa, T. Okuzono, and M. Doi, *Jpn. J. Appl. Phys.* **45**, 8817 (2006).

Coalescence of multiple sessile drops on a substrate

Antoine Bouvier^{1,2}, Etienne Reyssat¹, José Bico¹, Barbara Bouteille², Jérémie Teisseire²

¹ Laboratoire de Physique et Mécanique des Milieux Hétérogènes, PMMH UMR 7636 CNRS, ESPCI Paris, PSL, Sorbonne Université, Université Paris Cité, 7 Quai Saint-Bernard, 75005, Paris

² Saint-Gobain Research Paris, 39 Quai Lucien Lefranc, 93300 Aubervilliers

Corresponding author: antoine.bouvier@espci.fr

Wet coatings are of great interest in industrial processes as they allow for the protection or functionalization of surfaces by a thin film. Such films can be deposited in several ways including drop deposition techniques such as spraying or inkjet printing. In those cases, drops are deposited on a surface where they coalesce to form a continuous film. In the case of spraying, drops are distributed in sizes and positions [1] while inkjet printing allows for a well-controlled deposition of each drop [2]. These techniques rely on the coalescence of drops which has been widely studied for pairs of drops [4, 3]. However, coalescence mechanisms involving more drops remains an open question. In order to obtain uniform films all the drops have to merge. Otherwise, holes and other defects can appear. We present model experiments involving a small number of drops to study coalescence locally. For this purpose, an experimental set-up was designed to deposit glycerol drops on a glass plate according to specific patterns. An example of experiment is shown in fig. 1 in the case of three drops deposited on a triangular lattice.

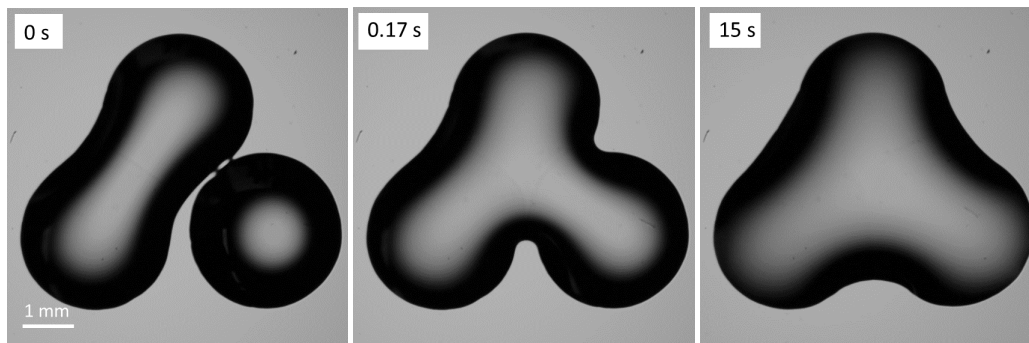


Figure 1: Snapshots of the coalescence for 3 drops of glycerol on a glass slide. The top drop successively touches its two neighbours.

We measure the dynamics of coalescence as well as the dimensions and geometry of liquid in the final state. During coalescence a liquid bridge grows between the two drops. Our experiments suggest that, in a viscous regime, the width of this bridge follows an exponential relaxation up to a final state. The number of drops involved and the deposition pattern both have a strong influence on the coalescence events. For a given system, the chronology of events is also of great interest as it significantly changes the dynamics. Indeed as soon as we consider more than two drops, they can touch each other following different sequences. Moreover we observe that contact angle hysteresis plays a major role in the geometry of the final state. It can lead to contact line pinning and prevent liquid drawback after merging. Accounting for geometry and chronology will bring a new point of view on multiple coalescence.

References

- [1] A. DALILI, K. SIDAWI, AND S. CHANDRA, *J. Coat. Technol. Res.* **17**, 207–217 (2020).
- [2] B. DERBY, K. SIDAWI, AND S. CHANDRA, *Annu. Rev. Mater. Res.* **40**, 395–414 (2010).
- [3] J.F. HERNÁNDEZ-SÁNCHEZ, L.A. KUBBERS, A. EDDI AND J.H. SNOEIJER, *Phys. Rev. Lett.* **109**, 184502 (2012).
- [4] W.D. RISTENPART, P.M. MCCALLA, R.V. ROY AND H.A. STONE, *Phys. Rev. Lett.* **97**, 064501 (2006).

Chromatographic Effects in Inkjet Printing

Gianmarco Venditti, Vignesh Murali, and Anton A. Darhuber

Department of Applied Physics, Eindhoven University of Technology, The Netherlands

Corresponding author: a.a.darhuber@tue.nl

We have studied the chromatographic separation of solvents and dyes after deposition of a dye solution on a paper substrate [1]. Due to their larger molecular size, dyes typically exhibit a stronger interaction with the paper constituents. Consequently, the imbibition process of the dye is usually delayed compared to that of the solvent, see Fig. 1 for an example. This impacts the achievable resolution and color homogeneity in inkjet printing. We present experiments and a comprehensive numerical model to illustrate and quantify these effects. The model accounts for the solvent evaporation, heat transfer, multicomponent unsaturated flow, and dye adsorption, as well as the presence of permeable fibers in the paper substrate. We identify the key parameters that can be tuned to optimize the pattern fidelity of the printing process.

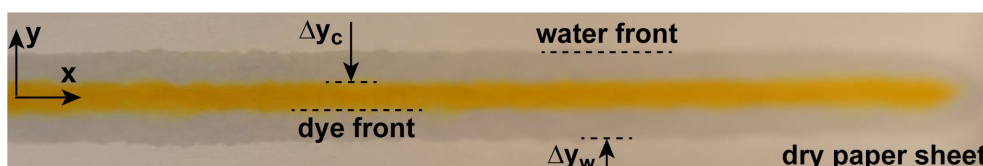


Fig. 1. Top-view photograph of commercial paper after inkjet printing a line of an aqueous fluorescein solution (initial concentration $c_0 = 0.05$ wt%; substrate speed $U_{\text{sub}} = 0.5$ mm/s). The water penetrates much further into the paper sheet than the dye due to chromatographic retention. Image height 6 mm.

Printing inks are typically multicomponent solutions of colorants, surfactants, humectants, and numerous other additives in aqueous or organic solvents. Upon contact with paper, capillary imbibition causes the flow of the solution. While progressive absorption of the solvent into the paper is usually desirable, it is generally undesirable if the ink colorants are transported significant distances from the ink deposition zone, as this diminishes the achievable resolution of the printing process. Similarly undesirable is the chromatographic separation of dye mixtures or non-homogeneous dye concentration profiles because these degrade the color uniformity and contribute to edge mottling.

The purpose of this paper is to present a numerical model for the imbibition and evaporation of a dye-based model ink containing a molecularly dissolved colorant in a solvent into and from paper substrates. The presence of fibers in the paper substrate is explicitly taken into account. The dye–paper interaction is described by the Langmuir-type rate equation for adsorption and desorption. The numerical simulations are complemented by experiments using anionic and cationic fluorescent dyes deposited either by drop-casting or inkjet printing.

References

1. G. Venditti, V. Murali, and A. A. Darhuber, *Langmuir* **37**, 11726–11736 (2021).

Inkjet printing of surfactant solutions onto thin moving porous media

Gianmarco Venditti, Vignesh Murali, and Anton A. Darhuber

Department of Applied Physics, Eindhoven University of Technology, The Netherlands

Corresponding author: a.a.darhuber@tue.nl

We have studied the combined imbibition and evaporation of surfactant solutions into thin porous media by means of experiments and numerical simulations. Solutions of anionic and non-ionic surfactants were deposited onto moving sheets of paper by a droplet-on-demand inkjet system. Optical transmission imaging and infrared thermography were used to monitor their lateral transport and evaporation. Moreover, we propose a theoretical model based on a dual-porosity approach that accounts for moisture and surfactant transport in both the pores and the fibers of the paper sheets as well as for surfactant adsorption. The numerical simulations reproduce the experimental data qualitatively well.

Surfactants are added to inkjet inks for a number of reasons. They tend to affect the contact angle on partially wetting substrates and thus control the ink wettability and the degree of droplet spreading. Surfactants can be used also as a dispersion agents that improve the colloidal suspension stability of colorant pigment particles. Surfactants can serve as emulsifiers, desizing or anti-foaming agents or promote the solubilization of dyes. Surfactants can reduce intercolor bleed and improve the ejection stability of ink droplets. Usually more than one surfactant species is present in a commercial ink formulation, and typically concentrations above the critical micelle concentration (cmc) are used.

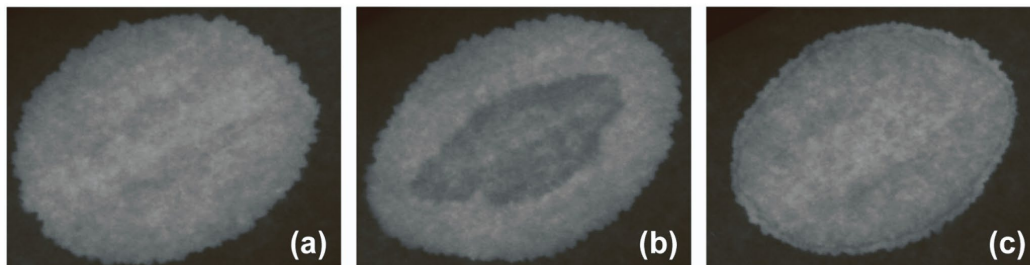


Fig. 1. Optical transmission images of wet zones in commercial inkjet printing paper substrates 300 s after deposition of droplets of (a) pure water and (b,c) sodium dodecyl sulfate (SDS) solutions of concentration $c = 1$ and 10 cmc, respectively. Image height 36 mm. The presence of the surfactant induces the formation of a darker region inside the wet zone, which reflects a locally reduced moisture content.

We studied the deposition of inkjet-deposited droplets and lines of an aqueous surfactant solution on a moving paper substrate by means of experiments and numerical simulations. We use light transmission and infrared thermography to characterize the moisture and temperature distributions due to wicking and evaporative cooling. In our model, we disregard the presence of liquid on top of the paper and thus effectively focus on the late stage of the simultaneous processes of imbibition of a surfactant solution into a paper substrate and evaporation of the solvent. We use a dual-porosity model of unsaturated flow based on the Richards equation, which explicitly accounts for the exchange between liquid residing in the pores and in the paper fibers. Moreover, we solve for surfactant adsorption on the fibers as well as for heat transfer to compare with the thermography measurements.

References

1. G. Venditti, V. Murali, and A. A. Darhuber, *Colloids Surf. A Physicochem. Eng. Asp.* **634**, 127832 (2022).

Muriel Mauron¹, Lucie Castens Vitanov¹, César Michaud¹, Raphaël Wenger¹, Derek Kiebalá²,
 Gilbert Gugler¹, Stephen Schrettl²

¹*iPrint Institute, HEIA-FR, University of Applied Sciences and Arts Western Switzerland, Fribourg CH-1700, Switzerland*

²*Adolphe Merkle Institute, University of Fribourg, Fribourg CH-1700, Switzerland*

Corresponding author: muriel.mauron@hefr.ch

Keywords: smart materials, functional surfaces, hardness gradient, multimaterial jetting, mechanochromic materials, inkjet

Inkjet printing technology has the advantage of being digital and extremely versatile by its nature: deposition of material through liquid phase processing, well controlled by the formation of pico-liter drops. In this case the droplet will be the smallest material unit called voxel. The ability to form such drops in a controlled manner enables the inkjet technique to not only be employed for graphical printing but also for the deposition of separated voxels on surfaces, possible even forming continuous layers. The spatially controlled deposition allows to functionalize surfaces, build materials gradients, and combine different materials to generate printed surfaces with new features. In this way, the preparation of surfaces and coatings with a tailored functionalization and performance on demand becomes possible. The process can be extended to the simultaneous deposition of several fluids by combining droplets on demand, maintaining a very high positional precision. In this way, new surfaces and materials in three dimensions, as for example materials with a controlled gradient of porosity, refractive indices or mechanical properties, can be engineered and fabricated.

Smart-Inks containing dissolved Polyurethanes (PU) with different hardness grades (Shore 35-80A) were formulated. A mechanochromic additive developed by the Adolphe Merkle Institute [1, 2], which changes its fluorescence absorption and color in response to mechanical forces (elongation) was added to the ink. This additive is a marker and has no impact on the properties of the PU. To ensure successful inkjet printing, the use of low-viscosity inks is required, which limits the current choice of materials. A big challenge was to find a suitable solvent compatible both with the additive and with commercially available inkjet printheads. Rheology of inks formulated with different solvents were measured at different PU concentrations and temperatures to judge their printability. A high boiling point solvent is preferred in inkjet to avoid drying of the ink at the nozzle. However, it turned out that a low boiling point solvent must be used due to the drying requirements of the additive. This resulted in a more difficult printing process, leading to a decrease of the PU concentration in the ink to remain jettable.

A multi-material inkjet platform was developed and printing process optimized, which allows to create gradient materials with new performances. Drops of selected inks were deposited by inkjet close to each other, then elongated up to 100% under the confocal microscope. Different substrates were tried out to find the optimal mechanochromic response. The intensity of the mechanochromic additive measured with the confocal microscope under UV light is different for each PU. It is possible to know with very high precision the hardness of the material by measuring this intensity (see Figure 1, 2 and 3). This visualization will help to simulate the behavior of the drops to create new tailored material with high precision deposition and resolution.

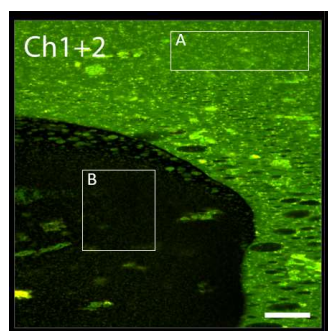


Figure 1: Confocal microscopy image of a sample made by dropcasting two inks, each comprised of a PU polymer of different hardness dissolved in dioxane along with the mechanochromic additive. A: Ink 1: PU with Shore 80A. B: Ink 2: PU with Shore 35A. 90% equibiaxial strain was applied to the sample before imaging.

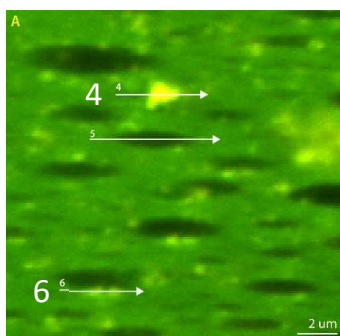
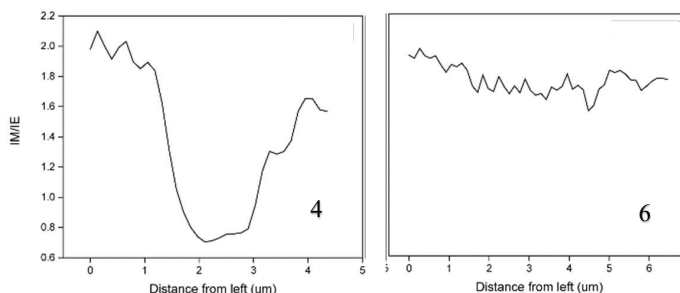


Figure 2 (left): A zoomed-in view of region A in Figure 1, showing phase-separated droplets of Ink 2 that have formed in Ink 1. Scale bar = 2 μm . Dark zone: softer PU. Light zone: harder PU.

Figure 3 (below): Plots of the local monomer-to-excimer ratio (I_M/I_E) in the sample along the lines shown in the direction indicated by the arrows. Note that regions of harder PU exhibit higher I_M/I_E values than softer PU. For line 6, only harder PU is present. The intensity can also be measured in the mixing zone between the two PU (line 4). Thanks to the mechanochromic additive and the measurement of its intensity, the hardness of the blend material can be measured.



References

1. Calvino, C.; Sagara, Y.; Buclin, V.; Haehnel, A. P.; del Prado, A.; Aeby, C.; Simon, Y. C.; Schrettl, S.; Weder, C. *Macromol. Rapid Commun.* **2019**, *40* (1), 1800705. <https://doi.org/10.1002/marc.201800705>.
2. Kiebalá, D. J.; Fan, Z.; Calvino, C.; Fehlmann, L.; Schrettl, S.; Weder. *Org. Mater.* **2020**, *02* (04), 313–322. <https://doi.org/10.1055/s-0040-1721052>.

The role of the dispersing agent on latency issues for water-based inkjet inks: drying aspect

Amélie Brogly¹, Gilbert Gugler², Gioele Balestra², Raphaël Wenger², Aurore Denneulin¹, Anne Blayo¹

¹Université Grenoble Alpes, LGP2, F-38000 Grenoble, France

²iPrint Center, HEIA-FR, HES-SO University of Applied Sciences and Arts Western Switzerland, 1700 Fribourg, Switzerland

Corresponding author: amelie.brogly@grenoble-inp.fr; anne.blayo@grenoble-inp.fr; aurore.denneulin@grenoble-inp.fr; gilbert.gugler@hefr.ch; gioele.balestra@hefr.ch; raphael.wenger@hefr.ch

Abstract

Inkjet inks and particularly water-based and pigmented inks are challenging to formulate. The requirements they need to achieve are strict in terms of viscosity, density, surface tension, etc (1). The pigment dispersion is a crucial step in ink preparation. The pigment needs to be stabilized with the help of dispersing agent during the grinding step. The level of colloidal stability achieved during this step will determine the shelf-life of the inks but also the quality of the jetting. A stable jetting is necessary to obtain good printing quality, depending on the application: textile, electronics, graphic industry, etc. The use of water-based inks seems a good start in the environmental transition. However, several issues are encountered with this type of fluid. One of the main problems is the latency phenomenon. Nozzles of the printhead are idle for a certain amount of time. This idle time can be short (seconds) during the printing or long (minutes) between the printing of two different designs. Latency appears when the jetting behavior is degraded after this idle time. This deterioration may be noticed by a decrease in drop speed, drop volume, or the non-appearance of drop. So far, this phenomenon was explained in the literature by a drying (2) of the ink at the interface of the nozzle meniscus. This paper tries to give a better understanding of this hypothesis.

Keywords: water-based inkjet inks, latency, drying, diffusion, dispersion, dispersing agent

Objectives

The objective of this paper is to understand better the phenomenon of latency seen in Figure 1. The role of the dispersing agent not correctly anchored to the pigment surface (free dispersing agent) seems to have an impact on this issue (3). Three inks with different percentages of free dispersing agent are studied in this article. Ink 1 does not have this excess of dispersant thanks to a special crosslinking step around the pigment particles, in inks 2 and 3, 1 wt.% and 3 wt.% of free dispersing agent respectively were added to the ink formulation. Latency was determined with the counting of non-firing strokes before first drop for different idle times at 500 Hz and 30°C. The impact of the humidity rate of the environment was also studied. Drying phenomenon was determined with the deposition of a thin layer of ink on aluminum foil. A transfer of the ink was made on paper at different drying times to evaluate this parameter.

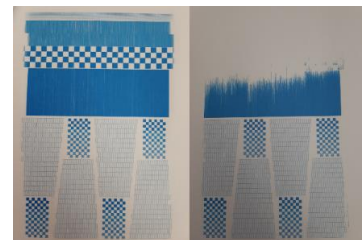


Figure 1: Pattern printed without latency (left) and with latency (right)

Results

The number of non-firing strokes (N_{nfs}) before first drop increases with idle time and with the percentage of free dispersing agent in Figure 2.

The drying of inks 2 and 3, including a part of free dispersing agent, seems longer than for the ink 1, without this excess of dispersant in Figure 3. This statement leads to the hypothesis of diffusion of dispersing agent molecules at the interface of the meniscus instead of a strong drying.

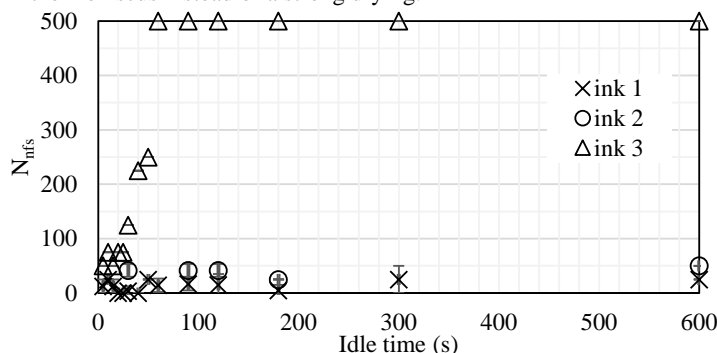


Figure 3: Number of non-firing strokes before first drop for inks with (2,3) or without (1) excess of dispersant

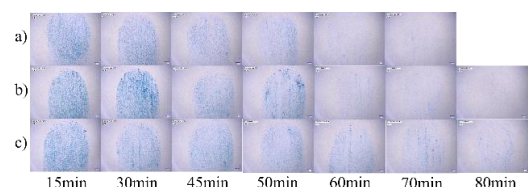


Figure 2: Transfer of the ink on paper after different drying times. a) refers to ink 1, b) refers to ink 2 and c) refers to ink 3

Bibliography

1. Hoath SD. Fundamentals of Inkjet Printing. 2016.
2. Magdassi S. The chemistry of inkjet inks. Singapore ; Hackensack, NJ: World Scientific; 2010. 345 p.
3. Jackson C. Aspects of Aqueous Pigment Ink Formulation : Latency, Dynamic Surface Tension, and Pigment Volume Concentration. 2016;55(6):9.

Falling films on a slippery wall: a revisited formulation

Khawla Msheik¹, Christian Ruyer-Quil²

¹ Institut Camilla Jordan UMR CNRS 5208, Université Lyon 1, Villeurbanne

² LOCIE UMR CNRS 5271, Université Savoie Mont Blanc, Chambéry

Corresponding author: christian.ruyer-quil@univ-smb.fr

We propose to revisit the problem of the wavy motion of a falling film on a slippery impermeable wall modeled by a Navier slip boundary condition. J.P. Pascal [1] showed that such a configuration is a convenient modeling of a permeable saturated porous substrate whenever the Beaver and Joseph boundary condition holds and the Darcian velocity in the porous medium is negligible with respect to the velocity in the film, i.e. at low permeabilities.

Modeling attempts on this problem either assume a small slip length l_s with respect to the film thickness [2] or lack mathematical structure as the model coefficients are functions of the local ratio of the slip length to film height l_s/h which is a function of time and space [3, 4]. As a consequence, the inclusion of inertia is limited to first-order consistency with respect to the film parameter $\epsilon = h_N/\lambda$, where h_N and λ refer to the Nusselt film thickness and typical wavelength respectively.

We will present a novel formulation which overcomes those difficulties. Our model is second-order accurate and present a clearer mathematical structure. In particular, coefficients are independent on l_s/h and the classical Saint-Venant averaged momentum balance is included in the model. This guarantees that the inviscid classical shallow-water equations are recovered in the limit $l_s \rightarrow \infty$. Besides, surface tension terms appear only in the averaged momentum equation, which enables to propose an augmented formulation of our model and therefore to account for complete surface tension forces, i.e. without the linear approximation of the curvature that is generally employed in thin-film studies [5]. The second-order four-equation model proposed by Ruyer-Quil and Manneville [6] is recovered in the appropriate limit. In particular, our new formulation being much simpler, is easily implemented numerically. An example of a time-dependent simulation of the response of the film to a periodic forcing is offered in figure 1. We are thus in a position to consider the accurate simulations of 2D flows on uneven geometries at an affordable cost.

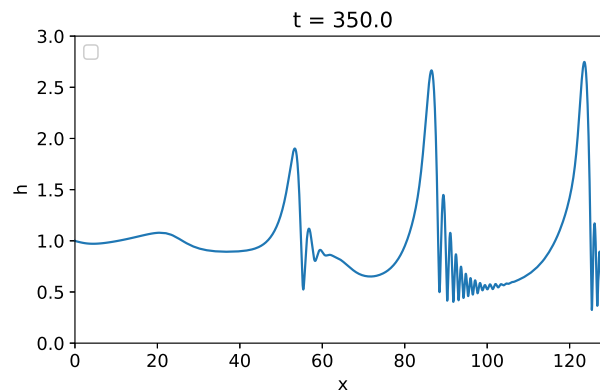


Figure 1: Simulation of a water film on a vertical wall ($Re = 69$, $Ka = 3650$, $l_s/h_N = 0.01$).

References

- [1] J.P. PASCAL, *J. Phys. D: App. Phys.* **32**, 417–422 (1999).
- [2] Y. CHAO, Z. DING, R. LIU, *Chem. Engng Sci.* **175**, 354–364 (2018).
- [3] A. SAMANTA, C. RUYER-QUIL, B. GOYEAU, *J. Fluid Mech.* **684**, 353–383 (2011).
- [4] H. JI, C. FALCON, A. SADEGHPOUR, Z. ZENG, Y.S. JU, A.L. BERTOZZI, *J. Fluid Mech.* **865**, 303–327 (2019).
- [5] D. BRESCH, N. CELLIER, F. COUDERC, M. GISCLON, P. NOBLE, G.-L. RICHARD, C. RUYER-QUIL, J.-P. VILA, *J. Comp. Phys.* **419**, 109670 (2020).
- [6] C. RUYER-QUIL AND P. MANNEVILLE, *Eur. Phys. J. B* **15**, 357–369 (2020).

Falling liquid film subject to a counter-current turbulent gas flow: beyond the absolute instability limit

Misa Ishimura^{1,3,4}, Sophie Mergui², Christian Ruyer-Quil³ and Georg F. Dietze¹

¹ Université Paris-Saclay, CNRS, FAST, 91405, Orsay, France.

² Sorbonne Université, Université Paris-Saclay, CNRS, FAST, 91405, Orsay, France.

³ Université Savoie Mont Blanc, CNRS, LOCIE, 73376, Le Bourget du Lac, France.

⁴ Department of Mechanical Engineering, Yokohama National University, Kanagawa, Japan.

Corresponding author: dietze@fast.u-psud.fr

Falling liquid films occur in several industrial processes involving heat/mass transfer operations, e.g. in distillation columns for cryogenic air separation. In that configuration, a gravity-driven liquid film is subject to a counter-current turbulent gas flow confined in a channel spanning approx. 10 mm. Surface waves, developing on the liquid film due to the Kapitza instability [1], are known to greatly intensify inter-phase heat/mass transfer. At the same time, they can trigger flooding events, such as channel obstruction and liquid reversal. Elucidating this dichotomic role of surface waves is key to identifying optimal wavy film regimes. The current work [2] contributes to this by investigating the effect of the counter-current gas flow on the waviness of the liquid film, with particular attention to regimes beyond the absolute instability (AI) limit of the Kapitza instability.

We apply three approaches: (1) experiments following [3], where Kapitza waves of forced frequency are allowed to develop in a protected zone before entering into contact with the counter-current gas flow, and where we characterize the waviness of the liquid film using shadowgraphy and film thickness measurements; (2) stability calculations based on the full Navier-Stokes equations in the liquid and RANS equations in the gas; and (3) nonlinear computations with a new low-dimensional model, which is based on the WRIBL approach [4] in the liquid and a long-wave asymptotic expansion [5] in the gas, and which we have validated versus our own experiments and literature data [6].

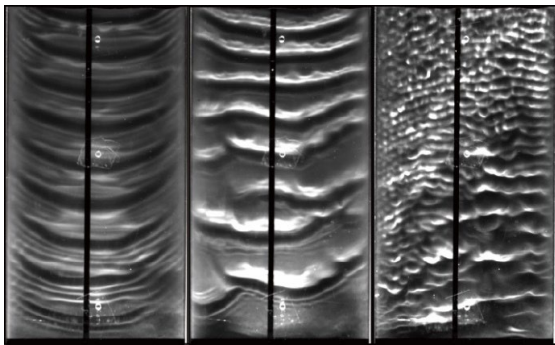


Fig. 1. Falling water film sheared by an increasingly strong counter-current confined turbulent air flow. *Left:* quiescent gas. Regular downward-travelling Kapitza waves; *middle:* counter-current gas. Coalescence of Kapitza waves; *right:* counter-current gas far beyond the AI limit. Upward-travelling short ripples leading to flooding.

Figure 1 shows the wave transition observed in our experiments under an increasingly strong counter-current gas flow. For a quiescent gas (left panel), regular downward-travelling Kapitza waves dominate the film surface. These waves start to coalesce when a sufficiently strong counter-current gas flow is applied (middle panel). However, no catastrophic events are observed when crossing the AI threshold. On the contrary, in the case of a natural wave evolution scenario, where the liquid film is sheared by the gas over its entire length, as we have simulated with our low-dimensional model, we find that AI acts as an effective wave selection mechanism, producing highly-regular downward-travelling Kapitza waves, allowing to preclude coalescence events, and, thus, to lower the flooding risk. Far beyond the AI limit (right panel), we observe upward-travelling short ripples that first compete with the long Kapitza waves and then dominate the latter. These ripples lead to an accumulation of liquid in the gas loop, marking the flooding threshold in our experiment.

With the help of linear stability analysis, we have identified a new short-wave interfacial instability mode that causes the upward-travelling ripples, and is associated with negative wave speeds. The onset of this mode requires the presence of turbulence in the gas flow, explaining why previous stability investigations based on the laminar Navier-Stokes equations [7,8] did not identify it. In our experiments, the short-wave ripples are observed only far beyond their linear instability threshold, because long Kapitza waves are privileged by the protected unshered region of our setup. In reality, their linear onset lies only slightly beyond the AI limit of the Kapitza instability. In this regime, the two instability modes compete. Then, at larger counter-current gas flow rates, the long-wave branch of the Kapitza mode and the short-wave branch of the short-wave mode merge, forming a new composite instability mode that covers a large range of wave numbers.

References

- [1] Kapitza, P. L., *Zhurn. Eksp. Teor. Fiz.*, **18**, 3-28 (1948).
- [2] Ishimura, M., Mergui, S., Ruyer-Quil, C. and Dietze, G. F., *Journal of Fluid Mechanics*, in press.
- [3] Mergui, S., Lavalle, G., Li, Y., Grenier, N. and Dietze, G. F., *Journal of Fluid Mechanics* **954**, A19 (2023).
- [4] Ruyer-Quil, C. and Manneville, P., *European Physical Journal B* **15**, 357-369 (2000).
- [5] Camassa, R., Ogrosky, H. R. and Olander, J., *Journal of Fluid Mechanics*, **825**, 1056-1090 (2017).
- [6] Kofman, N., Mergui, S. and Ruyer-Quil, C., *International Journal of Multiphase Flow* **95**, 22-34 (2017).
- [7] Schmidt, P., Naraigh, L., Lucquiaud, M. and Valluri, P., *Physics of Fluids* **28**, 042102 (2016).
- [8] Trifonov, Y. Y., *International Journal of Multiphase Flow* **95**, 144-154 (2017).

Modelling thin-film flow over a spinning disk

Laura Milne¹, Alexander W Wray¹, Omar K Matar², Marc Pradas³, Stephen K Wilson¹

¹ Department of Mathematics and Statistics, University of Strathclyde, Glasgow

² Department of Chemical Engineering, Imperial College London, London

³ School of Mathematics and Statistics, The Open University, Milton Keynes

Corresponding author: l.milne@strath.ac.uk

Film flows on spinning disks have a wide range of applications in industry, including heat and mass transfer, in which contexts the waves generated cause an increase in the surface area of the film which tends to augment heat and mass transfer processes. Furthermore, the dynamics of the flow lead to enhanced mixing, which is exploited in industrial processes such as the production of fine chemicals and pharmaceuticals [1]. Therefore, it is important to understand the dynamics of such flows so that we can optimise their behaviour. In the present work, we study the dynamics of a thin, axisymmetric film of Newtonian fluid on a uniformly rotating disk with topography. The system is modelled via a thin-film (i.e. lubrication) approximation together with the Method of Weighted Residuals [2] up to second order. The resulting model includes the effects of inertia, viscosity, centrifugation and capillarity. We obtain a closed initial-value problem for the film thickness and the radial and azimuthal fluxes, which we investigate both numerically and analytically; this system shows convective instability. We study a family of topographies with parameters controlling the asymmetry, smoothness, amplitude and frequency of the topography. The effect of topography on the flow of the film is investigated using an integral measure of the interfacial waviness denoted by $W(t)$, where t denotes time [3]. In particular, we find that the presence of topography can cause additional interfacial waves which can increase the surface area of the film, as shown in Figure 1.

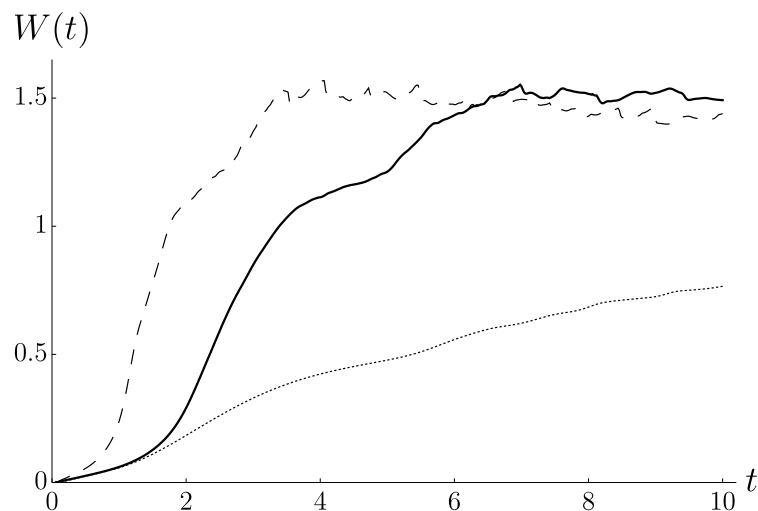


Figure 1: An integral measure of the interfacial waviness $W(t)$, for a planar disk (dotted curve), a disk with a left skewed, highly smoothed and low frequency topography (solid curve), and a disk with a right skewed, highly smoothed and low frequency topography (dashed curve).

References

- [1] A. AOUNE AND C. RAMSHAW, Process intensification: heat and mass transfer characteristics of liquid films on rotating discs, *International Journal of Heat and Mass Transfer*, **42**(14), 2543–2556 (1999).
- [2] C. RUYER-QUIL AND P. MANNEVILLE, Improved modelling of flows down inclined planes, *The European Physical Journal B—Condensed Matter and Complex Systems* **15**, 357–369 (2000).
- [3] O.K. MATAR, G.M. SISOEV AND C.J. LAWRENCE, Thin film flow over spinning discs: The effect of surface topography and flow rate modulation, *Chemical Engineering Science*, **63**(8), 2225–2232 (2008).

Fluid invasion front within a confined copper pillar array for microelectronic

Mary-Ann Gasser^{1,2}, Loïc Vanel² and Abdenacer Ait mani¹

¹ CEA LETI, Université Grenoble Alpes, 38054 Grenoble, France

² CNRS, Institut Lumière Matière, Univ. de Lyon, Univ. Claude Bernard Lyon1, F-69622 Villeurbanne, France

Corresponding author: mary-ann.gasser@cea.fr

Since electronic devices keep getting more powerful, there is a growing need to integrate more components without reducing performances. Flip chip hybridization is a key technology to reach this goal [1]. The top active component is hybridized onto the bottom readout component using in our case thermocompression (heat + force). To ensure a complete reliable structure, an essential step after hybridization is the underfill (Fig.1). Mostly based on epoxy resin, its main roles are to reduce the mismatch in thermal expansion impact and lower the thermomechanical stress on the interconnections elements. Moreover, the underfill protects the interconnections from an aggressive environment. In order for the underfill to be effective, it needs to be completely void-less and have a good adherence with all the materials present in Fig.1. This is a big challenge because flip chip components for display are typically 4cm² with over 450 000 interconnections. The interconnections are in the studied case 20 μ m high, 15 μ m wide with a 30 μ m pitch.

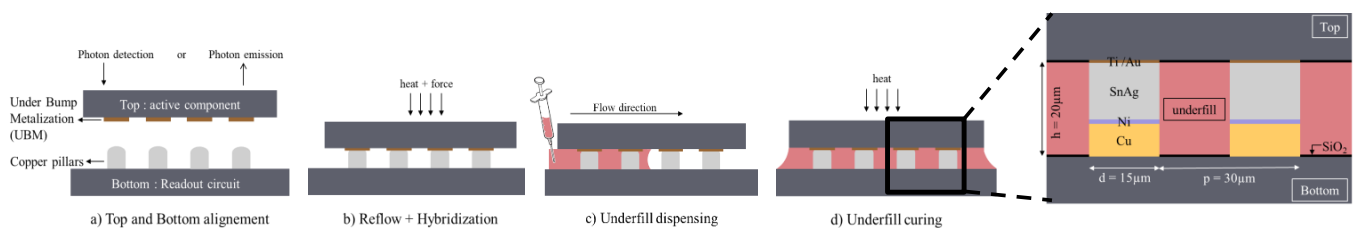


Fig. 1: Flip chip hybridization and underfill process with a presentation of all the materials.

This study is focused on understanding the propagation of the underfill in the micro pillar array. The epoxy glue has a very variable viscosity and its interfacial energy with the various materials of the hybridized structure varies (contact angle from 0° to 60°). To overcome these challenges, PDMS was used as a reference fluid, for its high wettability with the materials and well-known viscosity.

In order to understand the fluid flow, we conducted several experiments at different scales: large field and at the pillar level. We compare experiments on test vehicles with no pillar, where Washburn law applies, to experiments with hybridized circuits (CH). All these samples have a top made of glass to make it see through.

The large field's results allowed us to validate the experimental set up and compare the results of the front position as a function of time with models presented in literature [2], [3]. At the pillar level, we observe that the contact line advances by jumps on a forward pillar followed by lateral propagation of kinks to fill the line before jumping on to the next line as seen on Fig.2. We analyze the propagation dynamics of the kink, which velocity is much higher than the main front line velocity.

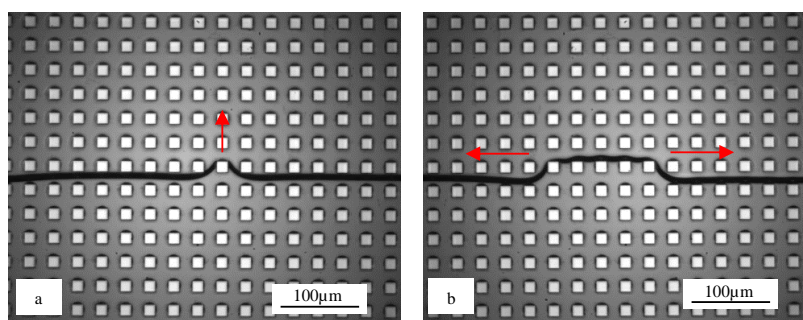


Fig. 2: Microscope images at the pillar level scale: PDMS kink propagation between pillars

a: the contact line advances on a pillar of the next line / b: the contact line propagates like kinks to fill the line

References

- [1] J. H. Lau, *Flip Chip Technologies*, McGraw-Hill, New York. 1996.
- [2] P.-G. de Gennes, F. Brochard-Wyart, and D. Quéré, *Capillarity and Wetting Phenomena*. New York, NY: Springer New York, 2004. doi: 10.1007/978-0-387-21656-0.
- [3] B. Darbois Texier, P. Laurent, S. Stoukatch, and S. Dorbolo, "Wicking through a confined micropillar array," *Microfluid. Nanofluidics*, vol. 20, no. 4, p. 53, Apr. 2016, doi: 10.1007/s10404-016-1724-3.

Thickness gradients induced by defects in liquid deposition

Gabrielle Di Mauro¹, Bertrand Heurtefeu², Jérémie Teisseire², François Lequeux³, Laurence Talini¹

¹ CNRS, Surface du Verre et Interfaces, Saint-Gobain, 93300 Aubervilliers

² Saint-Gobain Research Paris, 93300 Aubervilliers

³ CNRS Sciences et Ingénierie de la Matière Molle, ESPCI Paris, PSL Research University, Sorbonne Université 75005 Paris

Corresponding author: gabrielle.dimauro@saint-gobain.com

Drying a film of complex fluid on a solid substrate generally results in a spatially non uniform dry deposit. Thickness gradients can be induced by heterogeneities of the evaporation flux [1], [2]. The solvent then flows from the region where the evaporation flux is smaller to the region where the evaporation flux is larger, transporting solute to the latter regions. Thickness gradients can as well be caused by the presence of defects, such as dust particles from the atmosphere or topographic defects of the substrate. Thickness heterogeneities extending over distances up to ten times larger than the size of the defect can then be observed. In the literature, the influence of a substrate with topography on thin film drying has been studied numerically; a valley region has been shown to result in either a valley or a bump on the dry deposit, according to the interplay of capillary and Marangoni flows [3].

We aim at understanding the mechanism of solute transport in presence of defects that leads to such a large extent of thickness gradients. We spread films of amorphous polymer solutions (typical thickness $100\mu\text{m}$) on glass substrates and measure their thickness after they have dried in controlled conditions in presence of defects. We consider three kinds of model defects : hollows (made by impacting glass with a laser, bumps (formed by melted glass beads) and floating glass beads (scattered on the surface of the liquid film at the beginning of drying).

Thickness measurements of the dried film show that the extent of the thickness heterogeneity strongly depends on the nature of the defect. In case of defects of the substrate topography, the thickness gradient is induced over a distance of order of the size of the defect itself. In contrast, as shown in the figure below, the thickness gradient induced by a floating glass bead extends over a distance about ten times larger than the size of the bead. We show that in the latter case, polymer transport is caused by generation of a capillary wave as the bead impacts the surface of the liquid film. In contrast, the topography of the substrate results in a difference of evaporation flux, which is caused by a difference of polymer concentration and therefore of solvent activity at the interface. Ongoing work consists in systematically varying the size of the defects and the thickness of the liquid films in order to provide further insight on the thickness heterogeneities of dried films resulting from defects.

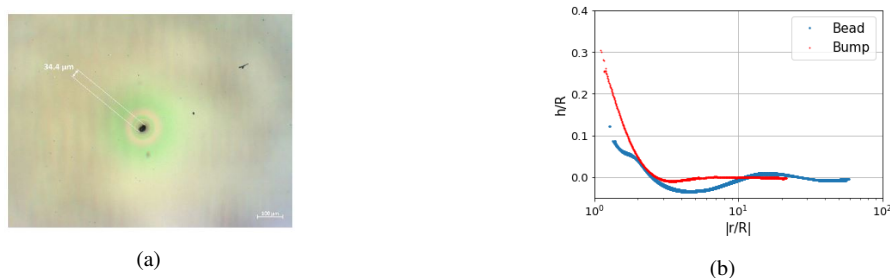


Figure 1: a) Photograph showing the thickness gradient of a coating observed with white light around a $34\mu\text{m}$ defect and extending over a distance of $150\mu\text{m}$. b) Thickness variation profil resulting from a floating bead and a bump normalised by the radius of the defect as function of the normalised distance to the center of the defect. The thickness variation is measured with respect to the thickness of the flat layer, far from the defect.

References

- [1] A. F. ROUTH, AND W. B. RUSSEL, *AIChE Journal* **12**, 2088–2098 (1998).
- [2] A. FAIDHERBE, M. WILMET, J. TEISSEIRE, F. LEQUEUX AND L. TALINI, *Langmuir* **39**, 3018–3028 (2013).
- [3] T. PHAM, X. CHENG AND S. KUMAR, *Journal of Polymer Science* (2016).

Drying liquid coatings with an evaporation mask

Apolline Faidherbe¹, Maxence Wilmet², Jérémie Teisseire², François Lequeux³ and Laurence Talini¹

¹ Surface du Verre et Interfaces, CNRS, Saint-Gobain, Aubervilliers, France

² Saint-Gobain Research Paris, Aubervilliers, France

³ Sciences et Ingénierie de la Matière Molle, ESPCI Paris, PSL Research University, Sorbonne Université, Paris, France

Corresponding author: laurence.talini@cnrs.fr

In an evaporating liquid film, the evaporation flux is larger at the edges than at the center; as a result, a flow is generated, which is directed from the region of smaller evaporation flux (i.e. the center) towards the regions of larger fluxes (i.e. the edges) [1]. If the liquid is a complex fluid, solute accumulates at the edges and the final dry deposit has a non uniform thickness. Quantitative understanding of this effect is lacking, and is required to improve the uniformity of layers obtained by wet coating processes.

We have studied the effect of a nonuniform evaporation flux on evaporating films of polymer solutions in a 1D geometry [2]. A region of zero evaporation has been induced at the center of liquid film using an evaporation mask, i.e. a solid that is placed above the surface of the film and locally stops evaporation by saturation of solvent vapor between the surface and the mask. As previously reported [1, 3], the solvent flows induced during drying result in a depressed region under the mask of the dry polymer layer, together with overthicknesses at its edges, which extend over distances that may be larger than the size of the mask (see Fig. 1).

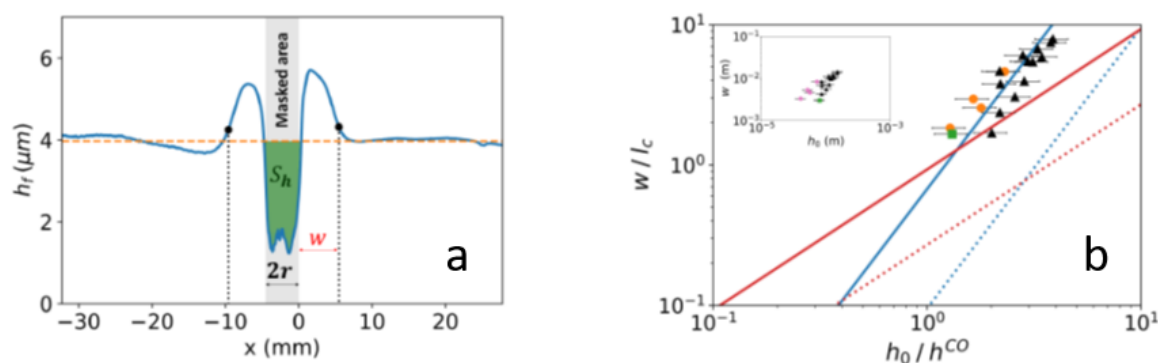


Fig. 1. (a) Thickness profile of a film formed by drying a polymer solution under an evaporation mask and definition of the extent w of the thickness heterogeneities, which experimental values (normalized by the capillary length) are shown in (b) as a function of the initial thickness of the film normalized by a crossover thickness. The experimental data is well described by the theoretical predictions for gravity-driven flows with a constant viscosity (full blue line).

Using a linear approximation, we have obtained analytical solutions for the thickness profiles during drying in the limits of either gravity or capillarity driven flows. We demonstrate that gravity can play a role in the deformations of the films, even if their initial thicknesses are one order of magnitude smaller than the capillary length. In addition, we examine two possible reference states for the linear approximation, i.e. far from the mask in the film of decreasing thickness and increasing viscosity, or under the mask where no evaporation occurs. We further compare these results with experimental ones obtained by drying thin films of polymer solutions under a mask. Both the extent and amplitude of the thickness heterogeneities of the dry film are quantitatively predicted by the linear analysis for a reference state under the mask.

Our study can be generalised to minimize thickness heterogeneities in any situation in which the evaporation flux is non uniform and therefore provides new insight on the mastering of thickness uniformity in wet coating processes.

References

1. A.F. Routh and W.B. Russel, *AIChE Journal* **44**, 2088–2098 (1998).
2. A. Faidherbe, M. Wilmet, J. Teisseire, F. Lequeux and L. Talini, *Langmuir* **39**, 3018–3028 (2023).
3. C. Parneix, P. Vandoolaeghe, V.S. Nikolayev, D. Quéré, J. Li and B. Cabane, *Physical Review Letters* **105**, 266103 (2010).

Stable and unstable coating flows on curved substrates

François Gallaire

Ecole Polytechnique Fédérale de Lausanne

Drainage and spreading processes in thin liquid films have received considerable attention in the past decades. Yet, our understanding of three-dimensional cases remains sparse, with only a few studies focusing on flat and axisymmetric substrates. Here, we exploit differential geometry to understand the drainage and spreading of thin films on curved substrates, under the assumption of negligible surface tension and hydrostatic gravity effects. We develop a solution for the drainage on a local maximum of a generic substrate. We then investigate the role of geometry in defining the spatial thickness distribution via an asymptotic expansion in the vicinity of this maximum, and analyze the competition between the variations of the substrate's slope and mean curvature in spheroids, tori and ellipsoids with three different axes. The solutions are in agreement with numerical simulations and experimental measurements obtained from the coating of a curing polymer on diverse substrates.

Leveraging the conservation of mass, an analytical solution for the average spreading front is obtained. We re-introduce surface tension effects and observe that, when the spreading takes place on a non-wetted substrate, a capillary ridge forms, which is prone to an instability with respect to transverse perturbations, resulting in the formation of fingers. In contrast to the classic case of a flow over an inclined plane, the gravity components along a cylindrical substrate vary in space and the draining flow is time-dependent, making a modal stability analysis inappropriate. A linear optimal transient growth analysis is instead performed to find the optimal transverse wavenumber.

We finally turn the substrate upside down and investigate the Rayleigh-Taylor instability of a thin liquid film coated on the inside of a cylinder whose axis is orthogonal to gravity. In this configuration, gravity not only yields the progressive drainage and stretching of the coating along the cylinder's wall, but it also acts as the destabilizing force at the origin of the instability. We find that this draining flow stabilizes the film, which is asymptotically stable to infinitesimal perturbations. However, the short-time algebraic growth that these perturbations can promote the formation of different patterns, whose nature depends on the Bond number that prescribes the relative magnitude of gravity and capillary forces. Our experiments indicate that a transverse instability arises and persists over time for moderate Bond numbers. The liquid accumulates in equally spaced rivulets whose dominant wavelength corresponds to the most amplified mode of the classical Rayleigh-Taylor instability. For higher Bond numbers, a two-dimensional stretched lattice of droplets is found to form on the top part of the cylinder. The transition between the two types of patterns can be rationalized by a linear optimal transient growth analysis and nonlinear numerical simulations.

Wetting flows with viscoelasticity

Jacco Snoeijer

Fac. of Science and Technology, University of Twente, NL

Coating flows typically involve high rates of deformation. When polymers are present in solution, we thus expect violent stretching of polymers and hence strong viscoelastic effects. In this talk we first present experiments on the very rapid initial stages of spreading of a droplet that is gently brought into contact with a solid. The influence of polymers is somewhat unexpected, and we relate our findings to recent insights in viscoelastic coalescence. We then turn to the late stages of drop spreading. Based on a newly derived viscoelastic lubrication equation, we establish a modified form of the classical Cox-Voinov theory that systematically accounts for the normal stress effect. We apply this theory to a variety of (de)wetting geometries and show how normal stress facilitates (inhibits) the motion of advancing (receding) contact lines.

Free surface flows and contact line motions with suspensions

Alice Pelosse¹, Élisabeth Guazzelli¹, Matthieu Roché¹

¹ Laboratoire Matière et Systèmes Complexes, Université Paris Cité, Paris
Corresponding author: alice.pelosse@ens-lyon.fr

Blood, paint, cement, mudslides or avalanches are suspensions, mixtures of particles suspended in a fluid. When the Brownian motion of the particles is negligible, we speak more specifically of granular suspensions, complex fluids that have surprisingly simple volume properties with a continuous medium approach. For example, for a concentrated monodisperse suspension with a solid fraction ϕ of 40%, the mixture remains Newtonian and its effective viscosity is 10 times that of the suspending fluid, whatever the particle size.

We focus on concentrated granular suspensions with free interfaces and, in particular, on the spreading of a drop [1]. The bulk properties of the continuous medium approach are challenged by a moving interface that must contend with the biphasic flow. In the vicinity of the contact line, the particles cannot approach due to their size. The size of the pure fluid zone increases with particle diameter. When the thickness is sufficient, a highly ordered monolayer is observed, a consequence of the extreme confinement of the particles. Further away, a disordered region follows as the confinement by the interface becomes less important.

An experimental and theoretical approach is used to study the influence of the particles on the wetting dynamics. The classical models (Cox-Voinov, Tanner) remain valid with effective viscosities. However, in contrast to the volume properties, the effective viscosity of a wetting suspension is strongly influenced by the particle size. In particular, for particles larger than 100 microns, the measured viscosity is that of the pure fluid. This characteristic size of the viscous "cutoff" is found by analysis of the spreading equations and confirmed experimentally. The study of bidisperse systems confirms the effects of size and order of the particles near a contact line in advance. Finally, the global spreading dynamics is studied and related to local observations near the contact line.

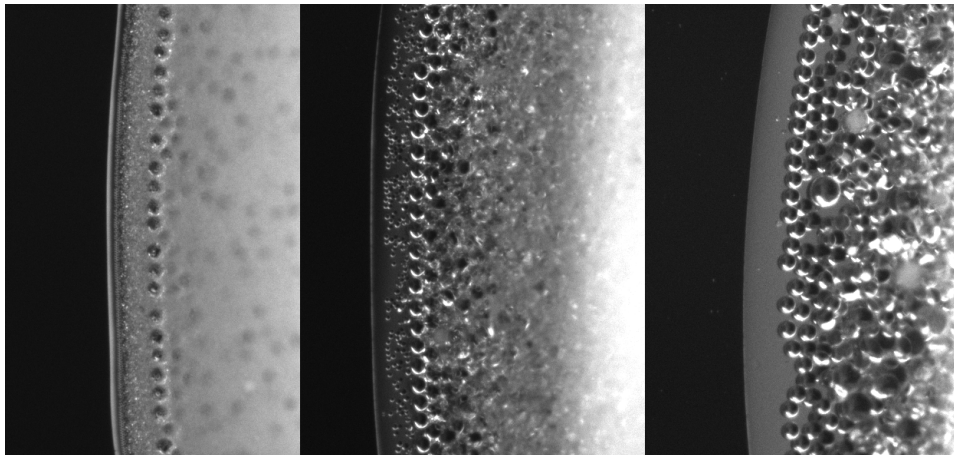


Figure 1: Vicinity of the contact line for drops of granular suspensions of (10-80), (20-80), and (80-250) micron particles (from left to right).

References

- [1] A PELOSSE, É GUAZZELLI, M ROCHÉ, *Journal of Fluid Mechanics*, **955**, A7 (2023).

Delayed coating of a liquid film on a soft substrate in a partially wetted condition

Anthony Varlet¹, Philippe Brunet¹, Laurent Limat¹, Julien Dervaux¹, Matthieu Roché¹

¹ Laboratoire Matière et Systèmes Complexes, UMR 7057/CNRS, Université Paris Cité, Paris

The dip-coating technique is a method for coating a solid by pulling it out of a liquid bath at constant velocity. This setup is suitable for studying the dynamics of wetting as the velocity at which the substrate is pulled out of the bath is a finely controlled parameter. Here we study the coating of a deformable silicone gel with a layer of Newtonian liquid under partial wetting conditions. The Young's modulus Y varied between 25 kPa and 1 MPa.

The observations with a rigid solid are fairly well known and understood. In total wetting, the solid is systematically coated with a liquid film of uniform thickness given by the Landau-Levich-Derjaguin relation, $h \propto Ca^{2/3}$ [1] (Ca is the capillary number, a dimensionless number comparing viscous and capillary forces such as $Ca = \frac{\eta U}{\gamma}$, where η is the dynamic viscosity of the liquid (Pa.s), γ the surface tension (J/m²) and U the pulling speed (m/s)). In the case of partial wetting, the solid is coated when Ca is above a threshold value, otherwise we observed only a meniscus at a stationary height above the liquid tank [2].

To this day, the coating of soft solids has been little studied [3]. We present here a hitherto unreported phenomenon which, to the best of our knowledge, is not observed in rigid solids : the entrainment of liquid occurs after a delay time τ (Fig. 2), within a range of Ca . Above a critical Ca , the entrainment is immediate, and below a lower threshold in Ca , the delay becomes too long to be accessible to our setup.

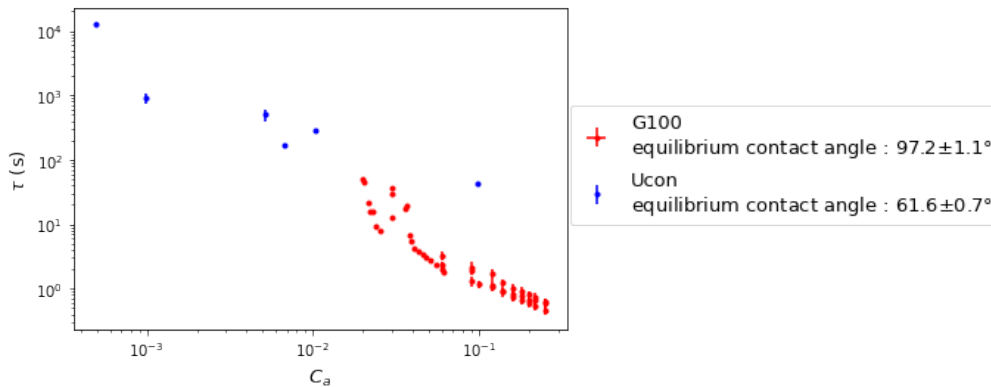


Figure 1: Delayed coating time τ as a function of the capillary number Ca .

For two liquid : Pure glycerol (G100, $\gamma \sim (63.1 \pm 0.5)10^{-3} \text{ J/m}^2$ and $\eta \sim 1.291 \pm 0.301 \text{ Pa.s}$) and a lubricant (Ucon, $\gamma \sim (40.7 \pm 0.9)10^{-3} \text{ J/m}^2$ and $\eta \sim 50.638 \pm 1.647 \text{ Pa.s}$).

The origin of this delay has not yet been clearly explained. In our presentation we will also discuss two possible mechanisms for this delay. The first mechanism involves the free, unreticulated chains present in our substrates, which cause a phenomenon of poroelasticity. The second be the slow, progressive growth of the deformation at the contact line, transported by the moving contact-line, which could then be related to the visco-plasticity of the substrate.

References

- [1] L. LANDAU, B. LEVICH, *Dynamics of Curved Fronts*, 141-153 (1988).
- [2] J. H. SNOEIJER, G. DELON, M. FERMIGIER, B. ANDREOTTI, *PHYSICAL REVIEW LETTERS*, **96**, 174504, (2006).
- [3] V. BERTIN, J. H. SNOEIJER, E. RAPHAËL, T. SALEZ, *PHYSICAL REVIEW FLUIDS*, **7**, L102002 (2022).

Acoustically-Induced Sinuous-Varicose Coupling in Falling Fluid Rivulets

Grégoire Le Lay¹, Adrian Daerr¹

¹ MSC Laboratory (UMR 7057), Université Paris Cité, Paris, France

Corresponding author: gregoire.le-lay@u-paris.fr

Oil injected between two vertical glass plates forms a liquid bridge, termed rivulet, which falls down under the effect of gravity. This simple system allows us to study the dynamics of a liquid file interaction with a surface without having to consider the complex contact lines dynamics that arise with partial wetting. The rivulet behaviour is nontrivial because of the coupling between the flow inside the rivulet and the geometry of its free surface [1].

We excite acoustically the rivulet using speakers placed on the side of the cell, creating a spatially homogeneous forcing. The rivulet behaves like a one-dimensional membrane and moves transversally, the straight downward flow of constant cross-section becoming unstable. The file then adopts a sinuous trajectory where the fluid is concentrated in heavy patches linked by thinner portions, as illustrated on fig. 1. We show that this instability is the result of a nonlinear coupling between the sinuosity of the rivulet path and the cross-section width heterogeneity which — to our knowing — hasn't yet been described in the literature.

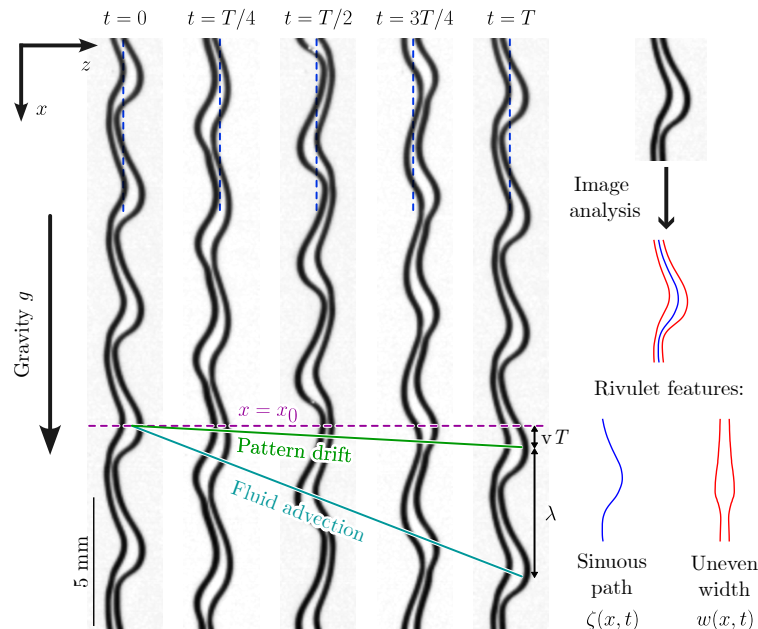


Figure 1: The rivulet free surface (in black, experimental data). At $t = T/4$ and $t = 3T/4$, the displacement of the space-averaged center of mass is maximal with respect to its mean value (blue dotted line). The sinuous path drifts with the slow speed v when the patches of fluid are advected at a greater speed.

While the periodic modulations of the rivulet cross-section are advected at a deterministic speed, the sinuous path followed by the rivulet drifts slowly or not at all. These features are the result of the interaction with the acoustic forcing, spatially homogeneous and oscillating in time. The instability is characterized by a wavelength and drift speed that depends on the flow rate and the excitation frequency, which we are able to explain using a resonance condition.

References

- [1] A. DAERR, J. EGGERS, L. LIMAT, AND N. VALADE, General Mechanism for the Meandering Instability of Rivulets of Newtonian Fluids, *Phys. Rev. Lett.* **106**, 184501 (2011).

Microfluidic study of evaporation through steady colloidal crust

Hrishikesh Pingulkar and Jean-Baptiste Salmon

LOF, UMR 5258 CNRS-Solvay-Université de Bordeaux

Corresponding author: hrishikesh.pingulkar-ext@solvay.com

This work explores the phenomenon of evaporation through colloidal crusts, which is encountered in a wide range of applications, from soil salinization, filtration to until recently electricity generation [1, 2, 3]. However, this complex phenomenon is still a subject of ongoing research and is influenced by various factors including colloidal concentration, crust length, particle size, temperature and relative humidity, RH.

In this work, effects of relative humidity and crust length on evaporation of water through colloidal crust are studied, using a PDMS chip with serpentine-shaped microchannel, as shown in 1. Different lengths of colloidal crusts are formed using aqueous dispersions of silica (Ludox) as well as polystyrene (Latex) particles. Our *in-situ* meniscus tracking method allows direct measurements of evaporation rate, J . The results show that for small colloidal crusts, J varies linearly with $1-RH$. In case of longer colloidal crusts, J again varies linearly with $1-RH$ until $RH \approx 0.6$, where it reaches a plateau for $RH \leq 0.6$. These results are consistent with recently published theoretical work [4], and provide the further experimental evidence of existence of the *capillary-limited regime* [4, 5], where J is observed to be independent of RH.

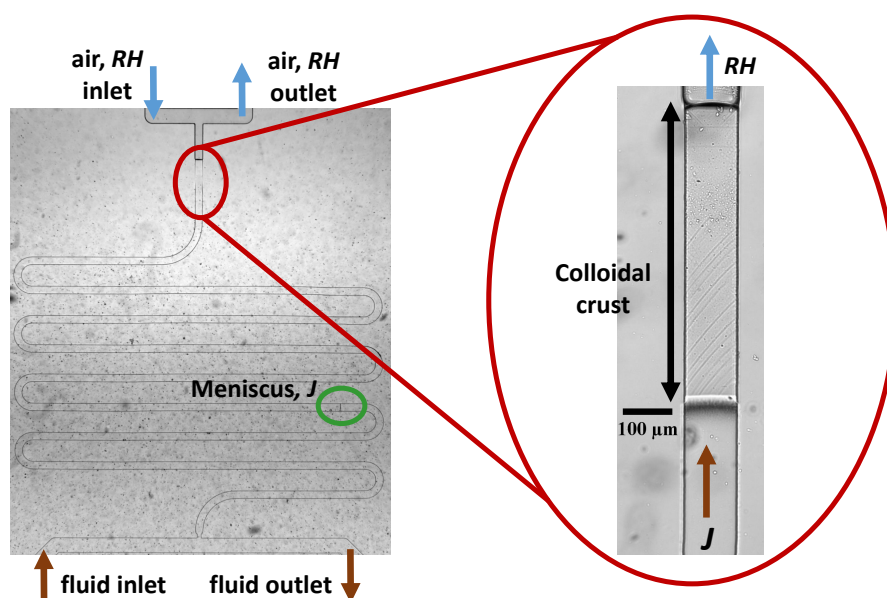


Figure 1: Overview of PDMS microfluidic chip used, with a zoomed view of colloidal crust formed through which evaporation of water occurs. The *in-situ* imaging of water-oil meniscus gives direct measurements of J for various values of RH.

References

- [1] SHOKRI-KUEHNI S. M. S. AND VETTER T. AND WEBB C. AND SHOKRI N., *Geophysical Research Letters* **44**, 15504-5510 (2017).
- [2] LINKHORST J. AND BECKMANN T. AND GO D. AND KUEHNE A. J. C. AND WESSLING M., *Scientific reports* **6**, 1-8 (2016).
- [3] SHEN D., DULEY W., PENG P., XIAO M., FENG J., LIU L., ZOU G. AND ZHOU Y. N., *Advanced Materials* **32**, 1-32 (2020).
- [4] PINGULKAR H., SALMON J.-B., *Soft Matter* **19**, 2176-2185 (2013).
- [5] VINCENT O., SZENICER A. AND STROOCK A. D., *Soft Matter* **12**, 6656-6661 (2016).

Capillary flow of evaporating liquid solutions in open rectangular microchannels

Panayiotis Kolliopoulos¹, Krystopher S. Jochem¹, Lorraine F. Francis¹ and Satish Kumar¹

¹ Department of Chemical Engineering and Materials Science, University of Minnesota, Minneapolis, MN 55455, USA

Corresponding author: kumar030@umn.edu

Capillary flow of liquids plays a key role in many applications including lab-on-a-chip devices, heat pipes and printed electronics manufacturing. Open rectangular microchannels often appear in these applications, with the lack of a top resulting in a complex free-surface morphology and evaporation (Fig. 1). In this work [1] we develop a theoretical model based on lubrication theory and kinetically limited evaporation to examine capillary flow of evaporating liquid solutions in open rectangular microchannels connected to circular reservoirs. The model accounts for the complex free-surface morphology, solvent evaporation, Marangoni flows due to gradients in solute concentration and temperature and finite-size reservoir effects. Significant differences are predicted in flow behavior between pure liquids and liquid solutions due to solvent evaporation and solute transport. Marangoni flows are found to promote more uniform solute deposition patterns after solvent evaporation. Model predictions of meniscus position evolution are in good agreement with prior capillary-flow experiments of aqueous poly(vinyl alcohol) solutions in the presence of evaporation. The model reveals that the principal mechanism through which evaporation influences the meniscus position in the experiments is the increase in viscosity with solute concentration.

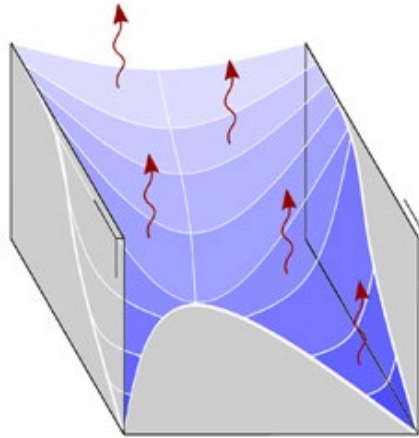


Fig. 1. Schematic of an evaporating liquid in an open rectangular microchannel

References

1. P. Kolliopoulos, K. S. Jochem, L. F. Francis, and S. Kumar, *J. Fluid Mech.* 938 (2022) A22.

Optomechanical measurement of single nanodroplet evaporation with millisecond time-resolution

Samantha Sbarra¹, **Louis Waquier**¹, Stephan Suffit¹, Aristide Lemaître² and Ivan Favero¹

¹ *Matériaux et Phénomènes Quantiques, Université Paris Cité, CNRS, UMR 7162, 75013, Paris, France*

² *Centre de Nanosciences et de Nanotechnologies, Université Paris-Saclay, CNRS, UMR 9001, 91120, Palaiseau, France*

Corresponding author: ivan.favero@u-paris.fr

Tracking the evolution of an individual nanodroplet of liquid in real-time remains an outstanding challenge. Here a miniature optomechanical resonator detects a single nanodroplet landing on a surface and measures its subsequent evaporation down to a volume of twenty attoliters. The ultra-high mechanical frequency and sensitivity of the device enable a time resolution below the millisecond, sufficient to resolve the fast evaporation dynamics under ambient conditions. Using the device dual optical and mechanical capability, we determine the evaporation in the first ten milliseconds to occur at constant contact radius with a dynamic ruled by the mere Kelvin effect, producing evaporation despite a saturated surrounding gas. Over the following hundreds of milliseconds, the droplet further shrinks while being accompanied by the spreading of an underlying puddle. In the final steady-state after evaporation, an extended thin liquid film is stabilized on the surface. Our optomechanical technique opens the unique possibility of monitoring all these stages in real-time.

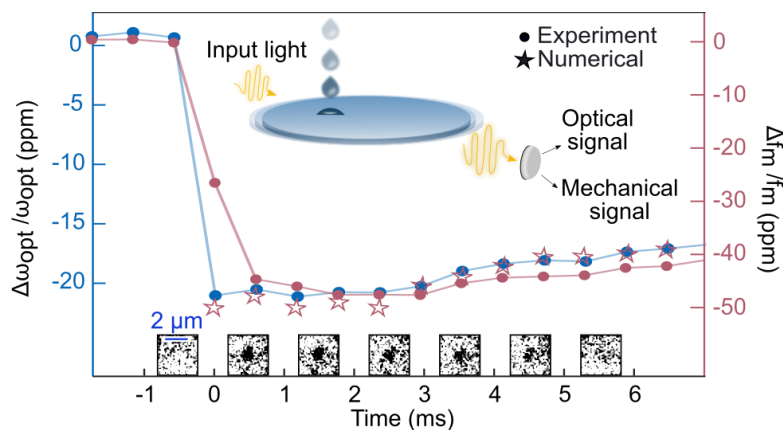


Fig. 1. A droplet of $1.3 \mu\text{m}$ diameter is deposited on an optomechanical disk resonator at $t=0$ making its optical (blue) and mechanical (red) resonances shifting to the red. Then its evaporation in the first milliseconds is tracked with both the optical and mechanical signals. Using these signals and under few assumptions, the mass of the nanodroplet, its contact radius and angle, can be measured all along the evaporation with a millisecond time resolution. The results are supported by a numerical finite element method analysis. A fast camera (frames along the time axis) images in real time the evaporation of the droplet.

References

Sbarra, S., Waquier, L., Suffit, S., Lemaître, A., & Favero, I. (2022). Optomechanical measurement of single nanodroplet evaporation with millisecond time-resolution. *Nature Communications*, 13(1), 6462.

Effect of gas wiping temperature on coating weight reduction in hot-dip galvanizing of steel strip

Hirokazu Kobayashi^{1,2}, Gentaro Takeda¹, Kenji Katoh² and Tatsuro Wakimoto²

¹ Steel Research Laboratory, JFE Steel Corporation, Fukuyama, Hiroshima, Japan

² Graduate School of Engineering, Osaka Metropolitan University, Osaka, Osaka, Japan

Corresponding author: hirok-kobayashi@jfe-steel.co.jp

Key words: Hot-dip galvanizing; Gas wiping; Air knife; Coating weight; Solidification

In the gas wiping process in hot-dip galvanizing, the wiping mechanism and performance are well-established theoretically, assuming that the pressure from the impinging jet and the shear force from the wall jet act on the liquid zinc film [1,2]. On the other hand, there are two limitations on reduction of the coating thickness: The first is the limit due to splashing of the liquid film of molten zinc, and the second is the limit on film thinning due to the wiping capacity of the equipment.

In this study, we investigated the possibility that wiping efficiency is reduced by the effect of zinc solidification due to cooling by the gas jet by conducting a gas wiping experiment under various temperature conditions. The experimental set-up is shown in Fig. 1. A galvanized steel strip with a width of 100 mm was immersed in a molten zinc bath in the air atmosphere, and the steel strip was heated by induction heating before wiping.

The results clarified the fact that high temperature conditions improved gas wiping efficiency. It is suggested that high wiping efficiency is prevented by an increase in viscosity due to an increased solid volume fraction in the liquid zinc film surface caused by microscopic solidification. In addition, it was also found that the development of the initial alloy layer reduced the liquid phase and prevented wiping.

Introduction

Zinc has excellent corrosion resistance by forming an oxide layer, sacrificial protection [1] with respect to iron and highly workability. Therefore, zinc is a difficult metal material to replace and is widely used in galvanized steel sheets. However, because resources are finite, there is demand for zinc saving by reducing the thickness of the galvanized coating in order to reduce the zinc usage ratio.

In the manufacturing process of thin steel strips, hot-dip galvanized steel strips are generally produced by continuously immersing steel strips in a bath of molten zinc. The hot-dip coating is thicker than in the electrogalvanizing process. Excess liquid zinc accompanying the running steel strip is reduced by a gas jet from a nozzle to control the coating weight. Gas wiping is widely used due to its excellent efficiency and uniformity, but in order to decrease the coating thickness, it is necessary to slow the strip speed and increase the gas pressure to improve gas wiping performance.

The gas wiping mechanism is theoretically established, assuming that the pressure from the jet and the shear force from the impinging wall jet act on the liquid film [2-4]. However, there are limitations on reduction of the coating thickness in hot-dip galvanizing.

In this study, we suspected that wiping efficiency might be decreased by the formation of a solid-liquid coexistence layer due to cooling, and conducted a gas wiping experiment to verify the effect of applying induction heating to improve the fluidity of the liquid zinc.

Experimental set-up

Fig. 1 shows a schematic image of the wiping experimental setup. Zinc was melted in a stainless steel pot equipped with an electric heater. In order to ensure wettability with the molten zinc, a galvanized steel strip with a coating weight of 40 g/m² was immersed in the pot. A gas wiping nozzle was installed on one side to control the coating thickness, and an induction heating coil was installed below the nozzle to increase the steel strip temperature. The heights from the zinc bath surface to the center of the heating coil and the gas nozzle were 130 mm and 170 mm, respectively.

Because a galvanized steel strip was used, double plating was a concern. However, cross-sectional observation after the experiment confirmed that the initial layer structure was melted and replaced, and it was possible to produce a thin plating with a coating weight of less than 40 g/m².

On the entry side of the zinc pot, the coiled galvanized steel strip was preheated. On the exit side, a tension reel was used to control the winding speed of the steel strip. The zinc bath temperature was set to 470 °C. The width and thickness of the steel

strip were 100 mm and 0.41 mm, respectively. The induction heating coil was a 10 x 10 mm square copper tube with a hollow shape and a wall thickness of 1 mm, and its inner side was water-cooled. The power output and frequency of 100 kW and 18.5 kHz were used in induction heating.

The zinc film thickness, that is, the coating weight, was measured by the weight difference after removing the coating. The coating weight was defined as the average value obtained with 5 galvanized steel sheet samples of 100 × 100 mm under the same experimental conditions.

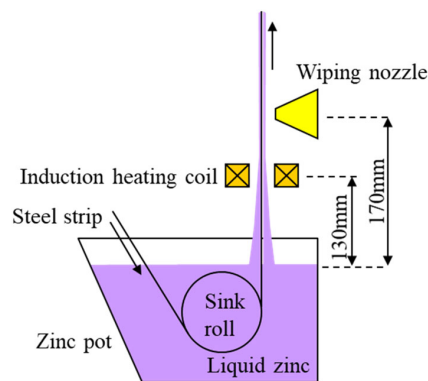


Fig. 1. Schematic image of experimental set-up

Results

Table 1 shows the experimental conditions, and Fig. 2 shows the experimental results of the zinc coating weight. For comparison, the analytical results by the method of Takeishi et al. [2] are also shown.

The coating weight decreased as the strip speed was reduced. Comparing the conditions with and without heating, it was found that the coating weight could be further reduced when the steel strip was heated by the induction coil. These results indicate that wiping efficiency is deteriorated by a phenomenon such as solidification due to gas cooling under the no-heating condition.

On the other hand, the analysis predicted a smaller coating weight than the experimental results. As the reason for this, it is thought that the analysis assumed a 100 % liquid layer, while in the experiment, a rigid initial alloy layer that formed near the boundary between the steel and the zinc and cooling solidification affected wiping efficiency. The analysis results also showed that the coating weight decreased at slower strip speeds. However, the experimental results without heating showed that the decrease in coating weight at 10 m/min was slightly smaller than the analysis result. Since the slower strip speed decreases the strip temperature, this result also indicates the same conclusion that cooling deteriorates gas wiping efficiency.

In the experiment, it was observed that the surface of the molten zinc flowed and was wiped off, indicating that the surface was not completely solidified. Therefore, it is possible that a solid-liquid coexistence layer is generated due to a microscopic solidification phenomenon. Regarding the viscosity coefficient increase in the solid-liquid coexistence layer, Thomas [5] reported experimental results of an investigation of the relationship between the solid volume fraction and the viscosity coefficient using shaped particles, and showed that if the solid volume fraction increases, the viscosity coefficient increases by several times to tens of times.

It is also known that the viscosity of a liquid metal is expressed by the following exponential function [6].

$$\mu = A \exp\left(\frac{B_\mu}{RT}\right) \quad (1)$$

where, A and B_μ are constants, R is the gas constant, and T is the absolute temperature. In the case of molten zinc, the constants are defined as $A = 0.5266$, $B_\mu = 10.91$. Thus, even if the zinc temperature is changed from 470 °C to 420 °C, that is, near the melting point of Zn, the difference in the viscosity coefficient is less than 1.2 times.

In order to explain the difference of the coating weights with and without heating at a strip speed of 30 m/min by wiping theory [2], a difference in the viscosity coefficient of approximately 1.6 times is required. Thus, in the experiment, there is a difference

in the wiping ability that cannot be explained only by the change in the viscosity of the liquid metal, so it is highly possible that the solid volume ratio caused the decrease in wiping efficiency.

Table 1 Experimental conditions

Wiping gas pressure	17 [kPa]
Gas nozzle - strip distance	5 [mm]
Nozzle slit gap	1 [mm]
Induction heater power	50 [kW]
Heating coil - strip distance	5 [mm]

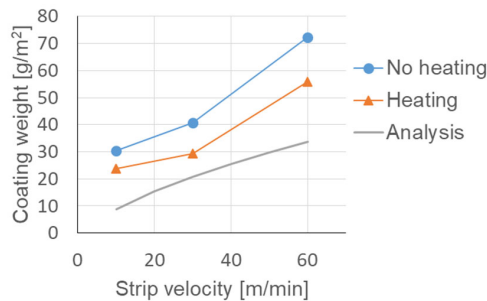


Fig. 2 Comparison of coating weight

Fig. 3 shows the results of a calculation of the steel strip temperature history in the experiment. The strip temperature at the exit side of the zinc bath was calculated from the relationship between the results of temperature measurements with a thermocouple and the immersion time. Since the immersion time is longer at slower strip speeds, the temperature at the exit side of the zinc bath (0 m) is higher at 10 m/min. The cooling ability of the wiping jet was calculated by Martin's equation [7] to predict the heat transfer coefficient in a single-slit nozzle, which is known to agree well with the experimental results. The temperature rise due to induction heating was calculated by considering the transit time under each condition from the thermocouple temperature measurement results for low-speed strip threading. In addition, the heat quantity below 420 °C was calculated by offsetting the heat quantities for supercooling and heating, assuming that the latent heats of solidification and melting are equal.

In the results, the steel strip temperature at the wiping position with heating is around 440 and 520 °C, which is higher than the 420 °C melting point of zinc. Table 2 shows the measured zinc coating Fe% of the galvanized steel sheet for the heating condition at various strip velocities. Since the largest temperature increase occurs at the strip velocity of 10 m/min, it can be understood that the Fe-Zn alloy layer was developed. In Fig. 2, it is thought that the difference between the analysis and experimental results at 10 m/min with heating occurs because the alloy layer affects wiping efficiency. On the other hand, since Fe% is low at 30 and 60 m/min, it is highly likely that wiping efficiency decreased due to insufficient heating, that is, due to the increase in viscosity caused by a microscopic solidification phenomenon. These results clarified the fact that the wiping temperature affected wiping efficiency by affecting the degree of alloying and the viscosity of the molten zinc.

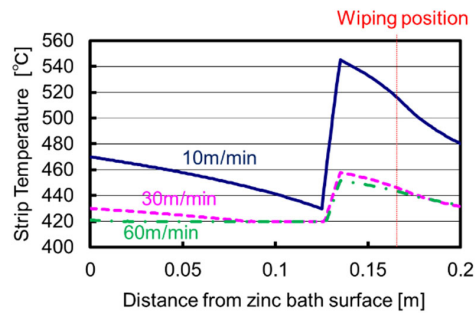


Fig. 3 Analysis of strip temperature

Table 2 Fe% of heated zinc coating

Strip velocity [m/min]	10	30	60
Fe [%]	7.1	1.7	0.5

Conclusion

Gas wiping experiments were conducted to investigate gas wiping efficiency in hot-dip galvanizing under conditions in which the strip temperature was changed by induction heating, and the difference between the experimental coating weight and an analysis based on wiping theory was also investigated.

The results of this research showed that the initial alloy layer reduces the thickness of the liquid layer that can be wiped off, and the solid-liquid coexistence layer caused by cooling increases the viscosity of the zinc, and these phenomena decrease gas wiping efficiency. Therefore, we concluded that it is necessary to consider the volume ratio of the liquid and solid phases in the gas wiping analysis.

References

- [1] Adaniya, T., *J. MMIJ*, **128**, 57-64 (2012).
- [2] Takeishi, Y., Yamauchi, A. and Miyachi, S., *Tetsu-to-Hagane*, **81** (6), 37-42 (1995).
- [3] Takeda, G., Takahashi, H. and Kabeya, K., *Tetsu-to-Hagane*, **102** (10), 24-30 (2016).
- [4] Yahyaee Soufiani, A., McDermid, J. R., Hrymak, A. N. and Goodwin, F. E., *J. Coat. Technol. Res.*, **14** (5), 1015-1028 (2017).
- [5] Thomas, D. G., *J. Colloid Science*, **20** (3), 267-277 (1965).
- [6] Iida, T., *J. The Japan Welding Society*, **63** (2), 70-75 (1994).
- [7] Martin, H., *Adv. Heat Transf.*, **13** (1), (1977).

Film Formation of Lithium-Ion- and Sodium-Ion-Battery Electrodes During Drying: Challenges and Opportunities due to Particle Properties and Process Conditions

Julian Klemens, David Burger, Philip Scharfer, Wilhelm Schabel

Thin Film Technology (TFT), Material Research Center for Energy Systems (MZE), Karlsruhe Institute of Technology (KIT), Karlsruhe, Germany

Corresponding author: julian.klemens@kit.edu

The microstructure formation of slurries for battery electrodes follows specific steps. After uniform film shrinkage, a saturated structure is formed in which all the resulting pores are filled with solvent. The components contained in the slurry (active material, conductive carbon black, dispersing additive, binder) are expected to be homogeneously distributed at this point. Subsequently, the solvent is removed from the pores by a mechanism controlled by capillary forces (pore emptying). Drying at higher, industry-relevant drying rates results in an inhomogeneous distribution of the binder, which is transported to the top of the electrode by capillary transport of the solvent. The inhomogeneous distribution blocks pathways through the pores, resulting in increased ionic resistance. This adversely affects the electrochemical properties of the electrodes. In addition, the decrease in binder concentration near the substrate leads to a deteriorated adhesion and, in extreme cases, delamination of the coating. It is known from the literature and recent studies with other particle morphology that the interaction of the particles with the other components of the slurry can result in a reduction or even suppression of binder transport. In this case, the structure still empties according to the capillary transport during pore emptying, but the binder seems to be bound more strongly by the interactions with other materials in the slurry and therefore migrates less or not at all. So far there is no fundamental understanding of the enhanced interaction of the binder and the particles and no mechanistic description for this process.

This work fundamentally and systematically addresses the material-process-property relationships (Fig. 1). It shows results on the influence of different particle systems on microstructure formation and on the mechanism of binder migration during pore emptying. Specifically, it is shown how the properties of electrodes with different materials change under identical processing and drying boundary conditions. Furthermore, the effect of the process conditions on the resulting properties of the electrodes is being investigated.

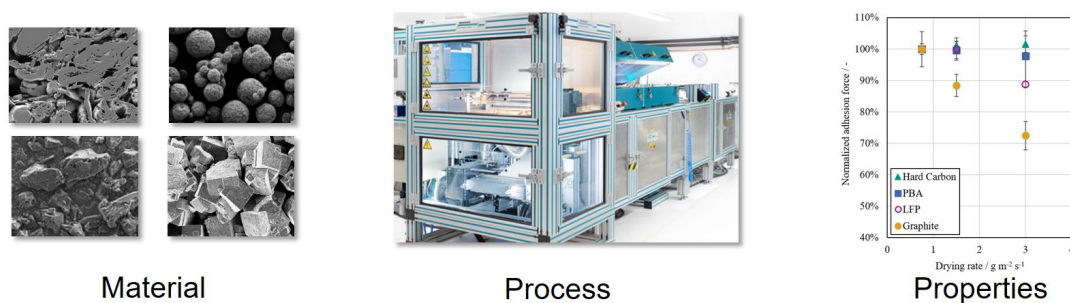


Fig. 1. Material-Process-Properties relationship: Illustration of different active materials for the anode and cathode of lithium-ion and sodium-ion batteries (left). Pilot plant as a representation of industry-relevant process conditions (middle). Trends in adhesion force with increasing drying rate for electrodes made of different active materials (right).

Furthermore, an additional important relationship that will be studied is the temperature of the drying slurry at a given drying rate. The drying rate is the driving force for the intensity of the capillary transport, and thus, the amount of the binder migration that occurs. The temperature of the film tends to be higher at higher drying rate, having a significant influence on the movement of the binder. An increased film temperature at the same drying rate proves to be a resistance to binder migration and can be reached by non-convective heat flux as radiation or conduction. It seems that the binder is more bound at higher film temperature and is less transported through the capillary emptying. This results in higher adhesion forces and lower ionic resistance, which suggests a homogeneous distribution of the binder. This work provides first approaches to the mechanistic understanding of this effect and should also contribute to the understanding of processing different particle systems.

This work was funded by the Deutsche Forschungsgemeinschaft (DFG, German Research Foundation) under Germany's Excellence Strategy – EXC 2154 – Project number 390874152 (POLiS Cluster of Excellence) and contributes to the research performed at CELEST (Center for Electrochemical Energy Storage Ulm Karlsruhe) and MZE (Material Research Center for Energy Systems).

Structural optimisation of catalyst layers for PEM electrolysis

Nadine Zimmerer^{1,2}, Philipp Quarz^{1,2}, Philipp Scharfer, Wilhelm Schabel^{1,2}

¹ Thin Film Technology (TFT), Karlsruhe Institute of Technology (KIT), Karlsruhe, Germany

² Material Research Centre for Energy Systems (MZE), Karlsruhe Institute of Technology (KIT), Karlsruhe, Germany

Corresponding author: nadine.zimmerer@kit.edu

In view of the desired energy transition and the increasing demand for energy storage systems with regard to renewable energies, hydrogen is an efficient and environmentally friendly energy carrier which can be stored and used without greenhouse gas or any harmful emissions. The polymer electrolyte membrane (PEM) water electrolysis offers the possibility to store energy from for example wind and solar energy sources by producing regenerative, green hydrogen [1].

The energy-converting reactions take place at the heart of the PEM stack, the catalyst coated membrane (CCM). The CCM consists of a perfluorosulfonic acid (PFSA) membrane, for instance Nafion™ membrane, which is coated on both sides with microporous catalyst layers. The efficiency of the system is based on the reaction at the triple phase boundaries within the CCM and is therefore significantly influenced by the porous microstructure of the catalyst layers, as it has a decisive influence on the electrochemical accessible surface and the supply and removal of the reactants.[2,3]

The materials and production of the CCMs, contribute decisively to the still high costs of the system. Thus, different approaches for the cost reduction target the optimization of the catalyst layers. The presented study focuses on the processing and optimization of anode electrodes. In the approach chosen here, the catalyst layer is built up from several layers, so that a multilayer structured electrode is created. The tailored individual layers are aimed at both improving the productivity of the overall system and reducing the material costs. A porosity gradient in the electrode, for example, can optimise the electrochemically active surface and the mass transport of the reactants and products [4]. Other approaches include a catalysis loading gradient to reduce the material costs [5] or an ionomer gradient to improve the performance by reducing the ionic resistance [6].

The production of the electrodes is particularly important with regard to catalyst layer optimisation by means of a porosity gradient. By adjusting the parameters during ink mixing, particle properties can be systematically influenced. In the next step, film consolidation is the decisive step for the resulting porosity and microstructure formation [7,8]. For this reason, the drying step of the (nano)particulate catalyst ink is in the focus of the investigations. Here, effects of coupled heat and mass transfer are investigated and related to electrode properties. Another phenomenon occurring in carbon-based catalyst layers is the formation of defects, e.g. cracks and pinholes, within the catalyst layers. In addition to the optimisation possibilities already mentioned previously, a multilayer structure of the catalyst layer produced by sequential or simultaneous coating also has an influence on defect formation. The investigation of these is also a focus of the research.

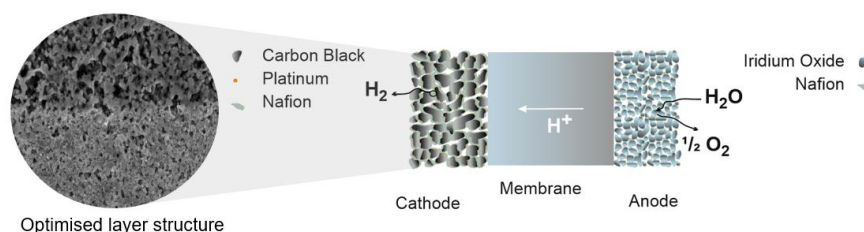


Fig. 1. Example of an PEM electrolyser CCM and the optimized electrode by the use of a multilayer with porosity gradient.

References

1. M. Carmo, D. L. Fritz, J. Mergek, De. Stolten, *Hydrogen Energy*, 38, 4901-4934 (2013).
2. U. Schelling; R. Zahoransky (Ed.), *Energietechnik* 8. Auflage (Springer Vieweg, Wiesbaden, 2019).
3. J. Shimanuki, S.Takahashi, H. Tohma, A. Ohma, A. Ishihara, Y. Ito, Y. Nishino, A. Mityazawa, *Microscopy*, 66, 204-208 (2017).
4. G. Liu, M. Wang, Y. Wang, Z. Tian, X. Wang, *Int. J. Energy Res.*, 37, 1313-1317 (2013).
5. H. Yu, A. Baricci, A. Bisello, A. Casalegno, L. Guetaz, L. Bonville, R. Maric, *Electrochimica Acta*, 247, 1155-1168 (2017).
6. Y.-G. Yoon, T.-H. Yang, G.-G. Park, W.-Y. Lee, C.-S. Kim, *Journal of Power Sources*, 118, 189-192 (2003).
7. S. Jaiser, M. Müller, M. Baunach, W. Bauer, P. Scharfer, W. Schabel, *Journal of Power Sources*, 318, 210-219 (2016).
8. J. Kumberg, W. Bauer, J. Schmatz, R. Diehm, M. Tönsmann, M. Müller, K. Ly, P. Scharfer, W. Schabel, *Energy Technology*, 9: 2100367 (2021).

Fabrication of Reduced Graphene Oxide Nanofiltration Membranes by an Integrated Roll-to-Roll (R2R) Process

Tequila A. L. Harris¹, Amirsalar R. Esfahani¹, Chen Ma², Uwezo A. Flewollen¹, Sankar Nair²

¹Woodruff School of Mechanical Engineering, Georgia Institute of Technology, Atlanta, GA, 30332, USA

²School of Chemical & Biomolecular Engineering, Georgia Institute of Technology, Atlanta, GA, 30332, USA

Corresponding author: tharris3@gatech.edu

There is an increasing demand in many industrial sectors for large-scale separation of complex aqueous streams to produce useable water, simultaneously recover/concentrate valuable resources (such as biomass components, salts, metals), and save energy relative to conventional separation processes such as distillation or liquid extraction [[1], [2], [3], [4]]. Economic fractionation of multicomponent biomass-derived streams is a key challenge in biobased fuels and chemicals production. Kraft black liquor (BL) is generated at ~1 billion tons/yr globally from biomass pulping and contains ~15 wt% total solids including lignin, hemicellulose fragments, and inorganics [5]. Membrane-based BL concentration is attractive but challenged by low solute rejections and poor stability in BL, which combines alkaline pH (~13), high dissolved solids content (15+ wt%) and high temperature (70-85°C). In this talk, we will discuss the scaled fabrication and characterization of reduced graphene oxide (rGO) nanofiltration membranes by slot die coating on a roll-to-roll (R2R) with integrated vacuum filtration. High-quality 90x30 cm rGO membranes (referred to as R2R-rGO membranes) with ~100 nm average thickness supported on porous poly(ethersulfone) (PES) sheets, and an effective area of 2700 cm², were fabricated. Characterizations of their microstructure and uniformity as mapped over large areas by scanning electron microscopy (SEM), ellipsometry, adhesion test and X-ray photoelectron spectroscopy (XPS), which will be discussed. The R2R-rGO membranes showed >98% lignin rejection with a steady state flux of ~12 LMH at 50 bar in a 15.7 wt% total solids (TS) kraft BL stream at 72°C and 2-3 gal/min crossflow rates. Slot die coating on a R2R platform with integrated vacuum filtration can enable rapid fabrication of high-quality GO membranes at scale without organic solvents or volatile organic compounds.

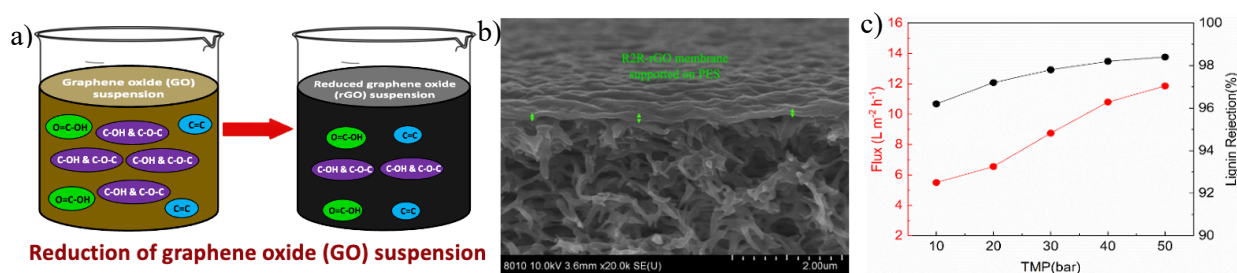


Figure 1. Schematic showing a) the chemical reduction, b) the fabricated membrane and c) typical results.

References

1. J.M. Dickhout, J. Moreno, P. Biesheuvel, L. Boels, R. Lammertink, W. De Vos, *Journal of colloid and interface science* 487 523-534, (2017).
2. E. Kavitha, E. Poonguzhali, D. Nanditha, A. Kapoor, G. Arthanareeswaran, S. Prabhakar, *Chemosphere* 291, 132690 (2022).
3. W. Rongwong, K. Goh, *Journal of Environmental Chemical Engineering* 8(5), 104242 (2020).
4. V. Kumar, S.K. Yadav, J. Kumar, V. Ahluwalia, *Bioresource technology* 299, 122633 (2020).
5. A. R. Esfahani, C. Ma, U. A. Flewollen, S. Nair, T. A.L. Harris, *Journal of membrane Science*, 678, 121669, (2023).

About the pore emptying during drying of water-based battery electrodes

David Burger, Julian Klemens, Philip Scharfer, Wilhelm Schabel

Thin Film Technology (TFT), Material Research Center for Energy Systems (MZE), Karlsruhe Institute of Technology (KIT), Karlsruhe

Corresponding author: david.burger@kit.edu

To meet the growing demand for batteries, it is important to make the manufacturing process as efficient as possible in order to reduce costs and the resources used. One limiting process in the roll-to-roll manufacturing is the drying, that needs to be fast to meet the economic demand for high throughput at limited dryer length. However, for high drying rates, migration of binder leads to possible delamination of the electrode coating and poor cell performance. The migration behavior of the thickener CMC and binder SBR must be considered, as well as that of further additives. Capillary-driven flow of solvent during drying whilst pore emptying is considered to be the main cause of binder migration [1].

One key role for the migration of binder plays the composition and processing of the slurry. Interactions between CMC and the particles' surface are thought of to suppress binder migration, for example reached by high shear mixing in a kneader [2]. Another way to strengthen the interactions between particles and the thickening polymer is the addition of synthetic nano-scale clay, to influence the slurries' microstructure and hence viscoelastic behavior [3]. It is to be investigated how the characteristics of pore emptying and the mechanical properties of the dry electrode rely on the slurries' microstructure and the drying conditions.

In this talk, the influence of different slurry compositions on the pore emptying is discussed for increasing drying rate and compared with the investigation of the coatings' microstructure by means of adhesion strength and image analysis of the local pore structure at the interface between the coating and a glass substrate (see Fig. 1).

Further to indirect measure with this setup the pore emptying can be tracked during drying. Differences in the increase of the empty pores' area share during drying indicate a slurry- and drying rate dependent pore emptying behavior. After comparison of single layer electrodes, focus is set on the use of promising slurry compositions in a multilayer configuration for a more efficient use of materials, i.e. the use of further additives only in the substrate near layer and an overall reduction of the passive material share.

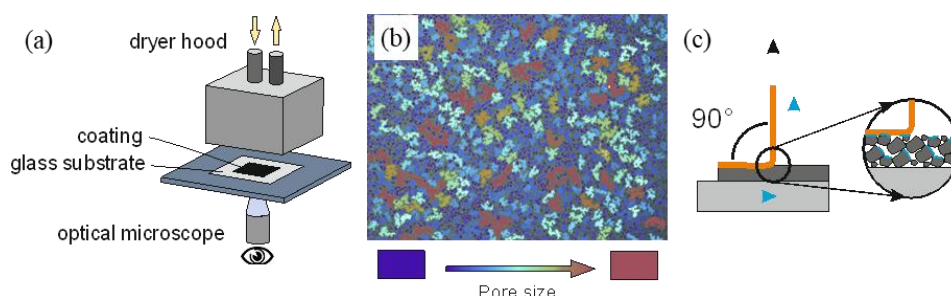


Fig. 1. Experimental setup for coating and drying (a) and in situ measurement of the pore structure (b), to be compared with adhesion strength via a 90° peel-test (c).

This work contributes to the research performed at CELEST (Center for Electrochemical Energy Storage Ulm Karlsruhe) and the Material Research Center for Energy Systems (MZE). The authors would like to acknowledge financial support of the Federal ministry of Education and Research (BMBF) via the ProZell cluster project "HiStructures" (Grant No. 03XP0243C) and by the Deutsche Forschungsgemeinschaft (DFG, German Research Foundation) under Germany's Excellence Strategy – EXC 2154 – Project number 390874152 (POLiS Cluster of Excellence).

References

1. S. Jaiser, et al., P. Scharfer, W. Schabel, Impact of drying conditions [...], *Drying Technology* **35**, 1807-1817 (2017).
2. J. Kumberg, et al., P. Scharfer, W. Schabel, Reduced Drying Time of Anodes [...], *Energy Technology* **9**, 2100367 (2021).
3. P. Xu, T. Erdem, E. Eiser, *Soft Matter* **16**, 5497-5505 (2020).

New methods for optimized inline monitoring of the drying process of battery electrodes

J. Mohacsi^{1,2}, A. Altvater^{1,2}, K. Ly^{1,2}, M. Birg¹, P. Scharfer^{1,2}, W. Schabel^{1,2}

¹*Thin Film Technology (TFT)*

²*Materialwissenschaftliches Zentrum für Energiesysteme (MZE)*

Corresponding author: jonas.mohacsi@kit.edu

The increasing demand for energy storage may position battery cells as one of the main players in the process of the energy transition. As electrification of the transport sector and digitalization continue to advance, the production of battery cells is set to increase significantly. However, to achieve this growth, it is crucial to optimize the manufacturing process by improving energy and material efficiency and ensuring cell quality.

In the manufacturing process of battery electrodes, reducing solvent loading through a suitable drying process is a critical step. One major challenge is minimizing high reject rates, which can significantly impact costs. Therefore, the aim is to achieve full monitoring of the drying process by integrating comprehensive sensor technology. By doing so, deviations from target parameters can be detected and eliminated at an early stage.

In this work, various sensors have been investigated to determine their suitability for inline monitoring of the drying process. They are to be integrated into the housing of a convective dryer developed in-house for a roll-to-roll system on a laboratory scale. This unique system offers special possibilities, including spatial integration of corresponding sensor technology.

An area-resolved measurement of the film temperature can be achieved by using an IR camera, which serves as an indicator of the progress of drying. Another parameter examined is the roughness of the film surface, which increases strongly during the drying process. This can be well resolved using of a scattered light sensor. These measurements are crucial for monitoring a three-stage drying process. Using the latest confocal point sensors, it is possible to monitor the film height distribution on the vibrating belt of the roll-to-roll system. Additionally, a further possibility for measuring the surface roughness could be achieved.

This work contributes to the research performed at CELEST (Center for Electrochemical Energy Storage Ulm Karlsruhe) and Material Research Center for Energy Systems (MZE). The authors would like to acknowledge financial support of the Federal Ministry of Education and Research (BMBF) under project ID 3XP0359A (IQ-El) and 03XP0295A (EPIC).

Friction of poroelastic contacts with hydrogel coatings

Antoine Chateauinois¹, Emilie Verneuil¹, Yvette Tran¹, Chung-Yuen Hui²

¹ SIMM Laboratory, ESPCI Paris, CNRS, PSL University, Sorbonne Université, F-75005 Paris, France

² Department of Mechanical and Aerospace Engineering, Cornell University, Ithaca, NY 14853, USA

Corresponding author: antoine.chateauinois@espci.fr; emilie.verneuil@espci.fr

The lubricating properties of polymer hydrogels in aqueous environments are of paramount importance in many biological systems (articular cartilages, mucin layers on the surface of cornea,...) and in biomedical engineering (contact lenses,...) where they can provide very low friction. The development of hydrogel coatings relies on a good control of their frictional response, in both steady-state and at the onset of sliding. One emerging issue is the ability of such systems to maintain low friction when sliding is initiated after prolonged static (non sliding) periods. Here, we report on the transient [2] and steady-state [1] frictional responses of contacts between a rigid spherical glass probe and a micrometer-thick poly(dimethylacrylamide) hydrogel film grafted onto a glass substrate when a lateral relative motion is applied to the contact initially at rest. From dedicated experiments with in situ contact visualization, both the friction force and the contact size are observed to vary well beyond the occurrence of a full sliding condition at the contact interface. Depending on the imposed velocity and on the static contact time before the motion is initiated, either an overshoot or an undershoot in the friction force is observed. Moreover, the steady-state contact size and friction force are both found to depend on the sliding velocity. These observations are rationalized by considering that the transient and steady-state contact sizes are predominantly driven by the flow of water within the stressed hydrogel networks. From the development of a poroelastic contact model using a thin film approximation, we provide a theoretical description of the main features of the frictional response. We especially rationalize the experimental observation that the relaxation of friction force $F_t(t)$ toward steady state is uniquely dictated by the time-dependence of the contact radius $a(t)$, independently on the sliding velocity and on the applied normal load.

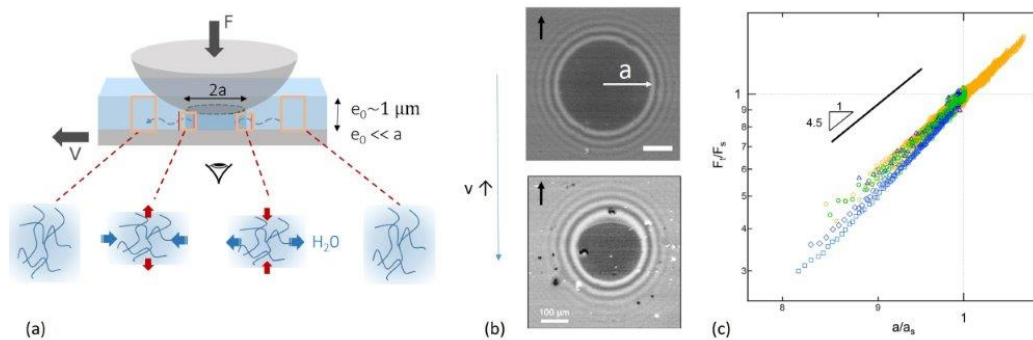


Figure 1: (a) Experimental set-up: a glass sphere is pressed against a thin hydrogel film of micrometer thickness e_0 . After a static contact time, the film is displaced laterally at constant velocity v and the friction force is measured over time. Water within the porous gel is squeezed out and in as the gel enters the contact zone. (b) The contact is imaged from below and its size a and shape are measured over time. They both depend on velocity. (c) The friction force is found to scale as a power law with contact radius a which is set by the poroelastic flow forced within the hydrogel in both transient and steady-state regimes.

References

- [1] J. DELAVOÏPIÈRE, Y. TRAN, E. VERNEUIL, B. HEURTEFEU, C. Y. HUI, AND A. CHATEAUMINOIS., *Langmuir* **34**, 9617–9626 (2018).
- [2] L. CIAPA, J. DELAVOÏPIÈRE, Y. TRAN, E. VERNEUIL, AND A. CHATEAUMINOIS. *Soft Matter*, **16** 6539–6548 (2020).

Hydrogel films as anti-fog coatings : swelling and debonding

Emilie Verneuil¹, Antoine Chateaubinois¹, Yvette Tran¹, Marc Fermigier², Chung-Yuen Hui³,

¹ SIMM Laboratory, ESPCI Paris, CNRS, PSL University, Sorbonne Université, F-75005 Paris, France

² Physique et Mécanique des Milieux Hétérogènes (PMMH), ESPCI Paris, PSL University, Sorbonne Université, CNRS, F-75005 Paris, France

³ Department of Mechanical and Aerospace Engineering, Cornell University, Ithaca, NY 14853, USA

Corresponding author: emilie.verneuil@espci.fr; antoine.chateaubinois@espci.fr

Hydrogel coatings absorb water vapor and, as such, are good candidates for antifog applications, but their efficiency requires a good control of both the kinetics of adsorption and their mechanical resistance to debonding. Here, the transfer of vapor from the atmosphere to hydrogel thin films is first measured in a situation where vapor flows alongside the cold coating (Fig. 1a). The effect of the physico-chemistry of the hydrogel film on the swelling kinetics is particularly investigated [1]. By using model thin films of surface-grafted polymer networks with controlled thickness, varied crosslinks density, and varied affinity for water, we were able to determine the effect of the film hygroscopy on the dynamics of swelling of the film (Fig. 1b). These experimental results are accounted for by a diffusion-advection model that is supplemented with a boundary condition at the hydrogel surface: we show that the latter can be determined from the equilibrium sorption isotherms of the polymer films. Altogether, we offer a predictive tool for the swelling kinetics of any hydrophilic hydrogel thin films.

Once the films are fully swollen, we further report on the delamination of the gel from the substrate starting from well-controlled line defects with low adhesion (Fig. 1c). We particularly investigate the effect of the strength of the coating/substrate interface on the propagation of the debonding. To do so, we control the chemical grafting density of the gel on a silanized silicon substrate by varying the surface density of reactive silanes. Debonding of the film propagates under the action of differential swelling stresses at the crack front [2]. A threshold film thickness for the onset of this delamination is evidenced which is increasing with grafting density, while the debonding velocity decreases. These observations are discussed within the framework of a nonlinear fracture mechanics model which assumes that the driving force for crack propagation is the swelling difference between the bonded and delaminated parts of the film. From this, the threshold energy for crack initiation is determined and discussed in relation to the grafting density.

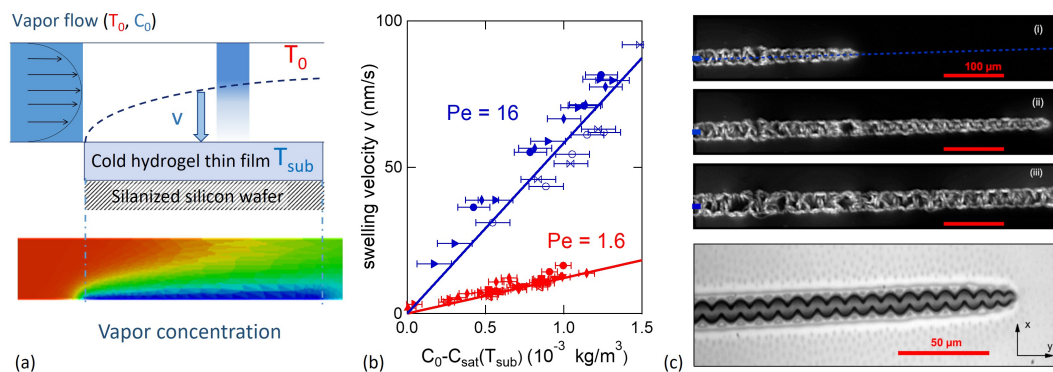


Figure 1: (a) Set-up: vapor flows in a chamber in which an initially dry hydrogel coating chemically grafted on a silicon wafer is set on a cold plate. As vapor diffuses to the coating, the film swells. (b) Swelling velocity is set by advection-diffusion of vapor and a boundary condition set by the polymer physico-chemistry. Lines: predictive model. (c) Timelapse images of delamination of hydrogel coatings induced from a line defect and promoted by swelling stresses showing propagation of debonding along and across the line defect.

References

- [1] J. DELAVOÏPIÈRE, B. HEURTEFEU, J. TEISSEIRE, A. CHATEAUBOINIS, Y. TRAN, M. FERMIGIER, AND E. VERNEUIL, *Langmuir* **34**, 15238–15244 (2018).
- [2] A. AUGUSTINE, M. VEILLEROT, N. GAUTHIER, B. ZHUC, C.-Y. HUI, Y. TRAN, E. VERNEUIL AND A. CHATEAUBOINIS, *Soft Matter* **x**, xx–xx (2023).

Transport and evaporation of aqueous co-solvent mixtures in thin porous media

M. G. Wijburg, S. Wang, and A. A. Darhuber

Department of Applied Physics, Eindhoven University of Technology, The Netherlands

Corresponding author: a.a.darhuber@tue.nl

We have studied the imbibition and drying of water/co-solvent mixtures in paper and glass microfiber filters [1]. The experiments reveal a rich interplay of solution imbibition, solvent evaporation and solvent-mediated pore-fiber transport. After deposition, liquids occupy the micron-scale inter-fiber pores of a paper sheet. In thermodynamic equilibrium, polar liquids such as water and co-solvents reside in the nm-scale intra-fiber pores of the cellulose fibers. The timescales for attaining equilibrium prove to depend sensitively on the water content, such that co-solvents can be temporarily trapped in a non-equilibrium configuration. The combination of two experimental methods allows the determination of both the overall co-solvent content and an estimation of what fractions reside in the pores and in the fibers of a paper sheet. The results are relevant to understanding the behavior of solutions in paper and provide insight into the dynamics of aqueous inkjet printing inks.

In Fig. 1(a-c), light transmission images for a tetra(ethylene glycol) (TEG) solution droplet are presented at different times after deposition. Bright regions indicate the presence of liquid in the pores. The wet zone has a slightly elongated, elliptical shape. Its major axis is aligned with the machine direction (MD) of the paper, due to the anisotropy of the cellulose fiber network. While the transmission intensity is relatively homogeneous at first, the formation of a ring structure is observed during later stages of the drying process.

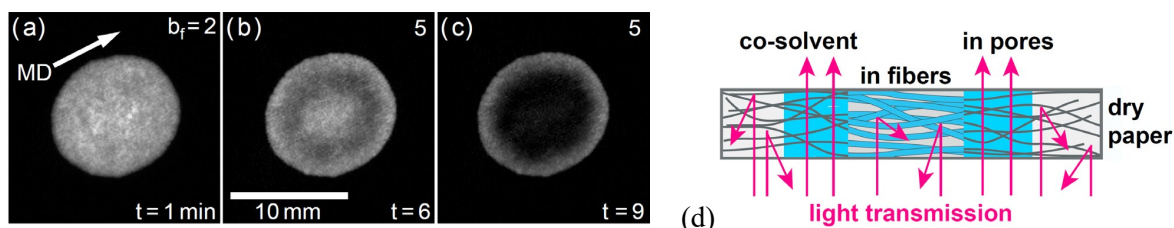


Fig. 1. (a-c) Light transmission intensity for a tetra(ethylene glycol) (TEG) solution droplet (volume $V = 5 \mu\text{l}$, weight fraction $c_0 = 40 \text{ wt}\%$) at times $t = 1, 6$ and 9 min after droplet deposition on commercial printing paper. The white arrow in (a) indicates the machine direction (MD) of the paper. The brightness of the images is enhanced by factors of (a) $b_f = 2$ and (b,c) 5 for improved visibility. (d) Cartoon explaining the ring formation in terms of solvent-assisted pore-fiber migration of the co-solvents.

The transmittance of a paper sheet is primarily determined by light scattering, which depends strongly on the lengthscale of the refractive index heterogeneities, i.e. the size of the pore fractions unoccupied by liquid. The inter-fiber pores of dry paper are in the micron size range, which highly scatter visible light and account for its relative intransparency. The intra-fiber pores are in a size range of 1–20 nm, which do not significantly contribute to the light scattering power. Thus, the migration of co-solvents from the pores into the fibers is accompanied by a strong increase in opacity. The pore-fiber migration rate is highly sensitive to the local co-solvent concentration, as water is required to first swell and plasticize the fiber walls, before co-solvents of high MW can pass into the fiber interior. Since the water concentration after droplet deposition tends to be lower at the perimeter of the wet zone, inhomogeneous pore-fiber distributions result. This induces the formation of a ring with increased transmittance at the perimeter of the wet zone. Its appearance is reminiscent of the well-known coffee stain effect, but it has a fundamentally different origin.

References

1. M.G. Wijburg, S. Wang, and A.A. Darhuber, *Colloids Surf. A Physicochem. Eng. Asp.* **656**, 130268 (2023).

Digital printing of coatings by direct-to-shape inkjet printing with industrial robot

Philip Kessler¹, Johannes Renner¹, Benoît Sahli¹, Vincent Schneuwly¹, Vincent Nidegger¹, Gilbert Gugler¹, Florian Fässler² and Danijel Tipura³

¹ iPrint Institute, HEIA-FR, HES-SO University of Applied Sciences and Arts Western Switzerland, Fribourg, Switzerland

² Polytype AG, Fribourg, Switzerland

³ MABI Robotic AG, Veltheim, Switzerland

Corresponding author: philip.kessler@hefr.ch

Digital inkjet printing has become a popular method for coating applications due to its precision, versatility, and speed. The process allows for a wide range of materials to be used, including aqueous and solvent-based inks, UV-curable inks, and functional materials such as conductive inks or adhesives. The digital printing system enables precise control over the deposition of the coating, enabling selective coatings without masking and the creation of intricate patterns and textures. Digital inkjet printing has found numerous applications in industries such as packaging, textiles, ceramics, and electronics, among others, due to its ability to produce high-quality, customizable coatings with minimal waste and cost.

Direct-to-shape (DTS) printing allows for images or coatings to be printed directly onto three-dimensional surfaces, such as bottles, automotive parts and other objects. DTS printing often uses specialized printers that are designed to accommodate the unique shape of the object being printed on and mostly rely on a static printing system and moving of the object to be printed on. To allow for printing on large and heavy objects and a more flexible process, iPrint has partnered up with MABI Robotic AG and Polytype AG to combine a printing system with a large industrial robot.

In the first phase of this study, a single-colour printing system (Fig. 1) was developed to print on a two-dimensional and three-dimensional (cylindrical) surface in different orientations and robot working spaces. An active ink pressure regulation system has been developed to compensate for the pressure variations caused by the dynamics to which the printing system is subjected. The different samples were scanned by a microscope to determine the relative drop position errors by image processing (Fig. 2) and to show the capability of the specifically used robot for DTS applications. (1) With the help of high-precision distance sensors built into the printing system, the drop placement error and the path accuracy of the robot could be correlated, thus proving the efficiency of the active ink pressure regulation.

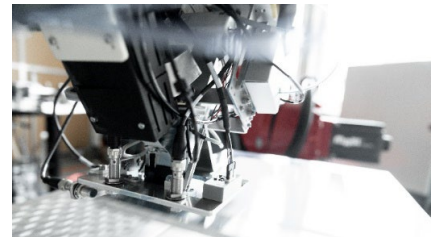


Fig. 1: Single-colour printing system

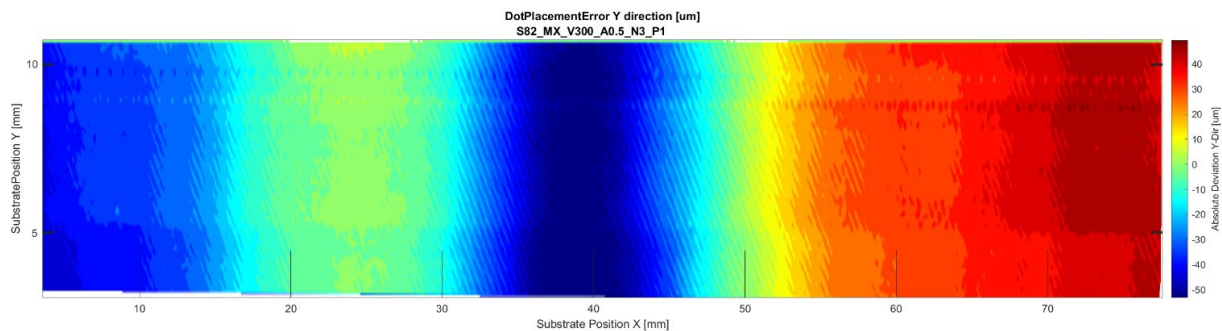


Fig. 2: Dot placement error contourplot

In a second phase, a four-colour printing system was developed to demonstrate the feasibility of high quality graphic printing and selective coatings in a use-case with an automotive part. In the process, aspects such as path generation, position error compensation, stitching quality, coating homogeneity, plasma pre-treatment and UV curing on 3-dimensional surfaces were addressed. We can conclude that the robot used is suitable for DTS applications on large surfaces and that in future numerous new applications can be exploited in graphical printing and digital coating.

References

1. Tipura, D. (2023, March 23) Inkjet Printheads on a MABI MAX 100: Results from Print Tests. InPrint, Munich, Germany

Freezing contact line

Thomas Séon

Institut d'Alembert, CNRS, Sorbonne Université, Paris, France

Ice accretion on airplane, wire or roadway, formation of ice fall, ice stalactite, frozen river or aufeis, are a few examples of ice structures formed by the solidification of capillary flows (drop, rivulet, film). Among the many scientific questions that remain open to understand these problems, the effect of freezing on the contact line motion is undoubtedly one of the most important and mysterious. In this talk, we experimentally investigate three situations where advancing and receding contact line is coupled to freezing : capillary and inertial spreading of a water droplet on a cold substrate and water film dewetting on its own ice. These configurations allow us to propose the main mechanisms that explain the arrest of a contact line due to solidification and to tackle the intricate problem of the wetting of water on ice.

